MODIFIED MESOPOROUS SILICA MEMBRANES FOR SEPARATION APPLICATIONS

A Thesis
Presented to
The Academic Faculty

by

Hyung Ju Kim

In Partial Fulfillment
of the Requirements for the Degree
Doctor of Philosophy in Chemical Engineering
in the School of Chemical & Biomolecular Engineering

Georgia Institute of Technology
August 2013

MODIFIED MESOPOROUS SILICA MEMBRANES FOR SEPARATION APPLICATIONS

Approved by:

Dr. Christopher W. Jones, Co-advisor
School of Chemical & Biomolecular Engineering
Georgia Institute of Technology

Dr. Sankar Nair, Co-advisor
School of Chemical & Biomolecular Engineering
Georgia Institute of Technology

Dr. William J. Koros
School of Chemical & Biomolecular Engineering
Georgia Institute of Technology

Dr. J. Carson Meredith
School of Chemical & Biomolecular Engineering
Georgia Institute of Technology

Dr. Angus P. Wilkinson
School of Chemistry & Biochemistry
Georgia Institute of Technology

Date Approved: June 11th, 2013

To my significant other

ACKNOWLEDGEMENTS

I would like to express my sincere gratitude to my advisors, Prof. Christopher W. Jones and Prof. Sankar Nair, for providing me an opportunity to work with them at Georgia Institute of Technology, and for extending continuous encouragement, support, and guidance. I am also grateful to my committee members, Prof. William J. Koros, Prof. J. Carson Meredith, and Prof. Angus P. Wilkinson, for providing valuable suggestions and for their critical reading of this thesis.

I would like to thank all members of Jones and Nair research groups for their kind help. I also extend my gratitude to my collaborator, Dr. Kwang-Suk Jang, for his support and scientific discussions.

TABLE OF CONTENTS

Page

ACKNOWLEDGEMENTS iv

LIST OF TABLES x

LIST OF FIGURES xii

SUMMARY xviii

CHAPTER

1 Introduction 1

1.1 Mesoporous Molecular Sieves 1

1.2 Mesoporous Silica Membranes 3

1.3 Modification of Mesoporous Silica Membranes 4

1.4 Fundamentals of Molecular Transport in Membranes 7

1.5 Overall Objectives and Strategy 8

2 Seeded Growth, Silylation, and Organic/Water Separation Properties of MCM-48 Membranes 11

2.1 Introduction 11

2.2 Experimental Section 13

2.2.1 Synthesis of MCM-48 seed particles 13

2.2.2 MCM-48 seed layer deposition 13

2.2.3 Synthesis and TEOS treatment of MCM-48 membranes 14

2.2.4 Surfactant removal 14

2.2.5 Silylation 15

2.2.6 Characterization methods 15

2.2.7 Gas permeation and pervaporation measurements 18

2.3 Results and Discussion 21

2.3.1 MCM-48 membrane synthesis by seeded growth 21

2.3.2 Silylation of MCM-48 membranes 35

2.3.3 Pervaporation 37

2.4 Conclusions 43

3 Silylated Mesoporous Silica Membranes on Polymeric Hollow Fiber Supports: Synthesis and Permeation Properties 44

3.1 Introduction 44

3.2 Experimental Section 47

3.2.1 Materials 47

3.2.2 Mesoporous silica membrane coating on Torlon® hollow fibers 47

3.2.3 Silylation of mesoporous membrane 48

3.2.4 Characterization methods 48

3.2.5 Gas permeation and pervaporation measurements 49

3.3 Results and Discussion 51

3.3.1 Mesoporous silica membrane synthesis 51

3.3.2 Evacuation and silylation of mesoporous membrane 59

3.3.3 Pervaporation 74

3.4 Conclusion 83

4 Synthesis and Gas Permeation Properties of Aziridine-Functionalized Mesoporous-Silica Membranes on Polymeric Hollow Fibers 85
4.1 Introduction 85
4.2 Materials and Methods 88
4.2.1 Materials 88
4.2.2 Synthesis of mesoporous silica membrane on Torlon® hollow fiber 88
4.2.3 Synthesis of aziridine 89
4.2.4 Aziridine functionalization of mesoporous silica membrane 89
4.2.5 Characterization methods 90
4.2.6 Gas permeation measurements 90
4.3 Results and Discussion 92
4.3.1 Membrane characterization 92
4.3.2 Gas permeation characteristics 93
4.4 Conclusions 103

5 Summary and Future Work 105
5.1 Summary 105
5.1.1 Silylated MCM-48 membrane on α-alumina disk for organic/water separation 105
5.1.2 Mesoporous silica membrane on polymeric hollow fiber for organic/water separation 106
5.1.3 Mesoporous silica membrane on polymeric hollow fiber for gas separation 107

5.2 Future Works 108

5.2.1 Extension of silylation techniques to other mesoporous M41S membranes 108

5.2.2 Direct characterization of organic loading and pore structure for modified mesoporous silica membranes 109

5.2.3 Application to dehydration of organic using hydrophilic mesoporous silica membranes 110

References 112

LIST OF TABLES

Page

Table 1-1. Properties of original and modified mesoporous silica membranes. 6

Table 2-1. Textural properties of seeded MCM-48 membranes. 29

Table 3-1. Pure-component gas permeation properties of mesoporous silica/Torlon® hollow fiber membranes at various stages of processing. All measurements were made at 308 K, and a feed pressure of 50 psig.[a] 58

Table 3-2. Concentration upgrade from feed to permeate at 303 K. 80

Table 3-3. Concentration upgrade from feed to permeate at 303 K for the template-extracted mesoporous silica/Torlon® hollow fiber membrane. 80

Table 3-4. Comparison of performance of hydrophobic membranes applied to organic/water pervaporation, including silylated mesoporous silica/Torlon® membranes in this work. PDMS: Polydimethylsiloxane, PVDF: polyvinylidene fluoride, POMS: polyoctylmethyl siloxane, TOA: trioctylamine, PTFE: polytetrafluoroethylene, PTMSP: poly(1-trimethylsilyl-1-propyne), PEBA: poly (ether) block amide, PVP: polyvinylpyrrolidone, HFP: hexafluoropropene, *: organic flux only reported. 82

Table 4-1. Steady-state single gas permeation results at 308 K. 103

LIST OF FIGURES

Page

Figure 1-1. Structure of ordered mesoporous materials [14-16]..... 2

Figure 1-2. Mechanism for the synthesis of mesoporous silica under basic conditions in the presence of a cationic surfactant [17]. 3

Figure 1-3. Scheme showing silica surface modification chemistry..... 7

Figure 2-1. Diagram of flange-based membrane adsorption cell [91]. 17

Figure 2-2. Schematic diagram of the experimental setup for permeation measurements [93]..... 19

Figure 2-3. Schematic diagram of experimental setup for pervaporation measurements.20

Figure 2-4. Illustration of disk membrane module for pervaporation experiments. 21

Figure 2-5. SEM images of **(a)** MCM-48 seed particles, **(b)** bare α-alumina disk, and **(c)** α-alumina disk seeded with MCM-48 particles..... 22

Figure 2-6. Pore size distributions of calcined MCM-48 seed particles. 22

Figure 2-7. Top-view SEM images of MCM-48 membrane: **(a)** as-synthesized, **(b)** TEOS VI treated, **(c)** calcined, and **(d)** surfactant-extracted respectively; and cross-sectional SEM images of the **(e)** calcined and **(f)** surfactant-extracted membranes, respectively. 24

Figure 2-8. (a) Cross-sectional SEM image of MCM-48 membrane indicating the distance over which composition analysis was carried out, and **(b)** Al and Si EDS line scan profiles. 25

Figure 2-9. XRD patterns of the **(a)** as-synthesized, **(b)** surfactant-extracted, and **(c)** calcined MCM-48 membranes..... 26

Figure 2-10. FT-ATR/IR absorption spectra of MCM-48 membranes..... 28

Figure 2-11. Nitrogen physisorption isotherms of **(a)** as-synthesized, **(b)** extracted, and **(c)** calcined MCM-48 membranes on the seeded α-alumina substrate. 30

Figure 2-12. Nitrogen physisorption isotherms of calcined MCM-48 membranes prepared by **(a)** seeded growth **(b)** unseeded (in situ) growth techniques, and **(c)** α-alumina support..... 31

Figure 2-13. PSDs of **(a)** calcined MCM-48 membrane, and **(b)** extracted MCM-48 membrane..... 32

Figure 2-14. Experimental gas permeabilities (blue squares) of calcined MCM-48 membranes at 308 K, and theoretically estimated permeabilities from the ideal Knudsen model (black circles) and after corrections for gas-solid interactions in the mesopores (black triangles). 34

Figure 2-15. XRD patterns of **(a)** calcined, and **(b)** HMDS-treated MCM-48 membranes. 36

Figure 2-16. Gas permeabilities of calcined and silylated MCM-48 membranes at 308 K. 37

Figure 2-17. Pervaporation (flux and separation factor) results **(a)** single component pervaporation of the seeded MCM-48 membrane, **(b)** single component pervaporation of the silyl-MCM-48 membrane, **(c)** 5 wt % mixture pervaporation of seeded MCM-48 membrane, and **(d)** 5 wt % mixture pervaporation of the silyl-MCM-48 membrane. 39

Figure 2-18. Pervaporation (permeability and selectivity) results **(a)** single component pervaporation of MCM-48 membrane, **(b)** single component pervaporation of silyl-

MCM-48 membrane, **(c)** 5 wt % mixture pervaporation of MCM-48 membrane, and **(d)** 5 wt % mixture pervaporation of silyl-MCM-48 membrane. 41

Figure 2-19. Pervaporation (permeance and selectivity) results from **(a)** single component pervaporation using the MCM-48 membrane, **(b)** single component pervaporation using the silyl-MCM-48 membrane, **(c)** 5 wt % mixture pervaporation using the MCM-48 membrane, and **(d)** 5 wt % mixture pervaporation using the silyl-MCM-48 membrane. 42

Figure 3-1. Illustration of mounted XRD sample. 49

Figure 3-2. Illustration of gas permeation module. 51

Figure 3-3. Illustration of pervaporation module. 51

Figure 3-4. Mesoporous silica/Torlon® hollow fiber membrane fabrication. 52

Figure 3-5. (a) Cross-section SEM image, and **(b)** low-angle XRD pattern of MCM-48 coated on Ultem® film. The XRD peaks are indexed as (210), (220), (332)/(422), and (440) of continuous cubic *Ia*3*d* structure. 53

Figure 3-6. Surface and cross-section SEM images of **(a),(b)** bare Torlon® hollow fiber supports; **(c),(d)** mesoporous silica/Torlon® hollow fiber membranes; and **(e),(f)** remaining silica layers after dissolving out the Torlon® supports, respectively. The mesoporous silica layer in **(e)** is free-standing, whereas the layer in **(f)** is adhered to an epoxy resin which was used to mount the fiber before polymer dissolution. 54

Figure 3-7. Cross-section SEM images of the mesoporous silica/Torlon® hollow fiber membrane after surfactant extraction. 56

Figure 3-8. Cross-section SEM image of the remaining silica layer after dissolving out the Torlon® support. The membrane was mounted in an epoxy resin before

dissolution of the Torlon® polymer. 56

Figure 3-9. EDS line scanning analysis of the mesoporous silica/Torlon® hollow fiber membrane..... 57

Figure 3-10. Pure-component gas permeation properties of mesoporous silica/Torlon® hollow fiber membranes at 308 K..... 59

Figure 3-11. SEM images of **(a)** top view and **(b)** cross section of evacuated mesoporous silica/Torlon® hollow fiber membranes; and **(c)** top view **(d)** cross section of HMDS-silylated mesoporous silica/Torlon® hollow fiber membranes. 61

Figure 3-12. N_2 and CO_2 single gas permeation results for (top) template extracted, (middle) evacuated, and (bottom) silylated mesoporous silica/Torlon® hollow fiber membranes. 63

Figure 3-13. N_2 and CO_2 single gas permeation results for (top) silica-free Torlon® hollow fiber, and (bottom) the silylated Torlon® hollow fiber..... 63

Figure 3-14. (a) Line scanning analysis of energy-dispersive X-ray spectroscopy (EDS) for the silylated Torlon® hollow fiber membrane, and **(b)** anticipated silylated Torlon® structure. 64

Figure 3-15. Line scanning analysis of energy-dispersive X-ray spectroscopy (EDS) for the Torlon® hollow fiber membrane. 66

Figure 3-16. XRD patterns of **(a)** template-extracted, **(b)** evacuated, and **(c)** silylated mesoporous membranes..... 67

Figure 3-17. TEM images of the **(a)** template-extracted, **(b)** evacuated, and **(c)** silylated mesoporous membrane layers after dissolution of the Torlon® fiber..... 69

Figure 3-18. TEM analysis (height, width) for the extracted mesoporous silica/Torlon®

hollow fiber membrane. 70

Figure 3-19. TEM analysis (height, width) for the evacuated mesoporous silica/Torlon® hollow fiber membrane. 71

Figure 3-20. TEM analysis (height, width) for the silylated mesoporous silica/Torlon® hollow fiber membrane. 72

Figure 3-21. Illustration of mounted FT-ATR/IR sample. 73

Figure 3-22. FT-ATR/IR absorption spectra of mesoporous silica/Torlon® hollow fiber membranes. The background spectrum is from the PS plate. 74

Figure 3-23. Pervaporation data (flux and organic/water separation factor) at 303 K and 323 K with 5 wt % organic/water feeds for **(a)** evacuated mesoporous membrane, and **(b)** silylated mesoporous membrane. Pervaporation data (permeance and water/organic selectivity) with 5 wt% organics/water feed mixtures for **(c)** evacuated mesoporous membrane, and **(d)** silylated mesoporous membrane. 75

Figure 3-24. Pervaporation (permeability and selectivity) data with 5 wt % organics/water feed mixtures for **(a)** evacuated mesoporous membrane before silylation, and **(b)** silylated mesoporous membrane. 76

Figure 3-25. Pervaporation data with 5 wt % organics/water feed mixtures for extracted mesoporous membrane **(a)** flux and separation factor, **(b)** permeance and selectivity, and **(c)** permeability and selectivity. 77

Figure 4-1. Schematic diagram of the experimental setup for permeation measurements. 91

Figure 4-2. Cross-sectional SEM images of aziridine functionalized membranes **(a)** without evacuation, and **(b)** with evacuation. 92

Figure 4-3. Top-view SEM images of aziridine functionalized membranes **(a)** without evacuation, and **(b)** with evacuation. 93

Figure 4-4. Cyclic dry gas permeation of CO_2 → N_2 → CO_2 → N_2 at 308 K for aziridine functionalized mesoporous silica/Torlon® hollow fiber membranes synthesized **(a)** without evacuation, and **(b)** after evacuation. 95

Figure 4-5. Cyclic dry gas permeation CO_2 → N_2 → CO_2 → N_2 for aziridine functionalized mesoporous silica/Torlon® hollow fiber membranes without evacuation at 308 K. 96

Figure 4-6. Cyclic dry gas permeation CO_2 → N_2 → CO_2 → N_2 for aziridine functionalized mesoporous silica/Torlon® hollow fiber membranes after evacuation at 308 K. 97

Figure 4-7. Mechanisms of CO_2 adsorption to the pairs of **(a)** primary-primary, **(b)** primary-secondary, and **(c)** secondary-secondary amines. 99

Figure 4-8. Mechanism of CO_2 gas adsorption through crosslinking (leading to reverse selectivity) by aziridine functionalized membrane. 100

Figure 4-9. Wet gas permeation of N_2 and CO_2 at 308 K for aziridine functionalized mesoporous silica/Torlon® hollow fiber membranes synthesized **(a)** without evacuation, and **(b)** after evacuation. 101

Figure 4-10. Surface reaction of tethered amine groups with CO_2. 102

Figure 5-1. Structures of mesoporous M41S materials: **(a)** MCM-41 (2D hexagonal, space group *p6mm*), **(b)** MCM-48 (cubic, space group *Ia3d*), and **(c)** MCM-50 (lamellar, space group *p2*) [45]. 109

Figure 5-2. Hydrophilic membranes used to remove water from a chemical or mixture of

chemicals. 111

SUMMARY

The main theme of this dissertation is the fabrication and analysis of modified mesoporous silica membranes for separation applications. Synthesis methods for mesoporous silica membranes have been developed to enhance the transport performance and quality of the membranes, such as permeability, pore volume, and surface area. Then, synthesized membranes were modified with different organic groups to tailor selectivity in separations. The collected studies of modified mesoporous silica membranes showed that appropriate functionalization on newly synthesized novel membranes leads to promising structural and permeation properties.

First, a seeded growth method was developed for synthesis of MCM-48 membranes on α-alumina supports, thereby extending the seeded growth technique used for zeolite membranes to mesoporous silica membrane synthesis. The surface properties of the MCM-48 membranes were then modified by silylation with hexamethyldisilazane (HMDS). In comparison to MCM-48 membranes previously synthesized by the *in situ* growth technique, much less silica infiltration into the alumina support was observed. The pore structure of the MCM-48 membranes demonstrated that a large accessible pore volume was available for molecular permeation and pore modification to tailor selectivity. The gas permeation properties of the calcined and silylated MCM-48 membranes were consistent with a Knudsen-like mechanism, albeit with a substantial influence of gas-solid interactions in the mesopores. The silylated MCM-48 membranes were evaluated for pervaporative separation of ethanol (EtOH), methyl ethyl ketone (MEK), and ethyl

acetate (EA) from their dilute aqueous solutions. The synthesized membranes exhibited high pervaporative separation factors and organic fluxes. The selective separation of organic/water mixtures with MCM-48 membranes were attributed to both the organophilic nature of the surface and the effective pore size of the silylated mesopores.

Next, the synthesis and organic/water separation properties of mesoporous silica membranes supported on low-cost and scalable polymeric (polyamide-imide) hollow fibers and modified by trimethylsilylation with HMDS was studied. Thin (1.6 μm), defect-free membranes that exhibited high gas permeances consistent with Knudsen-like diffusion through the mesopores were prepared. Silylation of these membranes did not affect the integrity of the mesoporous silica structure and the underlying polymeric hollow fiber, but led to capping of the surface silanol groups in the mesopores with trimethylsilyl groups. The silylated mesoporous membranes were evaluated for pervaporative separation of EtOH, MEK, EA, *iso*-butanol, and *n*-butanol from their dilute aqueous solutions. The membranes showed higher separation factors than those of flat membranes, along with high organic fluxes. The large increase in hydrophobicity of the membranes upon silylation allowed upgrading of the feed mixtures to permeate streams with considerably higher organic content. The selective separation of organic/water mixtures with the fiber-supported mesoporous silica membranes was attributed to both the organophilic nature of the surface (yielding good adsorption selectivity) and the effective pore size of the silylated mesopores (giving good fluxes). Comparison with other types of organic/water separation membranes revealed that the present silylated membrane platform shows good promise for use in organic/water separation applications

due to its high flux, scalable and low-cost fabrication methodology, and good separation factors that can be further enhanced by tailoring the mesopore modification chemistry.

Further, the gas transport properties of aziridine-functionalized mesoporous silica membranes on polymeric hollow fibers have also investigated. The mesoporous membranes were amine-functionalized with aziridine and their transport properties were studied to understand the effects of surface functionalization on gas separations. This new hybrid aminosilica membrane showed interesting and counter-intuitive N_2 selective permeation properties in dry CO_2/N_2 separations. Detailed characterization of the membrane structure and its permeation behavior showed that such behavior was due to the strong adsorption of CO_2, leading to reduced gas flux because of CO_2-induced amine crosslinking in the mesopores. This hyper-branched aminosilica membrane showed CO_2 selective properties when applied to humid gas permeation. Water molecules in the humid gas affected the adsorption of CO_2 molecules by causing a lower degree of crosslinking, allowing facilitated transport of CO_2.

CHAPTER 1

INTRODUCTION

1.1 Mesoporous Molecular Sieves

Mesoporous inorganic molecular sieves are good candidates as adsorbents or membrane materials for molecular separations due to their large specific surface areas, high pore volumes, and tunable pore sizes [1-4]. Among several types of mesoporous inorganic molecular sieves, mesoporous silicas have uniform pore structure and a high density of silanol groups [5, 6]. They are very promising candidate materials for both gas and liquid separations [7, 8]. M41S was the first ordered mesoporous silica material to be reported [2]. Their emerging applications in catalysis, adsorption, CO_2 capture, and separation have boosted the development of many other ordered mesoporous silica materials such as the families of SBA-n [9, 10], Fudan University Material (FDU) [11], Korea Advanced Institute of Science and Technology (KIT) [12], and anionic-surfactant-templated mesoporous silica (AMS) [13]. Figure 1-1 shows the schematic structure for several mesoporous materials [14-16]. Mesoporous materials are formed by a micelle-templating process (Figure 1-2), either following an electrostatically driven cooperative assembly pathway or the nonionic route in the presence of uncharged surfactants as structure directing agents [17]. There are numerous studies on the adsorption uptake of acid gases such as CO_2 by mesoporous silica molecular sieves [17-20]. It has been found that mesoporous silicas such as SBA-15, MCM-41, and MCM-48 are good adsorbents for CO_2, offering good selectivity over other gases like CH_4 and N_2 [19, 21-23]. Furthermore, modification of the molecular sieve with organic groups can further increase the sorption capacity of such materials [24, 25].

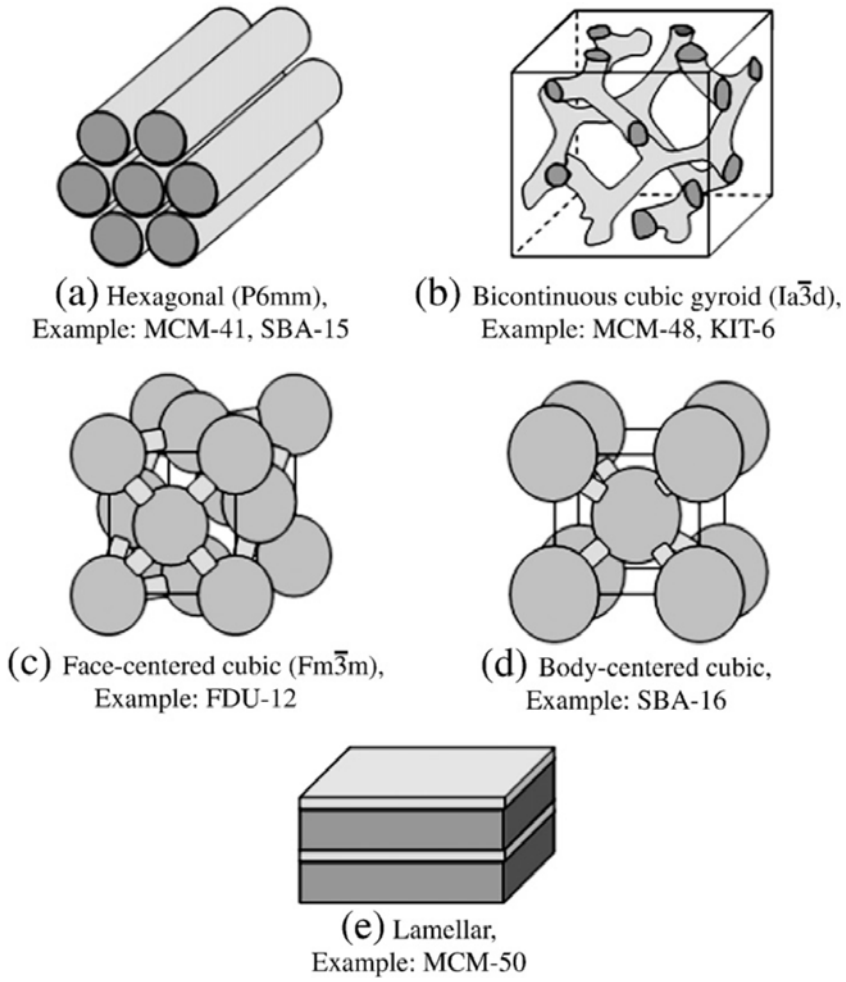

Figure 1-1. Structure of ordered mesoporous materials [14-16].

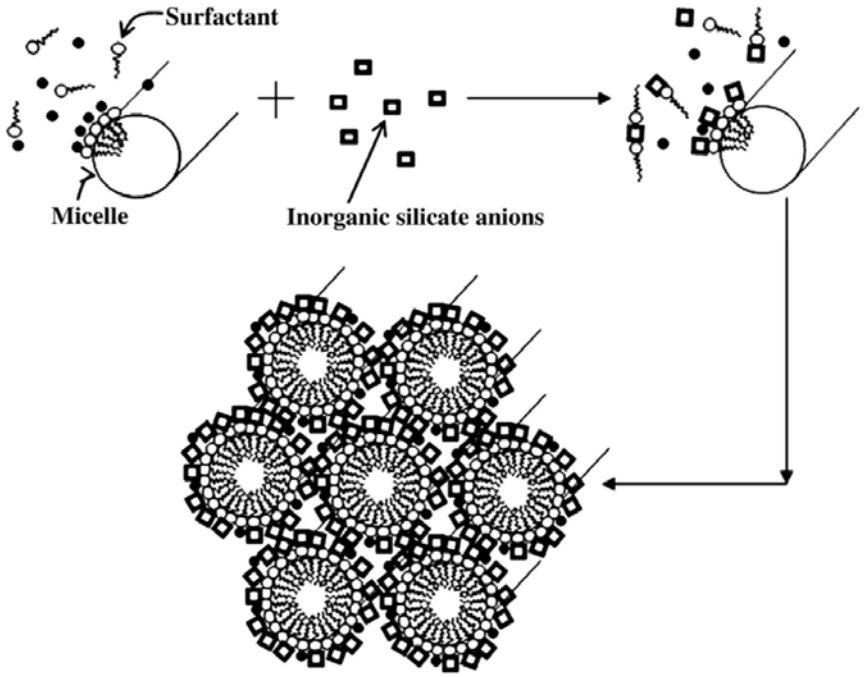

Figure 1-2. Mechanism for the synthesis of mesoporous silica under basic conditions in the presence of a cationic surfactant [17].

1.2 Mesoporous Silica Membranes

Mesoporous silica molecular sieves can be modified to tailor good selective properties, as discussed in the previous section. Adapting mesoporous silica molecular sieve powders into a membrane configuration while preserving their adsorptive properties presents an attractive but challenging possibility for developing new and novel separation processes [26, 27]. For instance, mesoporous silica in a membrane configuration allows the separation to be operated under steady state conditions wherein selective adsorption occurs on the feed side, followed by selective diffusion across the membrane, and continuous desorption occurs on the permeate side [28, 29]. In such a process, the molecules are chemisorbed on one side of the membrane (in the pore), diffuse through

the pores of the membrane and then desorb from the other side of the membrane [17, 30]. Thus, mesoporous materials in the form of a self-supporting membrane (symmetric membranes) or a thin film on a support (asymmetric membranes) could offer a number of advantages in many emerging applications [31, 32]. The membrane acts as a barrier to the mass transfer between phases to separate the phases under a driving force [7, 33]. In past work, a thin layer of a mesoporous silica membrane has been grown on a ceramic support to increase the mechanical stability of the membrane [34, 35].

1.3 Modification of Mesoporous Silica Membranes

The typical pore sizes (2-50 nm) of mesoporous silica membranes preclude direct application in separations involving small molecules [28, 36]. Thus, to increase selectivity or separation factors, further modification of silanol groups on the pore surface is necessary [29]. The surface chemistry of mesoporous silica can be effectively modified by chemical attachment of organic species. The most commonly applied method to functionalize mesoporous silica membranes is the one-pot co-condensation synthesis. However, some studies employing post-synthesis grafting have also been reported [37-41]. Post-synthesis grafting presents the following advantages as compared to the co-condensation route [37, 42]:

1. Treatment at high temperatures prior to functionalization results in a highly condensed inorganic framework and increases the stability of membranes.
2. The functionalization takes place only on pore surfaces.
3. No phase transition can happen with the incorporation of the organics, implying a conservation of the initial mesophase.

On the other hand, it has been recently shown that mesoporous silica powder materials (such as MCM or SBA materials) can be amine-functionalized to yield a high concentration of amine groups inside the pores [43]. This in turns leads to an unusually high CO_2 sorption capacity [43]. Similar results may be expected for H_2S sorption. Meanwhile, the surface modification of mesoporous silica powders by silylation is an effective technique in tailoring selective adsorbents for the removal of organic compounds from streams or wastewater [44]. Those silylated mesoporous silicas have been found superior to the non-silylated silica in terms of increasing the hydrophobicity of the inorganic/organic hybrid material [45].

The functionalization and gas permeation properties of various mesoporous silica membranes reported in literature are given in Table 1-1. Also, Figures 1-3 present schemes showing the modification chemistry in those cases. Sakamoto *et al*. achieved surface modification of MCM-48 pores with 3-aminopropyltrimethoxysilane [46]. The N_2 permeance across the membrane dropped significantly after the modification, suggesting pore filling of the MCM-48 membrane with amino groups. Kumar *et al*. modified the surface of an MCM-48 membrane with polyethyleneimine (PEI) containing primary, secondary, and tertiary amino groups [47]. A large drop in the N_2 permeance values was observed after PEI attachment, suggesting decreased pore sizes and volumes for the PEI-modified MCM-48 membranes as compared to the original MCM-48 membranes. Park *et al*. post-functionalized MCM-48 membranes with trimethylchlorosilane to enhance the hydrothermal stability and hydrophobicity [48]. The silylated MCM-48 membranes were used for the separation of organics in an aqueous solution. McCool and DeSisto [49] functionalized ordered mesoporous silica membranes with aminopropyl triethoxysilane to

form microporous organic-inorganic hybrid membranes for facilitated CO_2 transport. Park *et al*. modified MCM-48 membranes with trimethylchlorosilane or triethylchlorosilane to enhance hydrophobicity of membranes [50]. Higgins *et al*. recently reported alkyl modification of mesoporous silica membranes by covalent attachment of octadecyldimethylchlorosilane using triethylamine as a catalyst in supercritical CO_2 [51].

Table 1-1. Properties of original and modified mesoporous silica membranes.

Membrane	Grafted organic group	N_2 gas permeance (GPU)		Separation application	Ref.
		Unmodified	Modified		
MCM-48	3-Aminopropyltriethoxysilane	420	0.02	Gas	[46]
MCM-48	Trimethylchlorosilane	-	150	Liquid	[48]
MCM-48	Triethylchlorosilane	180	-	Liquid	[50]
Mesoporous silica	Trimethylchlorosilane	180	-	Gas	[50]
Mesoporous silica	Octadecyldimethylchlorosilane	2400	270	Gas	[51]

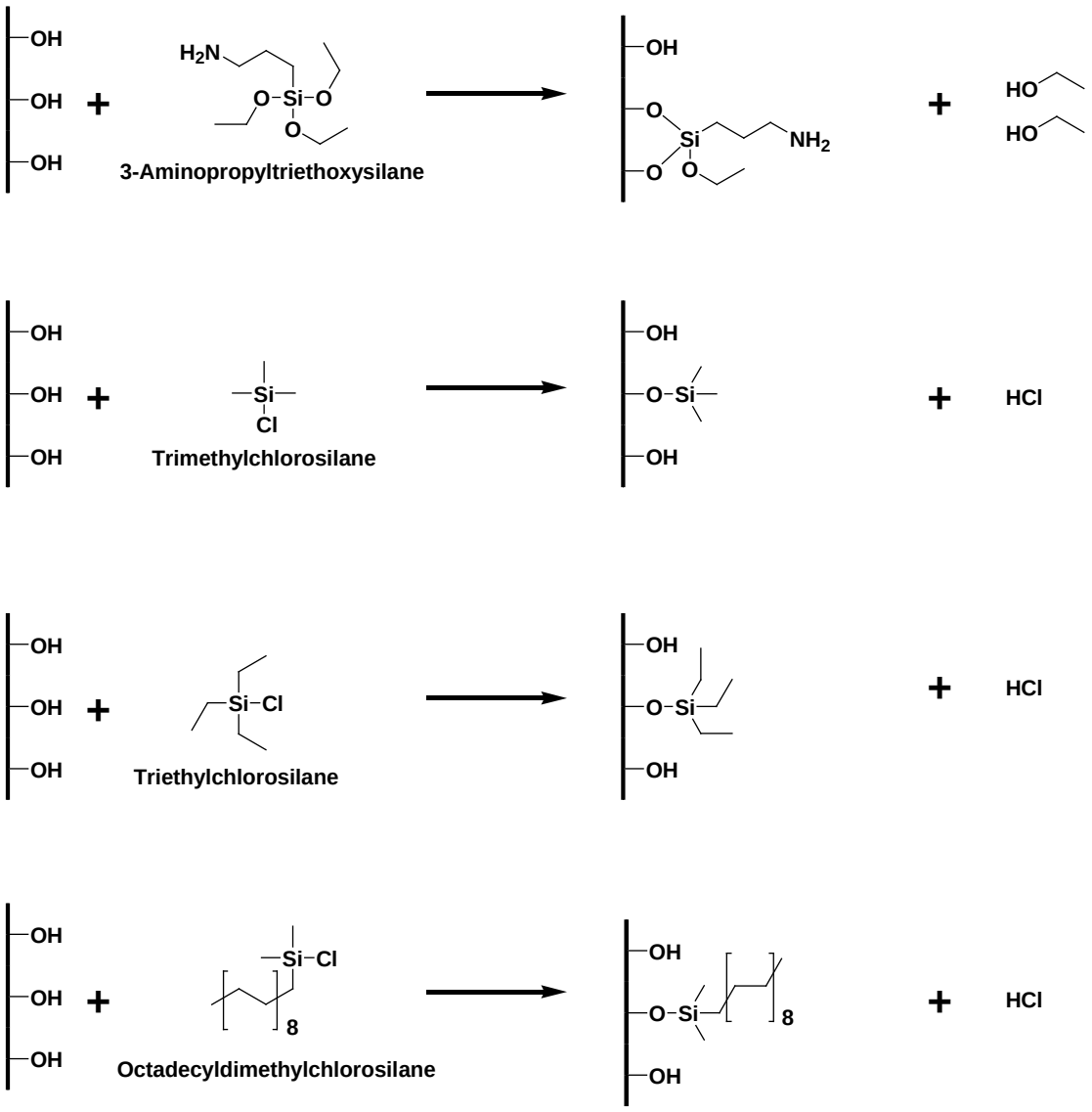

Figure 1-3. Scheme showing silica surface modification chemistry.

1.4 Fundamentals of Molecular Transport in Membranes

The permeability (P_A) of a molecule A in a membrane is given by:

$$P_A \equiv \frac{N_A l}{p_2 - p_1} \qquad (1)$$

where N_A is the steady-state flux of mixture through the membrane, l is the membrane thickness, and p_2 and p_1 are the upstream and downstream partial pressures of molecule A,

respectively. If the diffusion process obeys Fick's law, and the downstream pressure is much less than upstream pressure, the permeability is given by:

$$P_A = D_A S_A \qquad (2)$$

where D_A is the average effective diffusivity through the membrane, and S_A is the apparent sorption coefficient.

The ideal selectivity of a membrane for mixture A and B is hence the ratio of their permeabilities given by the equation:

$$\alpha_{A/B} = \frac{P_A}{P_B} = \left[\frac{D_A}{D_B}\right]\left[\frac{S_A}{S_B}\right] \qquad (3)$$

where D_A/D_B is the diffusivity selectivity, i.e. the ratio of the diffusion coefficients of molecules A and B. The ratio of the solubilities of molecules A and B, S_A/S_B, is the solubility selectivity. Diffusivity selectivity is strongly influenced by the size difference between the penetrant molecules and the size-sieving ability of the membrane material, whereas solubility selectivity is controlled by the relative adsorption/thermodynamic affinity between the penetrants and the membrane matrix [52].

1.5 Overall Objectives and Strategy

This thesis is focused on the fabrication of defect-free pore-modified mesoporous membranes and their applications in organic/water or CO_2/N_2 separations. The fabricated mesoporous silica membranes reported in the literature so far had cracks or pore collapse, and a low degree of pore activation. Even worse, the membrane characterization in many of those works was limited to silica powders, and properties of silica powder (pore structure and compositions) were regarded as properties of membranes. Thus, the present work is aimed at yield a more detailed understanding of adsorption and transport

phenomena by creating membranes using novel synthesis methods and new characterizations of obtained mesoporous silica membranes for their application in separation technologies. In chapter 2, the fabrication of defect-free MCM-48 membranes on α-alumina disks via seed layer deposition is described. The fabricated MCM-48 membranes have low silica infiltration into the support and high surface area and pore volume compared to unseeded MCM-48 membranes. In this study, the pore structure and compositions are thoroughly investigated by direct XRD, N_2 physisorption, FTIR-ATR/IR spectroscope, and gas permeation tests. Finally, the obtained membranes are successfully trimethylsilylated with hexamethyldisilazane to tailor the selectivity properties of the membrane and applied to organic/water separations. In chapter 3, the fabrication method of worm-like mesoporous silica membranes on polymeric hollow fiber supports has been developed, thereby suggesting a technologically scalable platform for separations. The silylation conditions were modified to tune the selective properties of the worm-like mesoporous silica membrane. Thus, it has hydrophobicity and can be used as a organic/water separation membrane. Meanwhile, the structural properties of these unmodified/modified membranes were thoroughly investigated. In chapter 4, to understand the effects of surface fucntionalization on gas separations, a study whereby aziridine was incorporated into the worm-like mesoporous silica membranes, forming hyper-branched amino-silica membranes, is described. The surface properties of the inorganic membrane were successfully tuned by modification, and detailed analysis of the permeation behavior elucidated CO_2 selective properties and counter-intuitive N_2 selectivity. Chapter 5 summarizes the work and discusses suggested future directions to engineer mesoporous materials for application in organic/water or gas separations.

Overall, the work described in this dissertation takes a significant step forward in the synthesis, characterization, and processing of functionalized mesoporous silica membranes that can be used in molecular transport and separation applications.

CHAPTER 2

SEEDED GROWTH, SILYLATION, AND ORGANIC/WATER SEPARATION PROPERTIES OF MCM-48 MEMBRANES

2.1 Introduction

Membrane-based separations continue to attract great interest for a number of applications [53, 54] because of their lower energy consumption, potentially low fabrication cost, and steady-state operation. Polymeric membranes are currently the predominant class of membranes in commercial applications, due to their easy processibility in large-scale fabrication processes. However, they also have intrinsic limitations on their performance due to a trade-off between their permeability and selectivity [55, 56], and issues with stability under harsh conditions [57]. Over the last two decades, inorganic membranes have been shown to possess high permeability, selectivity, and thermal and chemical resistance [58-60]. However, their applications have been somewhat limited by the difficulty of fabrication of continuous inorganic membrane structures on technologically scalable, low-cost platforms.

Ordered mesoporous silica materials, such as MCM-41/48 [5, 61] and SBA-15/16 [4, 46] are prepared by surfactant templating methods and have uniform pore channels with a diameter ranging from 2 to 10 nm. The mesopores allow rapid permeation by gases, but also can be modified with functional groups for specific purposes [62-70]. These materials are also thermally and chemically stable under non-steaming conditions. The above properties allow mesoporous silica materials to be useful host materials for a variety of separations. For example, mesoporous silica materials are

tunable for separation of small gas molecules as well as larger pharmaceutical or biological molecules [17, 32, 46, 71-76]. Among a number of mesoporous silica materials available, the M41S family of ordered mesoporous molecular sieves has been continuously developed since 1992 [2, 5]. The most common materials have uniform hexagonal (MCM-41), cubic (MCM-48), and lamellar (MCM-50) structures. MCM-48 is an attractive material to fabricate membranes for separations, because it yields a 3-D interconnected pore structure after surfactant removal. There are recent reports of the synthesis of MCM-48 membranes using *in situ* hydrothermal methods on ceramic substrates [17, 32, 46, 61, 77, 78]. However, the synthesis of defect-free MCM-48 membranes on these substrates has been challenging due to the presence of cracks and pinholes formed during synthesis and surfactant removal. The physical properties of the MCM-48 membranes reported so far in the literature have only been defined to a limited extent. Indeed, in most publications, the material characterization has mainly focused on MCM-48 powders and not the MCM-48 membranes themselves [31, 32, 79, 80].

The seeded synthesis approach for preparation of inorganic membranes was originally developed for the synthesis of continuous, low-defect-density zeolite membranes [81-83]. In this chapter, I extend this method (also known as 'secondary growth') to the synthesis of continuous, defect-free mesoporous silica (specifically, MCM-48) membranes on α-alumina disks as supports. The porosity of the membranes is activated by two different surfactant removal methods: calcination and solvent extraction. The structural and permeation properties of the resulting MCM-48 membranes are characterized in detail. The asymmetric MCM-48 membranes are shown to be continuous, defect-free, and have high gas flux.

To alter their adsorption and transport properties, the mesopores of the membranes are modified by post-synthesis silylation, thereby enhancing the organophilicity and hydrophobicity of the mesopore surfaces. Given that silylated MCM-48 membranes made by *in situ* growth can be used to selectively separate organics from aqueous mixtures [48], the new seeded-growth membranes are evaluated in the separation of model organic/water mixtures, in both silylated and non-silylated forms.

2.2 Experimental Section

2.2.1 Synthesis of MCM-48 seed particles

Cetyltrimethylammonium bromide (CTAB) template (2.4 g, 6.6 mmoles) was dissolved in deionized water (50 ml) and ethanol (EtOH) (50 ml, 0.87 moles) was added to the surfactant solution. After 10 min of stirring, aqueous ammonia (13.7 ml, 28 wt %, 0.20 moles) was added. The solution was stirred for another 10 min and tetraethyl orthosilicate (TEOS) (3.4 g, 98 %, 16 mmoles) was added. The molar composition of the gel was TEOS/12.5 NH_3/54 EtOH/0.4 template/174 H_2O. After stirring for 2 hours at room temperature, the resulting solid was recovered by centrifugation, washed with deionized water and dried in air at 333 K. The template was removed by calcination at 823 K for 6 hours in stagnant air [84].

2.2.2 MCM-48 seed layer deposition

To prepare a mesoporous silica suspension, 0.02 g of MCM-48 powder was mixed with 5 ml of *sec*-butanol and then vigorously stirred in a vial at room temperature for more than 6 days before use [85]. The concentration of the solids was 4 g/L. Large

pore α-alumina disks (Coorstek) of 1" diameter, 1 mm thickness, and 25 % porosity were used as supports for MCM-48 membrane preparation. To deposit the seed layer, 300 µl of the prepared suspension was spin-coated on the substrate at 5,000 rpm for 1 min. After coating, the seeded substrate was stored in an oven at 333 K for annealing.

2.2.3 Synthesis and TEOS treatment of MCM-48 membranes

The MCM-48 membrane was prepared as follows: sodium hydroxide was dissolved in deionized water for 10 min, and CTAB, the structure-directing agent (SDA), was also dissolved in that solution. After 1 hour of stirring, TEOS was added dropwise to the solution under constant stirring. The molar composition of the mixture was SiO_2: 0.425 CTAB: 0.525 NaOH: 62 H_2O [31, 32, 80, 86, 87]. After the mixture was stirred for 2 hours, it was transferred to an autoclave and the seeded α-alumina disk was placed in the autoclave horizontally. After 3 days of autoclaving at 373 K, the membrane was removed and washed with deionized water [31]. It was subsequently treated with TEOS by the Vapor Infiltration (TEOS VI) method. The as-synthesized MCM-48 membrane was exposed to TEOS vapor in a closed vessel at 373 K for 24 hours [50, 61, 88, 89]. This procedure supplies additional silicon atoms to stabilize the MCM-48 framework.

2.2.4 Surfactant removal

Calcination and solvent extraction methods were applied to remove the surfactant from the pores of the mesoporous silica. In the calcination method, the as-synthesized sample was heat-treated at 773 K for 4 hours under air flow following a temperature ramp of 1 K/min. After 4 hours of calcination, the oven was cooled slowly to room

temperature. In the extraction method, MCM-48 membranes were extracted with a 1 M HCl/EtOH solution for 24 hours under constant stirring [79].

2.2.5 Silylation

Prior to silylation, the MCM-48 membrane was evacuated in a vacuum oven to remove physically adsorbed moisture at 373 K. Then, the MCM-48 membrane was exposed to hexamethyldisilazane (HMDS) vapor in a closed vessel at 373 K for 24 hours. The membrane was washed with deionized water after silylation.

2.2.6 Characterization methods

Scanning Electron Microscopy (SEM) images and energy dispersive X-ray spectroscopy (EDS) analysis were obtained on a JEOL LEO-1530 at a landing energy of 15 kV using the 'In Lens' mode detector. The powder and membrane samples were prepared on carbon tape and coated with gold to prevent surface charging effects. X-ray diffraction (XRD) patterns of the membranes were obtained using a PANalytical X'pert diffractometer using a Cu-K-alpha X-ray source, diffracted beam collimator, and a proportional detector. FT-ATR/IR (Attenuated total reflectance) spectra were obtained using a Bruker Vertex 80v Fourier Transform Infrared (FT-IR) spectrometer coupled to a Hyperion 2000 IR microscope at 20X magnification.

Nitrogen physisorption isotherms were measured using a specially designed adsorption vessel developed at UMassAmherst, that is capable of measuring adsorption and desorption isotherms on intact supported porous membranes [90, 91]. Samples were placed in the adsorption vessel as shown in Figure 2-1 [90], which uses a re-sealable

stainless steel container with sufficiently large diameter and depth to hold the membrane disks without having to be cut, delaminated or otherwise damaged. The container flanges are sealed with copper gaskets and evacuated using a turbomolecular pump. Samples were heated slowly over 4-5 hours to 573 K. Each sample was maintained at this temperature for 24 hours or more, and then cooled to room temperature over 5 hours. The sample cell was then cooled below 173 K slowly by placing the liquid nitrogen bath under the sample such that the sample was cooled by the air over the bath. The sample container was then immersed in the liquid nitrogen bath to its final temperature (77 K). This somewhat complex procedure enabled us to maintain vacuum integrity over the samples while the temperatures were lowered by more than 200 K. Adsorption and desorption isotherms were measured at 77 K using an apparatus that employs a volumetric dosing system and accurate low-pressure transducers with ranges of 0-1,000 torr and 0-2 torr on the adsorption manifold. Nitrogen was used as the adsorbate, while the dead space measurements were conducted using helium. Saturation pressures were determined by condensing or subliming the adsorbate in the sample container at the end of the experiment. All gases used in the experiments were ultra-high purity grade (AirGas Corporation). Membrane or support disks were stacked in the sample cell, spaced by glass beads. Multiple membranes were measured simultaneously in order to obtain sufficient surface area for accuracy of the measurement. The surface areas and micropore volumes of the membranes were determined using the BET equation, and then dividing by the number of membranes measured. The surface area contribution from the membrane was determined by subtraction of the weight of the bare support disks from the membrane-containing support disks.

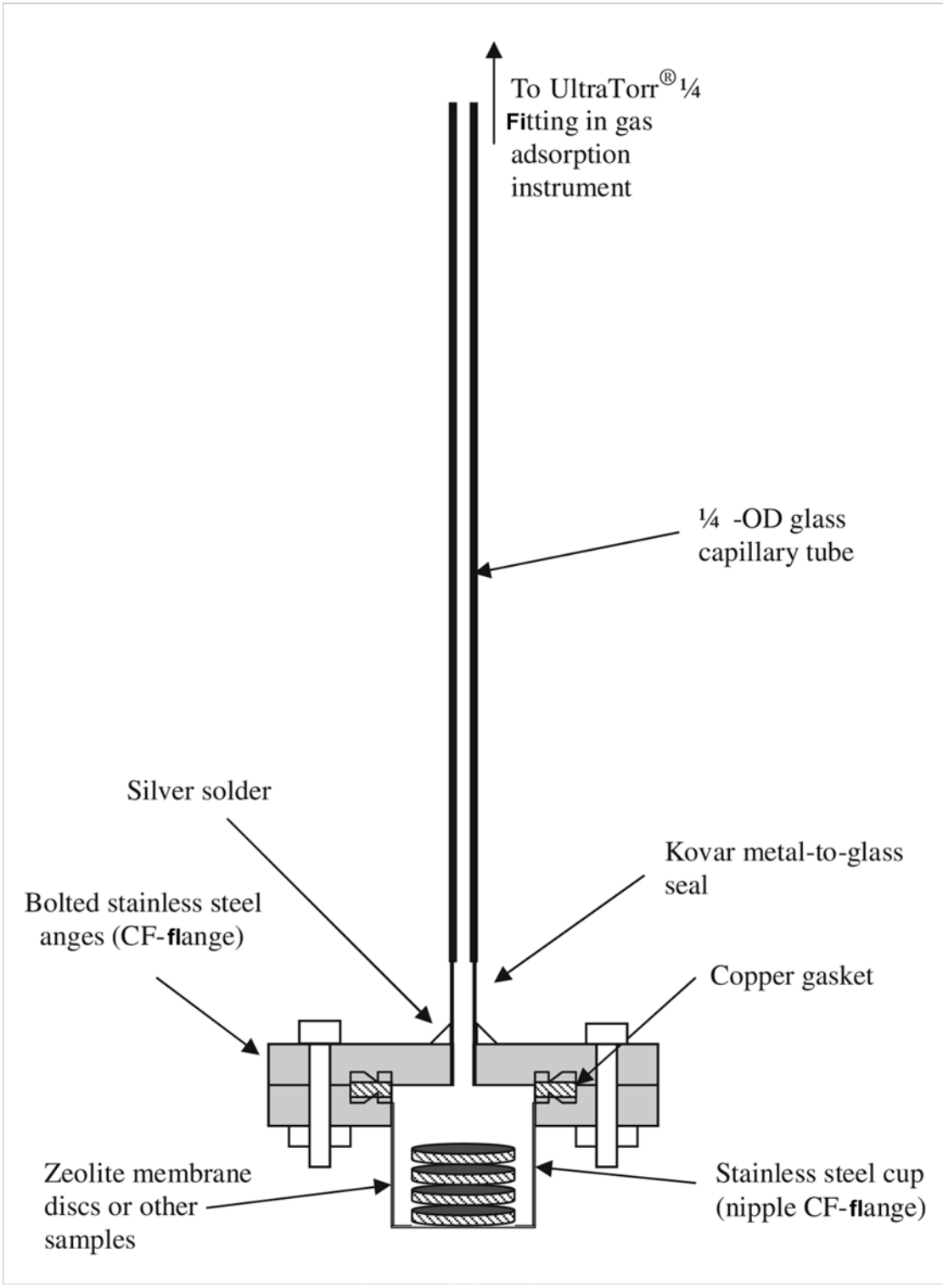

Figure 2-1. Diagram of flange-based membrane adsorption cell [90].

2.2.7 Gas permeation and pervaporation measurements

Single-gas permeation measurements were carried out using N_2, CO_2, CH_4, and SF_6 at 308 K with a custom-built unit. The schematic diagram of experimental setup for permeation measurements is shown in Figure 2-2. The feed side was maintained at 30 psi, and the permeate side was evacuated to 0.55 psi using a vacuum pump. The gas flux was measured by isolating the vacuum and recording the rate of pressure rise in a collection vessel of known volume on the permeate side. Pervaporation measurements were carried out with water, EtOH, methyl ethyl ketone (MEK), ethyl acetate (EA), and aqueous mixture of those organics at 303 K and 343 K using a custom-built unit (Figure 2-3). The permeate was collected in a liquid-N_2-cooled trap. The total flux was measured by the mass of permeate collected in a given measurement time, whereas the composition of the permeate was characterized by gas chromatography (GC). Membrane modules were prepared using epoxy as shown in Figure 2-4.

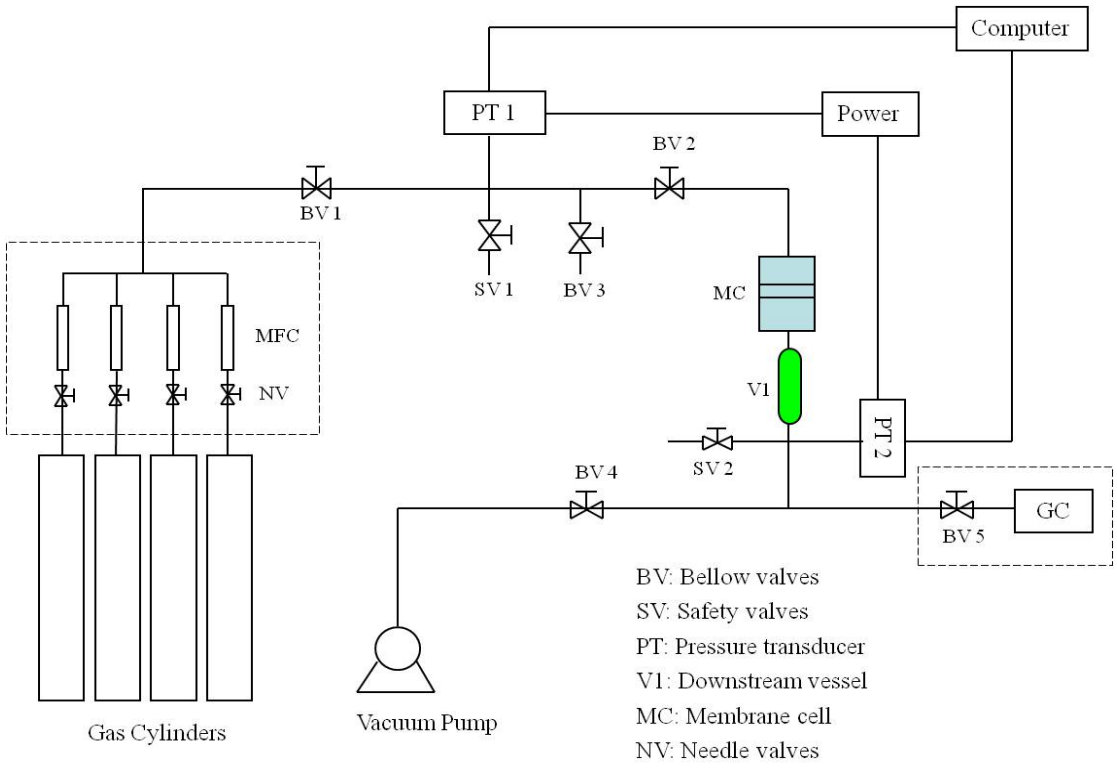

Figure 2-2. Schematic diagram of the experimental setup for permeation measurements [92].

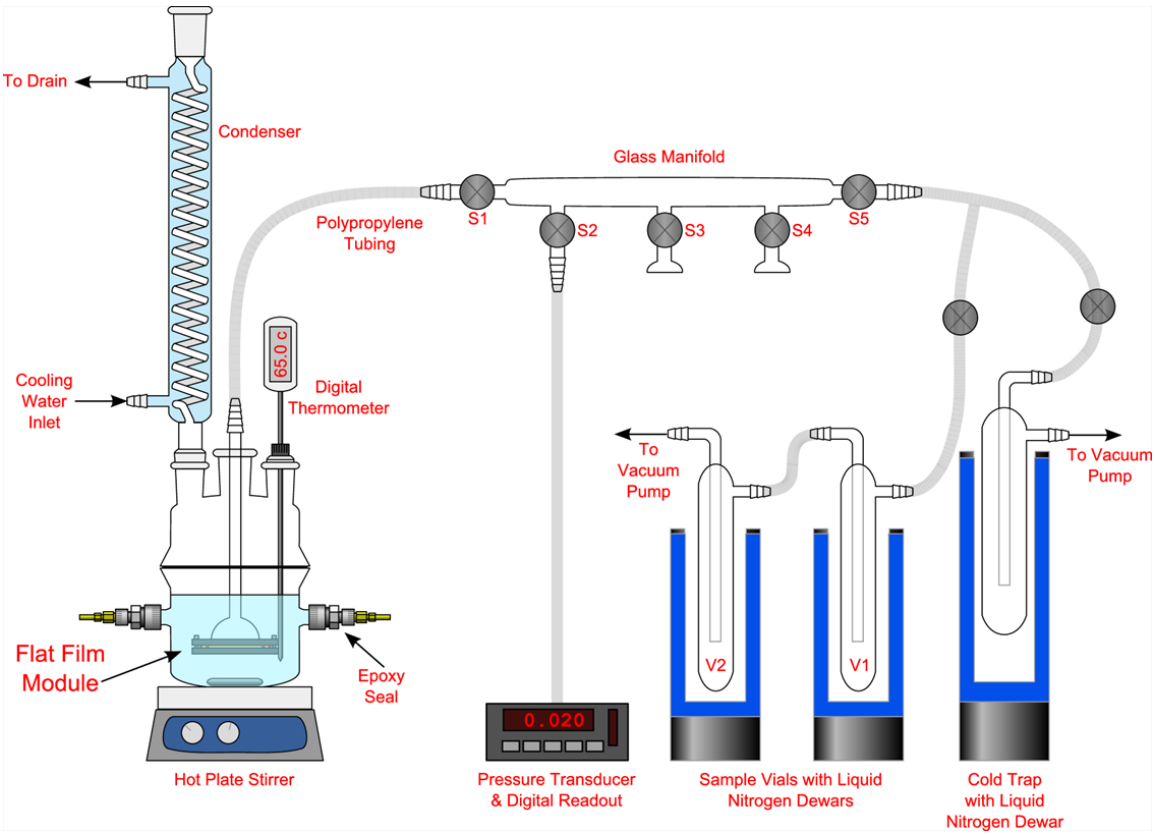

Figure 2-3. Schematic diagram of experimental setup for pervaporation measurements.

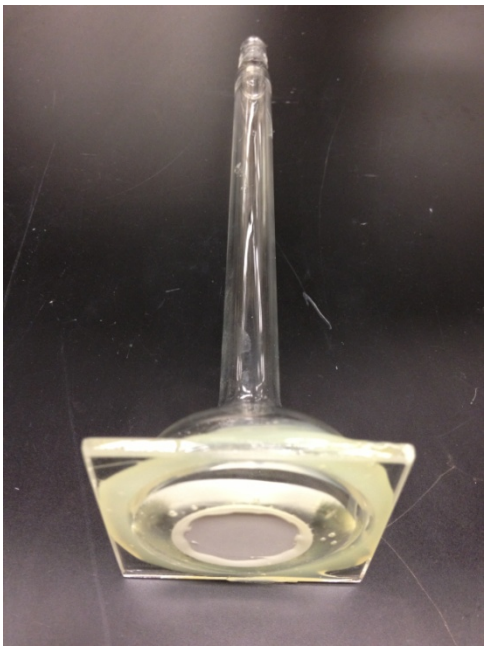

Figure 2-4. Illustration of disk membrane module for pervaporation experiments.

2.3 Results and Discussion

2.3.1 MCM-48 membrane synthesis by seeded growth

Figure 2-5(a) shows an SEM image of the synthesized MCM-48 seed particles. The particles are roughly spherical in shape and the size ranges from 300-500 nm, making them appropriate for use in seed layers. These particles have a surface area of ~1,200 m^2/g (C_{BET} = 100) as determined from nitrogen physisorption. The pore size distribution calculated from the physisorption isotherm by the BdB-FHH (Broekhoff–deBoer–Frenkel–Halsey–Hill) method [93] shows a narrow pore size distribution (PSD) centered on 2.8 nm (Figure 2-6). Figures 2-5(b) and 2-5(c) show SEM images of the bare α-alumina disk and the disk after MCM-48 seed deposition. The bare support has a non-homogeneous surface, and the use of *in situ* growth led to formation of relatively poor-quality MCM-48 membranes. After deposition of seeds by spin-coating, the surface was

uniformly covered by MCM-48 particles.

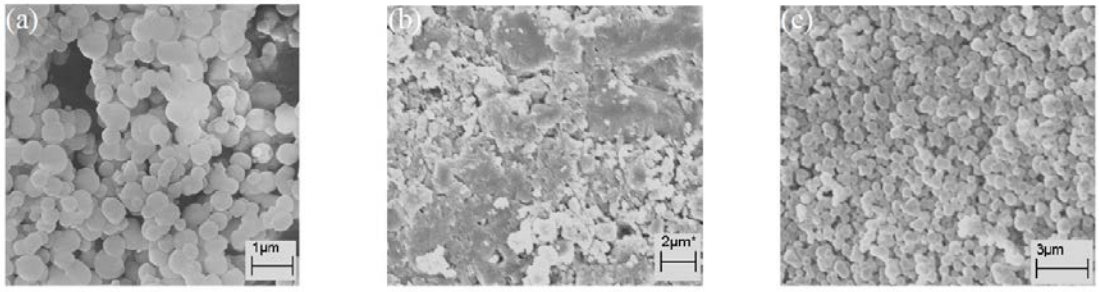

Figure 2-5. SEM images of **(a)** MCM-48 seed particles, **(b)** bare α-alumina disk, and **(c)** α-alumina disk seeded with MCM-48 particles.

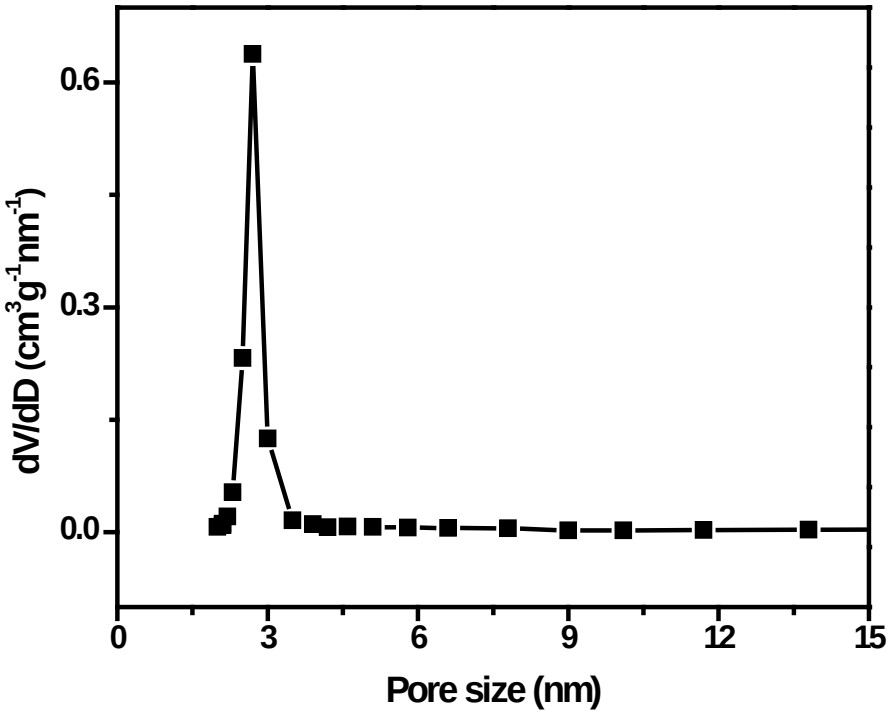

Figure 2-6. Pore size distributions of calcined MCM-48 seed particles.

Figure 2-7 shows SEM images of a representative MCM-48 membrane sample after each step of the synthesis. As shown in Figure 2-7(a), there are a large number of cracks in the top layer of the as-synthesized membranes, but these cracks are filled during the TEOS VI treatment as shown in Figure 2-7(b) [50, 61, 88, 89]. It is suggested that the TEOS VI step stabilizes the as-synthesized framework by providing reactive silicon species that complete the MCM-48 framework initially formed in the as-synthesized film. The densified silica wall of the TEOS VI-treated MCM-48 has a much higher structural stability. Surfactant removal was performed *via* two routes, calcination and liquid extraction. Many apparently large cracks were observed on the surface of calcined samples as shown in Figure 2-7(c), while relatively small cracks were found on the surface of extracted samples, as depicted in Figure 2-7(d). SEM imaging of the cross-sections of the films was also carried out (Figures 2-7(e) and 2-7(f)). The cross-sectional images reveal that the apparent cracks seen in the top views are only spaces between globular MCM-48 structures present on the top surface of the membrane, whereas a continuous and crack-free membrane layer exists below these surface structures. The membrane layer is seen to have a thickness of approximately 6 μm.

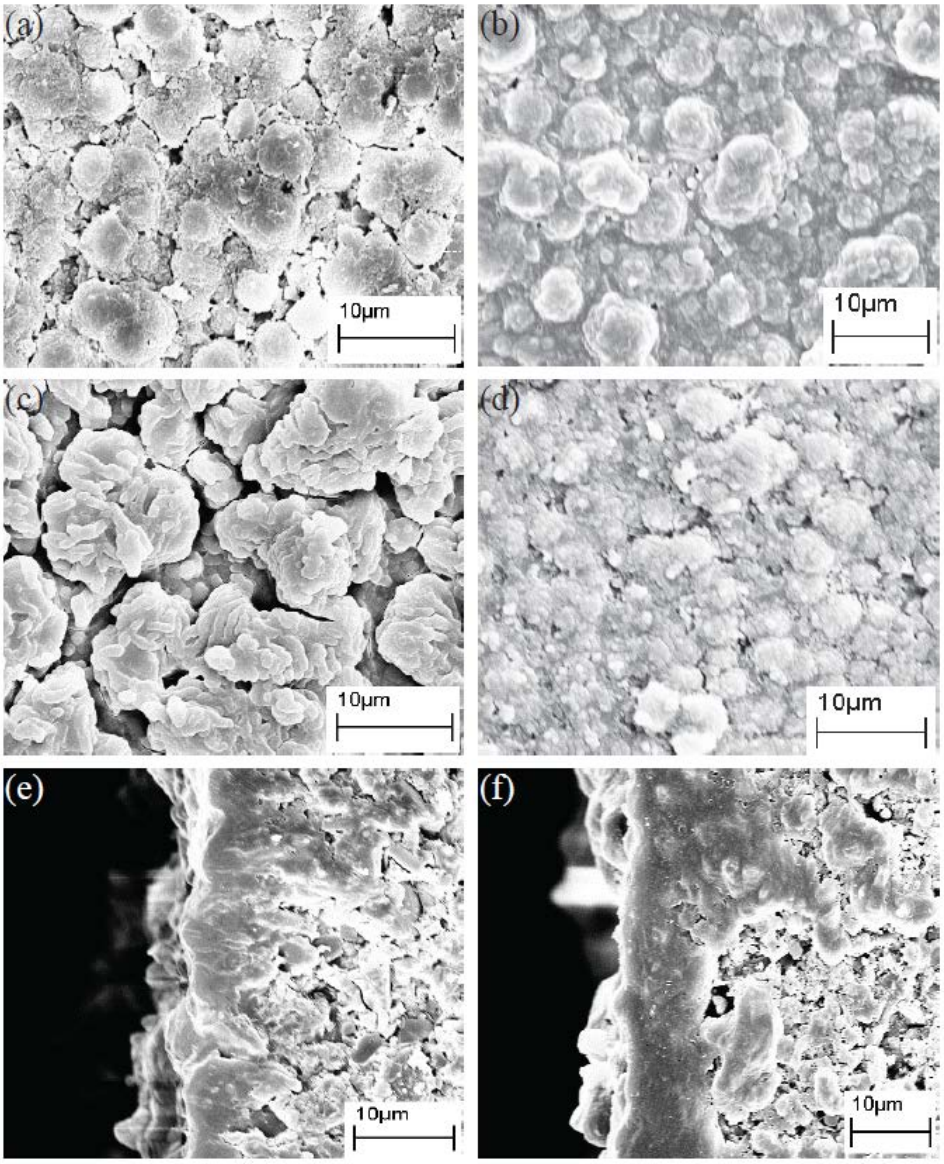

Figure 2-7. Top-view SEM images of MCM-48 membrane: **(a)** as-synthesized, **(b)** TEOS VI treated, **(c)** calcined, and **(d)** surfactant-extracted respectively; and cross-sectional SEM images of the **(e)** calcined and **(f)** surfactant-extracted membranes, respectively.

To investigate the distribution of silica in the membrane layer and the support layer, the cross-sectional Si and Al composition profile of the MCM-48 membrane was evaluated by EDS analysis (Figure 2-8). The Si composition profile shows a region of

~2.5 μm populated by the globular MCM-48 surface structures, followed by a ~6 μm continuous membrane. The transition region between the membrane and the support is about ~2.5 μm in thickness, beyond which a small amount of silica persists in the support over a distance of ~10 μm. However, there is overall a low degree of penetration of silica into the *α*-alumina support. This is likely due to the seed layer, which initially consumes silica reactants at the membrane surface and inhibits nucleation in the pores of the support, thereby largely confining the membrane growth to the top of the support. In contrast, MCM-48 membranes made by *in situ* methods show substantial penetration of silica into the support, up to about 500 μm [31, 32].

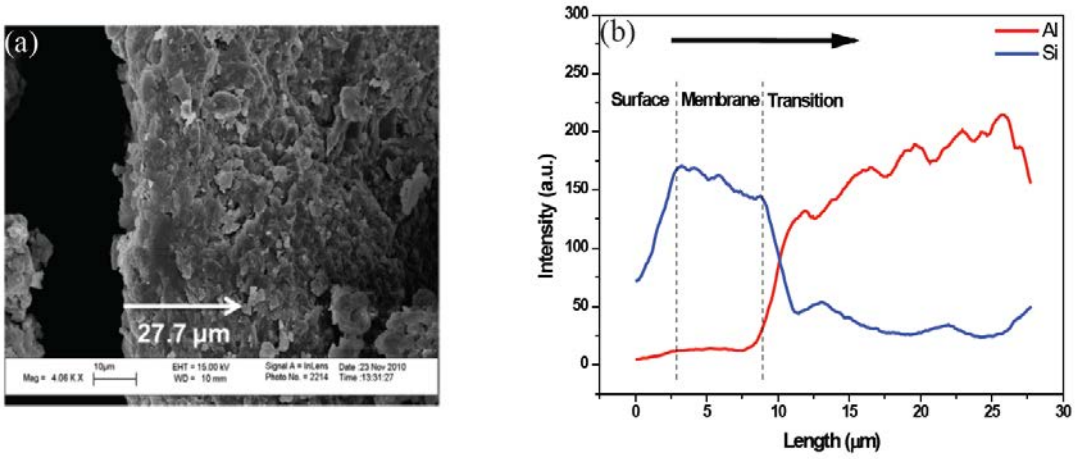

Figure 2-8. (a) Cross-sectional SEM image of MCM-48 membrane indicating the distance over which composition analysis was carried out, and **(b)** Al and Si EDS line scan profiles.

The XRD patterns of the seeded membranes before and after surfactant removal are shown in Figure 2-9. All the patterns have an intense (211) reflection with a less

intense (220) peak, corresponding to the cubic *Ia3d* symmetry of the MCM-48 pore structure [2]. After calcination at 773 K or surfactant extraction with a 1M HCl/EtOH solution, the XRD pattern shows that the MCM-48 structure is maintained. Comparing the as-synthesized membrane to the calcined or surfactant-extracted membranes, it is noteworthy that the peak positions are shifted to slightly higher angles (and therefore the *d*-spacings decrease slightly) upon surfactant removal. As the surfactant is removed, there is shrinkage of the structure.

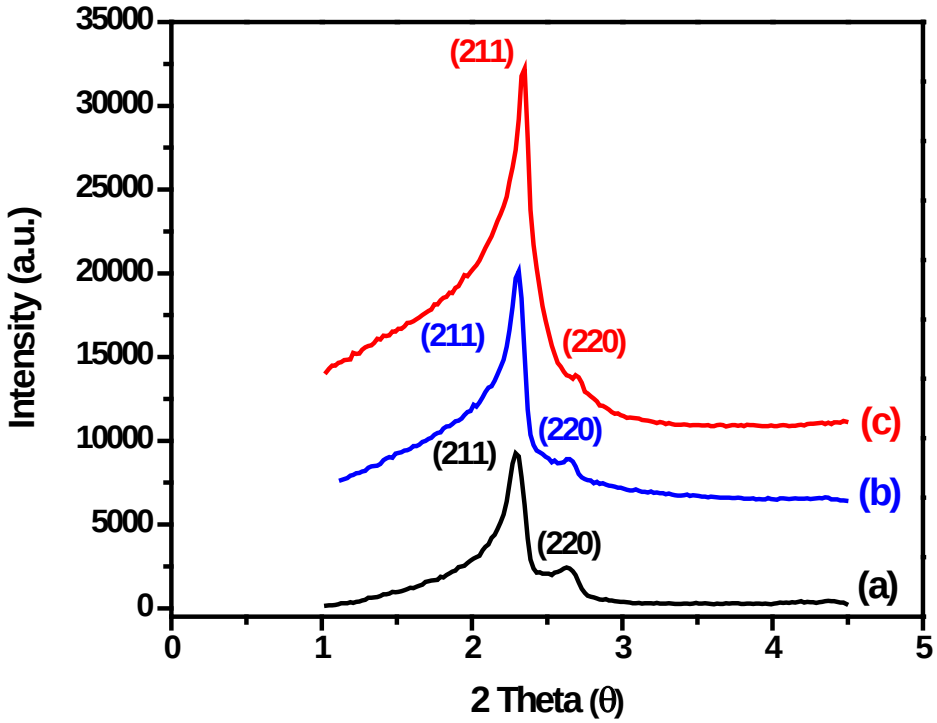

Figure 2-9. XRD patterns of the **(a)** as-synthesized, **(b)** surfactant-extracted, and **(c)** calcined MCM-48 membranes.

Figure 2-10 shows FT-ATR/IR absorption spectra of the MCM-48 membranes

before and after surfactant removal. The as-synthesized membrane shows two distinct bands in the 2850-2950 cm^{-1} region that are associated with the asymmetric and symmetric stretching vibrations of the $-CH_2-$ units of the surfactant aggregates. After extraction in 1 M HCl/EtOH solution for 12 hours, the intensity of the two CH_2-stretching bands significantly decreased, which implies that some of the surfactant had been extracted from the surface. After extraction for 24 hours, the bands almost completely disappeared, and thus most (but not all) of the surfactant near the membrane surface had been extracted. The amount of residual surfactant in the MCM-48 membrane cannot be detected easily by thermogravimetric analysis, unlike the case of MCM-48 powders, because the α-alumina support dominates the sample mass. However, the surfactant near the surface of the membrane can be detected by FT-ATR/IR spectroscopy [79], as seen from Figure 2-10.

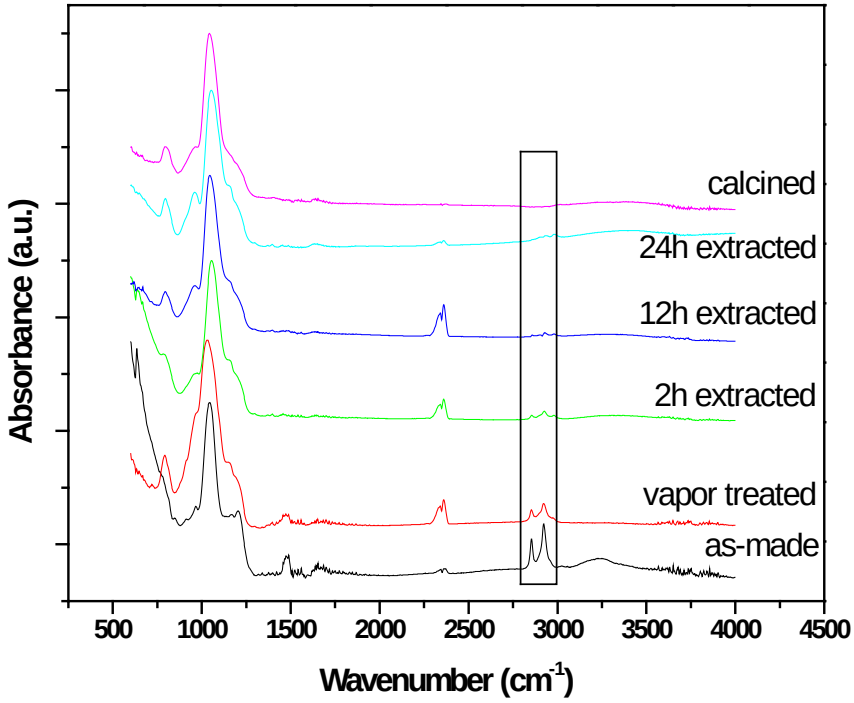

Figure 2-10. FT-ATR/IR absorption spectra of MCM-48 membranes.

The presence of unextracted surfactant inside the membrane layer could not be ruled out by the FT-ATR/IR measurements, which only have a penetration depth of ~1 μm [94, 95]. To examine this issue further, nitrogen physisorption measurements were performed on the MCM-48 membranes (Figure 2-11). As expected, the as-synthesized MCM-48 membrane had a very low pore volume, indicating that it was essentially non-porous before surfactant removal. The MCM-48 membrane after 24 hours of surfactant extraction had a similar pore volume as the as-synthesized membrane. In combination with the results of the FT-ATR/IR measurements, it appears that the surfactant in a thin top layer of the membrane may be completely extracted, but that substantial surfactant

remains deeper inside the membrane. On the other hand, the nitrogen physisorption isotherm of the calcined MCM-48 membrane shows a large pore volume of 410 cm^3/g, surface area of 656 m^2/g (C_{BET} = 115), and an estimated mean pore diameter of 3.9 nm (Table 2-1). The isotherm can be classified as Type IV according to the IUPAC nomenclature [96]. The physisorption isotherm of the calcined MCM-48 membrane shows hysteresis from capillary condensation, as is characteristic for mesoporous materials.

Table 2-1. Textural properties of seeded MCM-48 membranes.

	BET surface area (m^2/g)	Pore volume (cm^3/g)	Estimated mean pore diameter (nm)
As-made	34.2	40	-
Extracted	69.5	58	5.2
Calcined	656	410	3.9

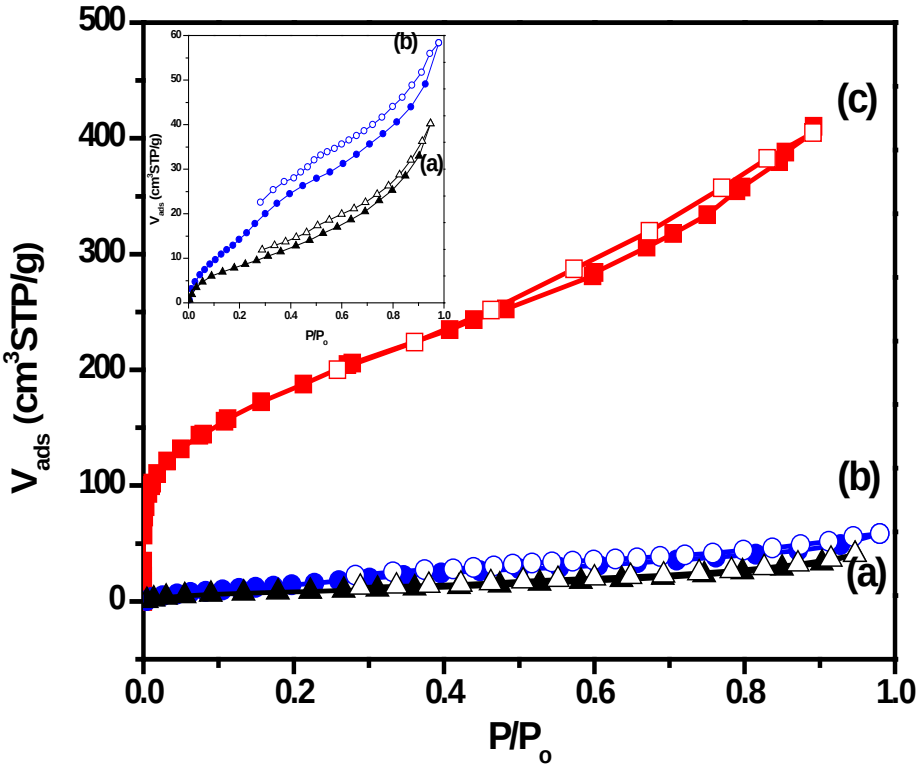

Figure 2-11. Nitrogen physisorption isotherms of **(a)** as-synthesized, **(b)** extracted, and **(c)** calcined MCM-48 membranes on the seeded α-alumina substrate.

For comparison, Figure 2-12 shows the nitrogen physisorption isotherms for calcined MCM-48 membranes prepared by seeded or unseeded (*in situ*) growth. The MCM-48 membrane synthesized with the seeded growth method had the twice larger pore volume of the membrane prepared by previously developed unseeded growth methods. The use of an MCM-48 seed layer limits the formation of dense silica regions in the membrane layer or in the support. Despite variations of the surfactant extraction process, calcination was found to be superior technique for activating the MCM-48

membranes and was therefore used for the membranes reported in the remainder of this chapter. The PSDs of calcined and extracted membranes, obtained from the isotherms, are shown in the Figure 2-13 and compared to the PSD of a calcined MCM-48 powder (Figure 2-6). All the PSDs are consistent with the presence of a mesoporous material. In contrast to the high-quality PSD obtained for the powder, the membrane PSDs are less well-defined. This is due to intrinsic limits of the membrane physisorption apparatus. The total amount of sample on the stacked membrane disks is very small as compared to the powder sample, and it is difficult to obtain data that can be used for high-quality PSDs.

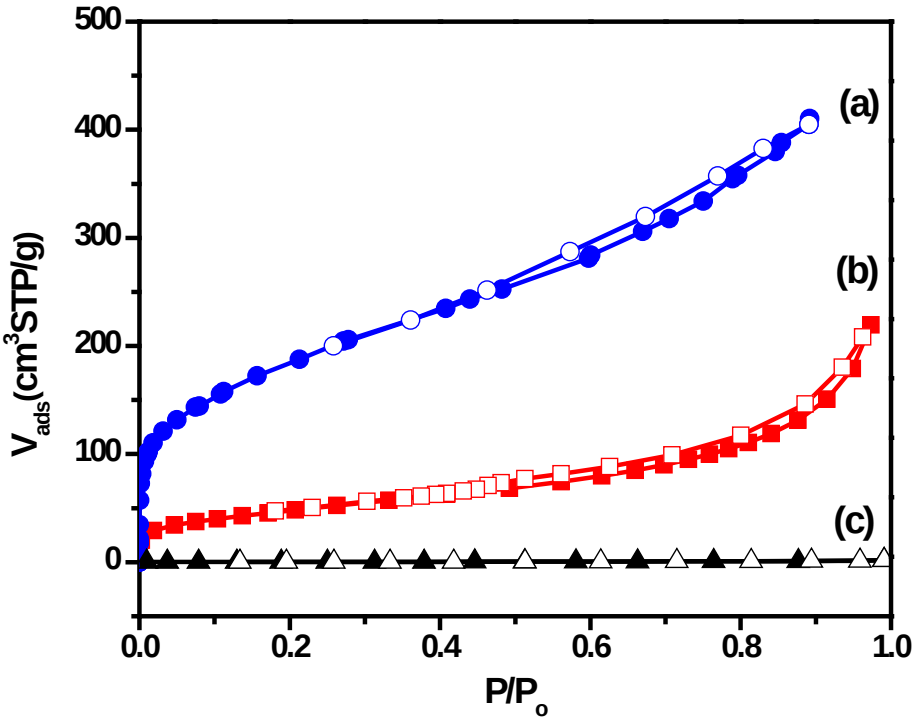

Figure 2-12. Nitrogen physisorption isotherms of calcined MCM-48 membranes prepared by **(a)** seeded growth **(b)** unseeded (in situ) growth techniques, and **(c)** α-alumina support.

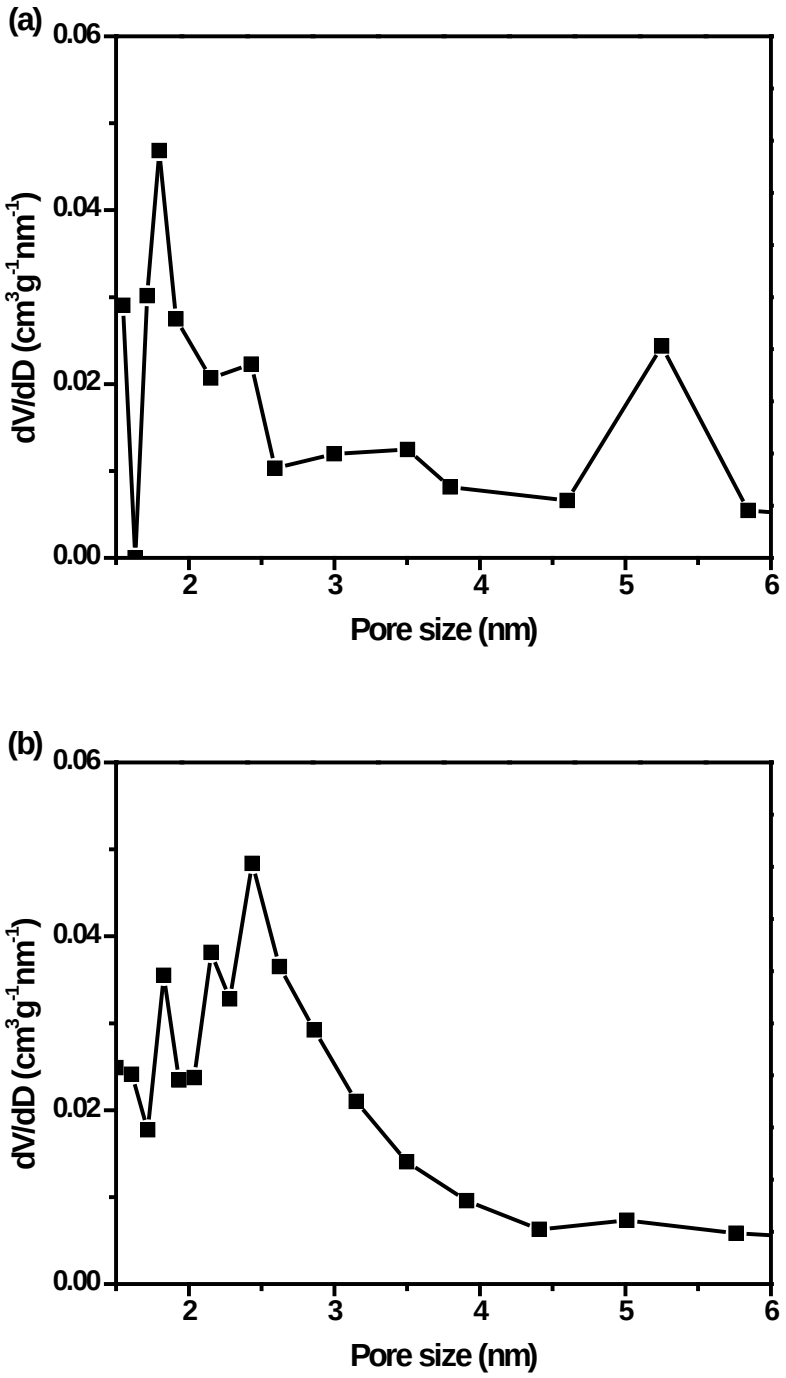

Figure 2-13. PSDs of **(a)** calcined MCM-48 membrane, and **(b)** extracted MCM-48 membrane.

Single gas permeation measurements on the calcined MCM-48 membranes were performed with N_2, CO_2, CH_4, and SF_6. The as-synthesized MCM-48 membrane was nearly impermeable to N_2, which means the permeability was less than 100 Barrer (1 Barrer = 10^{-10} cm^3 (STP) cm cm^{-2} s^{-1} $cmHg^{-1}$). The nonzero permeability before surfactant removal is associated with gas molecules that permeate through the low-density surfactant phase in the mesopores [72]. After surfactant removal, the membranes became highly permeable. Figure 2-14 summarizes pure-component gas permeabilities of the surfactant-free MCM-48 membranes versus the reciprocal square root of the gas molecular weight (M_w). The estimated theoretical permeabilities for Knudsen transport are also shown, using the structural tortuosity factor of 3 for MCM-48. Although the experimental data show the expected Knudsen-like trend with M_w, the observed permeability values are much smaller (by more than an order of magnitude) than theoretically expected. The theoretical estimate can be further corrected for the presence of significant gas-solid interactions (adsorption of gases on the mesopore walls) rather than an ideal Knudsen mechanism. This correction is based on parameters obtained directly from the recent work of Bhatia *et al* [97, 98] for silica mesopores of approximately 3 nm diameter. It is seen that adsorption likely plays a large role in decreasing the permeability from the ideal Knudsen value. The corrected theoretical permeabilities of the calcined MCM-48 membrane are still about 5-10 times larger than the experimental values, which then indicate additional permeation resistances from pore constrictions (e.g., by residual silica from the synthesis, coke formation during calcination of the surfactant, or local pore collapse during calcination) or dense material at the MCM-48/α-alumina interface. Nevertheless, it is clear that the gas permeabilities

of the seed-grown calcined MCM-48 membranes are well comparable to, and even much higher than, other MCM-48 membranes [32, 46, 79]. The slight deviation of CO_2 from the molecular weight trend may be due its stronger adsorption, both on the silica surface and on any remaining surfactant.

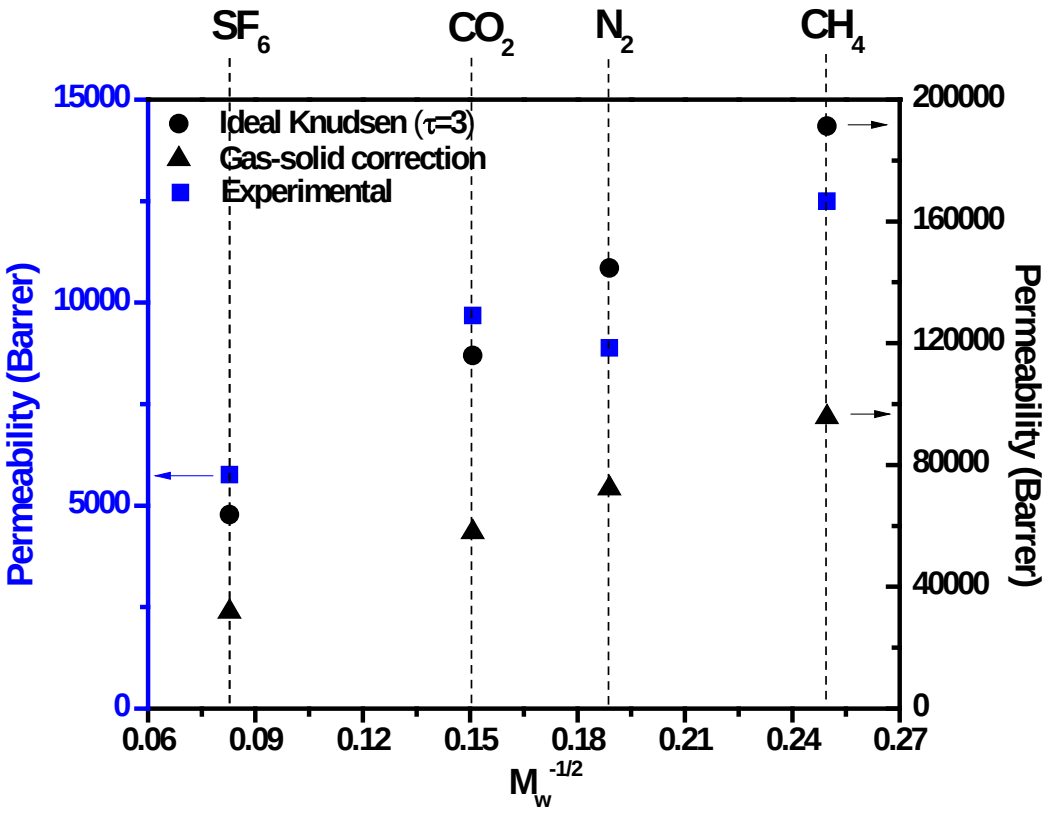

Figure 2-14. Experimental gas permeabilities (blue squares) of calcined MCM-48 membranes at 308 K, and theoretically estimated permeabilities from the ideal Knudsen model (black circles) and after corrections for gas-solid interactions in the mesopores (black triangles).

2.3.2 Silylation of MCM-48 membranes

The open mesopores of the MCM-48 membrane can be filled or modified with a variety of functional groups to tailor their molecular discrimination properties. In this work, HMDS was used as a functionalizing agent to enhance the organophilicity of the pore walls for organic/water separations [99]. Figure 2-15 shows the XRD patterns of the MCM-48 membrane before and after HMDS functionalization. The decrease in peak intensity compared to the calcined MCM-48 membrane indicates a reduction of electron density contrast between the mesopores and the silica walls, consistent with modification of the pores with organosiloxane species. The peak positions of the HMDS-treated MCM-48 membrane did not change after silylation, and hence the silylation does not cause structural changes in the MCM-48 membrane.

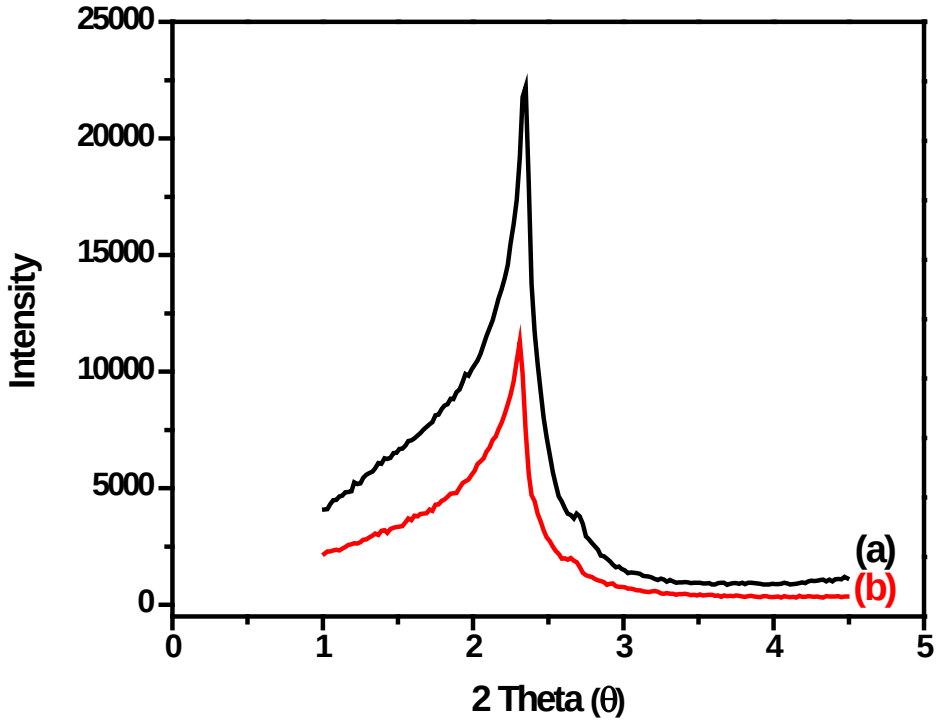

Figure 2-15. XRD patterns of **(a)** calcined, and **(b)** HMDS-treated MCM-48 membranes.

The silylation of the MCM-48 membrane was further established by gas permeation data (Figure 2-16). Permeabilities of the four different gases decreased substantially after silylation, consistent with reduction in porosity due to pore functionalization with organic groups. The order of decrease is similar for all four gases; however, CO_2 showed the sharpest reduction, possibly due to the additional effect of decrease in adsorption affinity with the organosiloxane-modified pores. As in the case of the calcined MCM-48 membrane, the HMDS-treated MCM-48 membrane also maintained the trend, consistent with gas molecule transport being governed by a Knudsen-like mechanism.

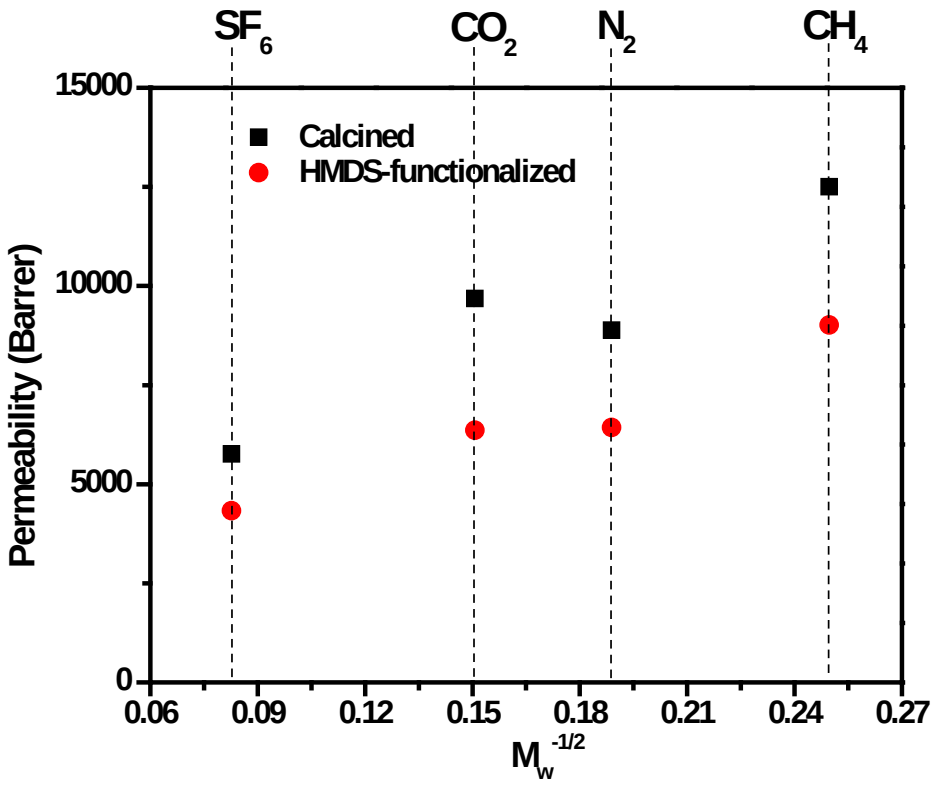

Figure 2-16. Gas permeabilities of calcined and silylated MCM-48 membranes at 308 K.

2.3.3 Pervaporation

Pervaporation data for single components and three different organic/water mixtures are summarized in Figures 2-17, 2-18, and 2-19. To allow a comprehensive understanding of the permeation properties [100], the data are expressed in terms of flux, separation factor, permeance, permeability, and selectivity for calcined MCM-48 membranes and HMDS-treated MCM-48 membranes, respectively. The feed mixtures used were (5/95 w/w) EtOH/water, MEK/water, and EA/water. The permeation experiments were performed at 303 K and 343 K.

Figure 2-17 shows the fluxes and separation factors from the single component pervaporation experiments. The fluxes increased with temperature. It is noteworthy that the silylated MCM-48 membrane shows higher fluxes for all the organics than for water, whereas the fluxes for the untreated membrane were comparable. In the mixture pervaporation experiments, the separation factors of all the organic/water mixtures through the calcined (non-silylated) MCM-48 membranes were lower than 1, indicating that the calcined MCM-48 membrane is intrinsically hydrophilic. These membranes preferentially permeate water due to the high density of silanol groups on the pore walls and the small size of the water molecules in comparison to the organic molecules. The separation factors increase substantially after silylation, as this treatment renders the pore surface hydrophobic *via* replacement of silanols with trimethylsilyl groups. Total fluxes decreased after silylation, and more importantly, the fluxes of water significantly decreased after silylation. The separation factors (of organics over water) of the HMDS-treated MCM-48 membrane varied with the organic components in the order: EA (35) > MEK (23) > EtOH (6). Both organic and water fluxes increased with temperature, but the water fluxes had a relatively larger increase, leading to decreased separation factors at high temperature.

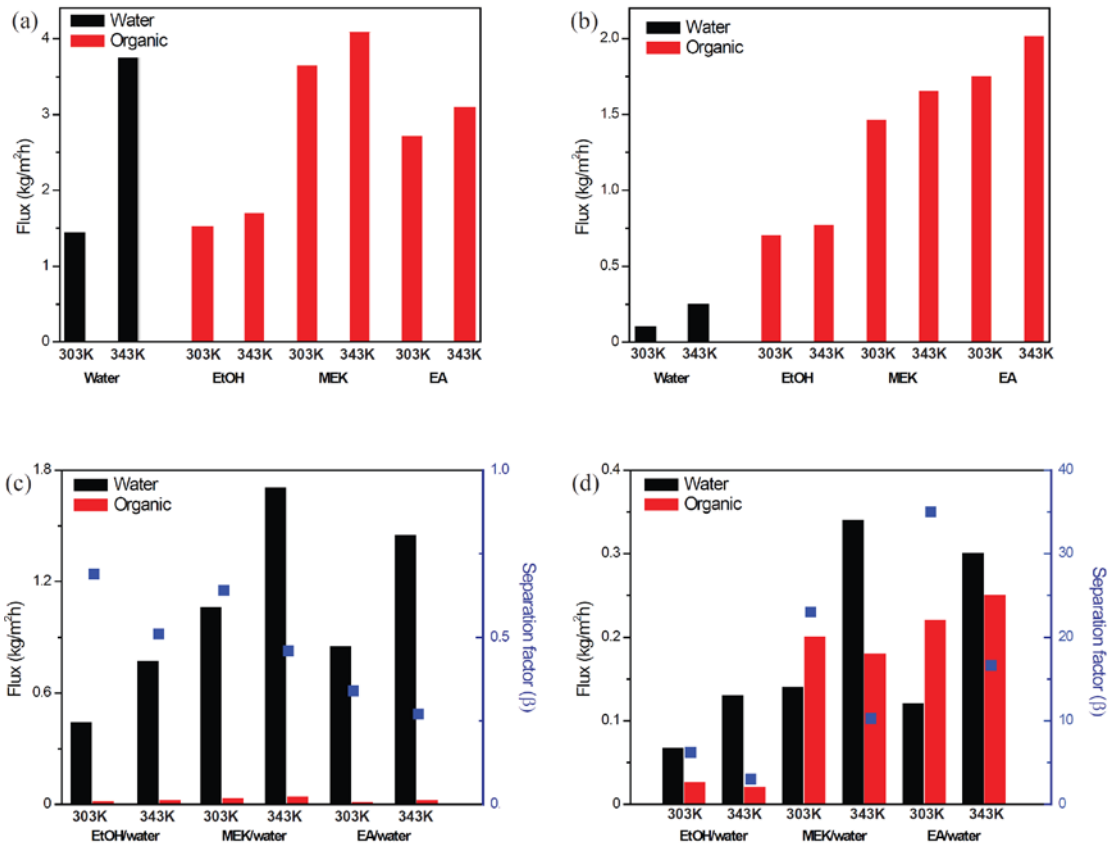

Figure 2-17. Pervaporation (flux and separation factor) results **(a)** single component pervaporation of the seeded MCM-48 membrane, **(b)** single component pervaporation of the silyl-MCM-48 membrane, **(c)** 5 wt % mixture pervaporation of seeded MCM-48 membrane, and **(d)** 5 wt % mixture pervaporation of the silyl-MCM-48 membrane.

Figure 2-18 shows the permeabilities and selectivities (ratio of component permeabilities) for the two membranes, calculated from the measured fluxes according to the well-known governing equation of pervaporation: $J_i = \left(P_{m,i}/l_m\right)(\gamma_i x_i p_i^{sat} - y_i p_p)$. Interestingly, the permeability decreased at 343 K. This result means that the permeability is more highly dependent on adsorption of the components into the mesopores (which decreases with increasing temperature) rather than diffusivity in the mesopores (which

increases with temperature). Even though the silylated MCM-48 membrane had high organic separation factors (Figure 2-17), its water/organic selectivity was still ~1 for single component pervaporation, and between 5-40 for mixture pervaporation. This is because the calcined MCM-48 membrane is highly hydrophilic. Even though the trimethylsilyl groups significantly decreased the fluxes of water through the membrane, it was still the same order of magnitude as the organic fluxes. The mixture pervaporation experiments showed higher selectivities than single component pervaporation, indicating a mechanism of competitive preferential adsorption of the organics in the membrane and relative exclusion of water.

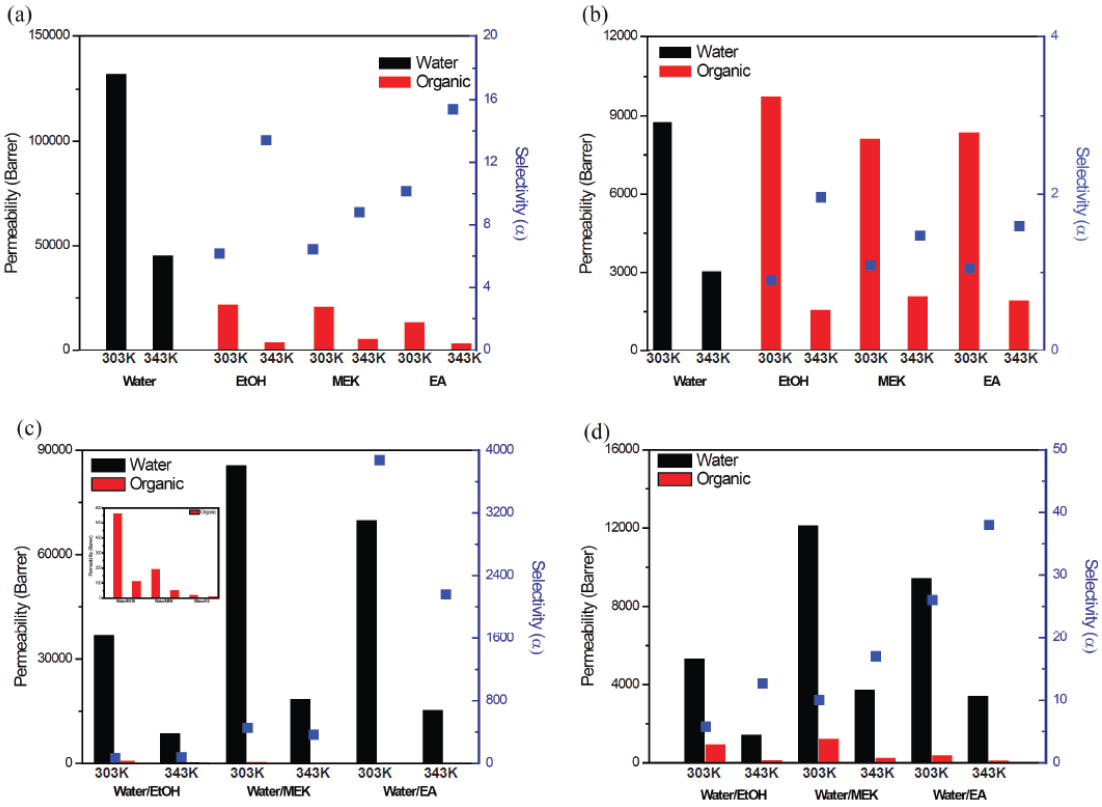

Figure 2-18. Pervaporation (permeability and selectivity) results **(a)** single component pervaporation of MCM-48 membrane, **(b)** single component pervaporation of silyl-MCM-48 membrane, **(c)** 5 wt % mixture pervaporation of MCM-48 membrane, and **(d)** 5 wt % mixture pervaporation of silyl-MCM-48 membrane.

For completeness, Figure 2-19 shows the same information as Figure 2-18, except permeance is displayed instead of permeability. It can be seen that the silylated membranes displayed high permeances (on the order of 1,000 GPU) for organics. As a result, the 5 wt % organic feed mixtures were upgraded to 28 % EtOH, 57 % MEK, and 64 % EA permeate streams at 303 K. With further optimization of the silylation conditions (silyl loading and type of silyl group), it is expected that the selectivities can be further improved. Additionally, reduction of membrane thickness or the applications of

the silylation approach to the recently-demonstrated mesoporous silica membranes on polymeric hollow fibers have potential for significant performance enhancements (carried out this study in chapter 3).

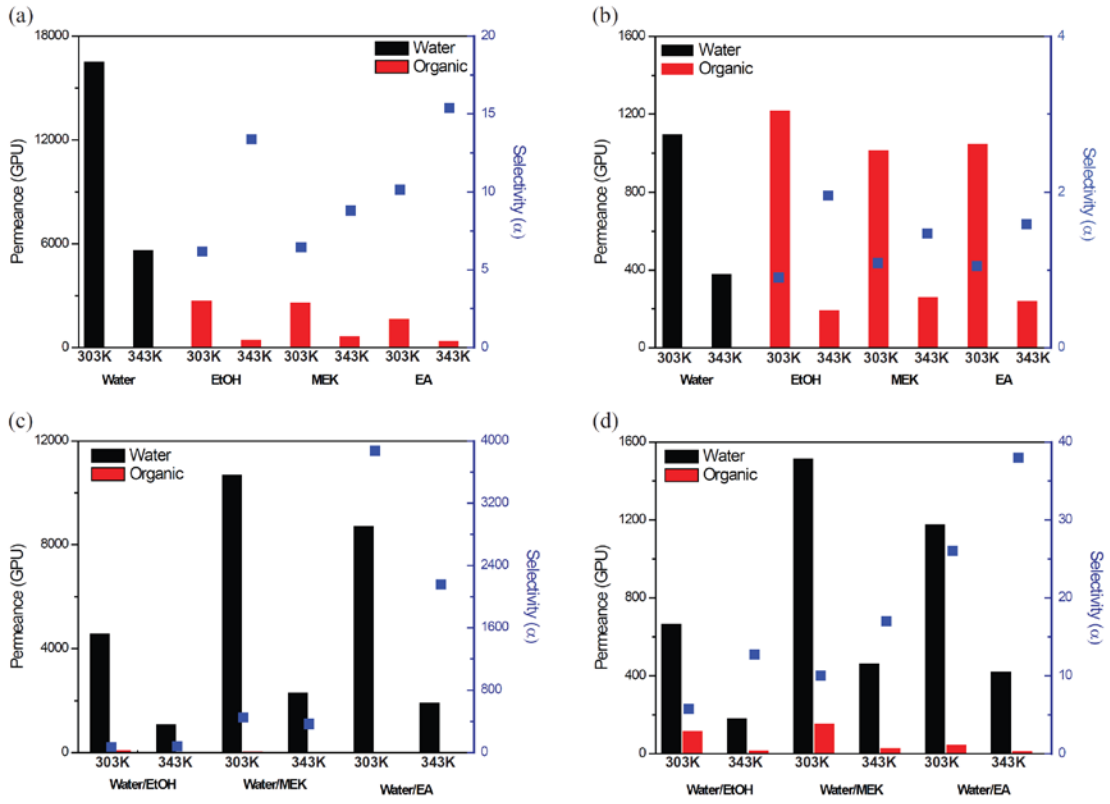

Figure 2-19. Pervaporation (permeance and selectivity) results from **(a)** single component pervaporation using the MCM-48 membrane, **(b)** single component pervaporation using the silyl-MCM-48 membrane, **(c)** 5 wt % mixture pervaporation using the MCM-48 membrane, and **(d)** 5 wt % mixture pervaporation using the silyl-MCM-48 membrane.

2.4 Conclusions

The fabrication of continuous MCM-48 membranes on α-alumina disks via seed layer deposition and hydrothermal growth has been demonstrated. The seeded MCM-48 membranes have low defect density and high gas fluxes, which are governed by a Knudsen-like behavior coupled with a significant influence of gas-solid interactions. By means of the seed layer deposition, MCM-48 membranes can be formed on the top of α-alumina supports with little silica infiltration into the macroporous supports. Also, the porosity of intact MCM-48 membranes has been assessed by nitrogen physisorption for the first time. Compared to the unseeded MCM-48 membrane, the seeded membrane has a larger pore volume and surface area.

The obtained membranes were silylated with HMDS to tailor selective properties of the membrane. The HMDS-treated MCM-48 membranes were selective for permeation of organic molecules in mixed EtOH/water, MEK/water, and EA/water permeation experiments, whereas the unmodified membranes were significantly selective for water. The good separation performance in organic/water mixtures was attributed primarily to the hydrophobic nature of the silylated pores and the preferential adsorption of the organics in the membrane.

CHAPTER 3

SILYLATED MESOPOROUS SILICA MEMBRANES ON POLYMERIC HOLLOW FIBER SUPPORTS: SYNTHESIS AND PERMEATION PROPERTIES

3.1 Introduction

Membrane-based separations are becoming increasingly competitive for a number of applications, such as hydrogen recovery, air separation, CO_2 separation, and organics recovery [101-103] due to their low energy requirements, potentially low fabrication cost, and steady-state operation. Polymeric membranes (e.g., in the form of hollow fibers) are amenable to large-scale fabrication processes and typically have large surface area to volume ratios (>1000 m^2/m^3) [104]. However, they also have an intrinsic "upper bound" on their performance, reflecting a trade-off between their permeability and selectivity [19, 105]. Although the trade-off is well-studied in the context of gas separations, it also exists in organic/water separations [106-109]. Such separations are of importance in the production of biofuels, bio-based chemicals, pharmaceuticals, and biomolecules [110-112]. In many cases, it is desired to recover the organic molecules from an aqueous dilute solution. The availability of an efficient and low-cost membrane platform capable of upgrading these dilute solutions to higher concentrations would allow a significant improvement in the economics of the above processes. The upgraded streams could then be further purified by more conventional processes to remove the remaining water (e.g., drying/adsorption with hydrophilic molecular sieves or membrane separations with hydrophilic polymer membranes) [113, 114].

Over the last decade, inorganic membranes have been shown to possess high permeability, tunable selectivity, and good thermal and chemical resistance [115-119]. Their widespread application is limited by the difficulty of fabricating them in a technologically scalable and low-cost manner. Certain types of hydrophilic zeolite membranes have successfully been fabricated on polymeric support tubes, and show excellent separation factors for water over organics of over 10,000 [116]. These membranes address the 'finishing step' of dehydration from an already concentrated product, and not the initial upgrading step from a dilute feed stream. For the latter case, several researchers have investigated the use of nanocomposite membranes that combine a hydrophobic and permeable polymer (typically a silicone elastomer) with hydrophobic molecular sieves such as pure-silica MFI [120-122]. Such membranes can potentially be scaled up to spiral-wound modules [123]; however, there is currently no reliable method of producing these membranes on high-surface-area platforms such as hollow fibers.

Here, a different approach is taken towards a scalable membrane platform for organic/water separations. This work was initiated by Dr. Kwang-Suk Jang in the Nair research group. For the purpose of creating appropriate background for my work on this aspect of the thesis, the work led by Dr. Jang (corresponding to Figures 3-4 to 3-8) is first described, before discussing my work on the detailed characterization, pore activation, silylation, and separation properties of these membranes.

Mesoporous silica materials prepared using long-chain surfactant templates have pore channels with a diameter range of 2-10 nm. The mesopores allow for rapid diffusion

of target molecules, and can be modified [124-128] in a variety of ways to impart selectivity to the permeation characteristics, thereby allowing for specific separation applications over a range of molecular sizes. Mesoporous silica membranes have been proposed as potential candidates for separation applications. Such membranes have been synthesized on ceramic substrates [129-133] and modified further to tailor the selective properties [129-137]. For example, Kumar synthesized an MCM-48 membrane on α-alumina, functionalized it with poly(ethyleneimine), and used it for CO_2/N_2 separations [138]. Nishiyama modified an MCM-48 membrane with trimethylchlorosilane groups and studied the separation of organic/water mixtures [139]. In chapter 2, I reported a seeded growth technique for MCM-48 membranes on α-alumina, and their subsequent silylation for use in organic/water separations [92].

In this chapter, the technologically scalable fabrication of an inorganic membrane platform based upon mesoporous silica membranes on polymeric hollow fibers is discussed. These asymmetric mesoporous silica membranes are continuous over large areas, are defect-free, and have high gas flux. Further, I perform the fabrication, characterization, and measurement of permeation properties of silylated mesoporous silica membranes on polymeric hollow fibers. I characterize in detail the structure and composition of the mesoporous silica membrane. Pervaporation of five different organic/water mixtures is studied to understand the permeation characteristics of the silylated mesoporous membranes. The effects of temperature on the separation performance, and the mechanism of separation with the silylated mesoporous silica hollow fiber membranes, are also discussed.

3.2 Experimental Section

3.2.1 Materials

The following chemicals were used as received: tetraethylorthosilicate (TEOS, 98% Sigma-Aldrich), cetyl trimethylammonium bromide (CTAB, Sigma-Aldrich), 1 N aqueous hydrochloric acid (HCl) solution (Sigma-Aldrich), hexamethyldisilazane (HMDS, Alfa Aesar), ethanol (EtOH, BDH), methylethyl ketone (MEK, Sigma-Aldrich), ethyl acetate (EA, Sigma-Aldrich), *iso*-butanol (*i*-BuOH, EMD), *n*-butanol (*n*-BuOH, Sigma-Aldrich), Ultem® 1000 (SABIC), and Torlon® 4000T-LV (Solvay Advanced Polymers).

3.2.2 Mesoporous silica membrane coating on Torlon® hollow fibers

Macroporous Torlon® (polyamide-imide) hollow fiber supports were fabricated by a dry-jet/wet-quench method, described in detail by us elsewhere [140]. The outer and inner diameters of the support fibers were *ca*. 380 μm and 230 μm, respectively. The fibers did not possess skin layers and had open pores of ~100 nm size at the outer surface. Before the membrane coating, both ends of the fiber support were sealed with epoxy to prevent the membrane growth in the interior of the fiber support. The support Torlon® hollow fibers were immersed in the coating solution for 5 hours at room temperature. The mixture had the molar composition of 1 TEOS : 0.425 CTAB : 0.00560 HCI : 62.2 H_2O. I switched from basic synthesis to acidic synthesis for the fibers, because Torlon® hollow fibers are not stable in acidic conditions. The prepared hollow fiber membranes were aged with saturated TEOS vapor prior to use. A 22 cm-long fiber membrane was placed with 25 μL of TEOS in a closed vessel at 373 K for 24 hours. For surfactant extraction,

the fiber membranes were washed with 0.05 N HCl/ethanol under stirring for 24 hours.

3.2.3 Silylation of mesoporous membrane

Prior to silylation, the surfactant-extracted mesoporous silica membranes were evacuated in a vacuum oven at 423 K under 0.07 atm, to remove physically adsorbed moisture and residual surfactant. Then, the membranes were exposed to HMDS vapor in a closed vessel at 373 K for 24 hours. After silylation, the membranes were washed with deionized water for 30 min in a separate container under stirring. Then, the coated membranes were dried at 363 K before preparing the pervaporation measurement module.

3.2.4 Characterization methods

Scanning electron microscopy (SEM) was performed with LEO 1530 and Zeiss Ultra60 instrument to examine the membranes. The membrane samples were prepared on carbon tape and coated with gold to prevent image distortion due to surface charging. Energy dispersive X-ray spectroscopy (EDS) was used to investigate the elemental composition of mesoporous silica/Torlon® hollow fiber membrane. X-ray diffraction (XRD) patterns of the membranes were obtained using a PANalytical X'pert diffractometer using a Cu-K-alpha X-ray source, diffracted beam collimator, and a proportional detector. For XRD, the samples were aligned on the center of an aluminum mount and attached to the surface with double-sided tape as shown in Figure 3-1. FT-ATR (Attenuated total reflectance) / IR spectra were obtained using a Bruker Vertex 80v Fourier Transform Infrared (FT-IR) spectrometer coupled to a Hyperion 2000 IR microscope at 20X magnification. High-resolution transmission electron microscopy

(TEM) was performed on a FEI Tecnai G^2 F30 TEM at 300 kV. For TEM, the samples were prepared after dissolving away the Torlon® support fiber using a strong solvent, N,N-dimethylformamide. Based on TEM images, pore sizes were estimated using NIH ImageJ software. In the selected area of worm-like mesopores, the pore size can be estimated by recognizing the pores as particles and using their width and height given by ImageJ [141, 142].

Figure 3-1. Illustration of mounted XRD sample.

3.2.5 Gas permeation and pervaporation measurements

Gas permeation was measured using a hollow fiber module (Figure 3-2) and a permeation testing system, constructed in-house as described by Koros *et al.* [143, 144]. Gases were fed into the bore ("tube side") of the fiber interior at one end of the module. The temperature of the system was maintained at 308 K during the measurement. The flux through the walls of the fiber was measured on the "shell side" connected to a bubble flow meter. Atmospheric pressure was maintained on the downstream side. The flux was

converted to permeance and permeability, a preferred way of reporting pervaporation performance data [145]. Permeances are expressed in GPUs (Gas Permeation Units, 1 GPU = 10^{-6} cm^3 (STP) cm^{-2} s^{-1} $cmHg^{-1}$) and permeabilities are given as Barrers (1 Barrer = 10^{-10} cm^3 (STP) cm cm^{-2} s^{-1} $cmHg^{-1}$). Pervaporation measurements were carried out using an aqueous mixture of a specific organics (5 wt % organic) at 303 K and 323 K using a custom-built unit. The permeate was collected in a liquid nitrogen cooled trap. In contrast to the gas permeation tests, liquid mixtures were fed into the shell side and vaporized, whereby they flowed through to the tube side. The hollow fiber module for pervaporation is shown in Figure 3-3. The total flux was obtained by measuring the mass of permeate collected in a given measurement time, and the composition of the permeate was characterized by gas chromatography (GC) and ^1H nuclear magnetic resonance (NMR) in deuterated acetone.

Figure 3-2. Illustration of gas permeation module.

Figure 3-3. Illustration of pervaporation module.

3.3 Results and Discussion

3.3.1 Mesoporous silica membrane synthesis

Figure 3-4 shows the membrane fabrication process, which was described in detail in the Experimental Section. As in chapter 2, MCM-48, a mesoporous silica with

three-dimensional channels of 2.7 nm diameter, was selected for investigation. The process comprises the fabrication of a macroporous polymeric hollow fiber, followed by the formation of a thin mesoporous silica layer on the hollow fiber at room temperature by static immersion in an acidic silica/surfactant precursor solution. The initial mesoporous framework formed in this process is then fully condensed by supplying additional silica species *via* a TEOS vapor treatment at 373 K, and the mesopores are then activated by a room temperature surfactant extraction step.

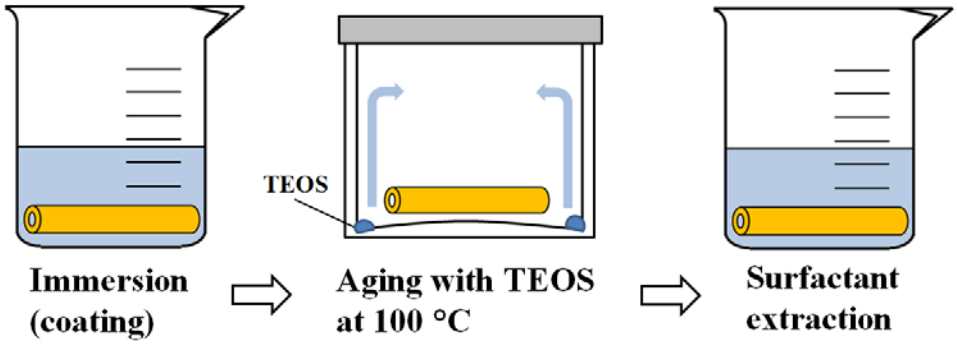

Figure 3-4. Mesoporous silica/Torlon® hollow fiber membrane fabrication.

Initial experiments to grow MCM-48 films were carried out on flat, nonporous surfaces of the poly(etherimide), Ultem®, coated on glass substrates. Figure 3-5 shows an SEM image and XRD pattern of the thin (150 nm) MCM-48 coating. It is hypothesized that the formation of the mesoporous silica film on the polymer substrate is initiated by the adsorption and micellar self-assembly of the surfactant molecules on the hydrophobic surface of the substrate.

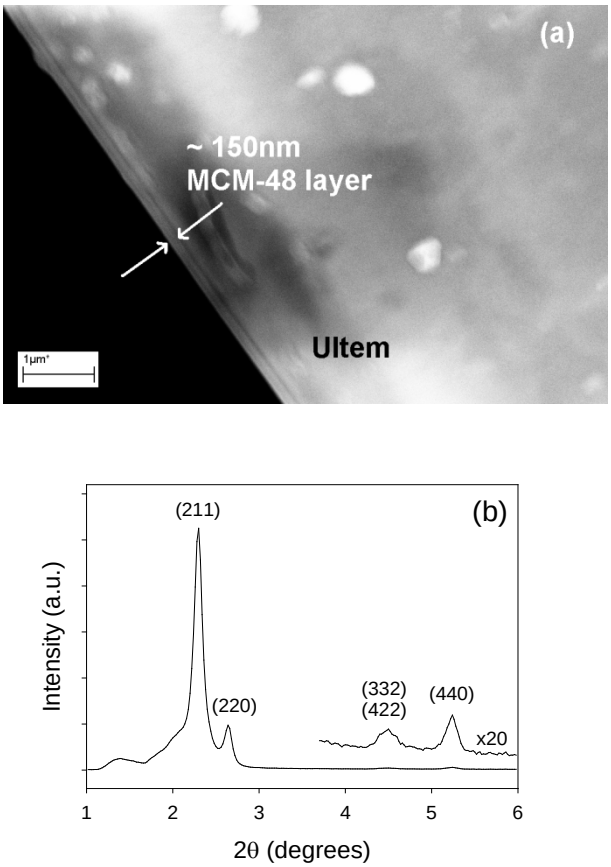

Figure 3-5. (a) Cross-section SEM image, and **(b)** low-angle XRD pattern of MCM-48 coated on Ultem® film. The XRD peaks are indexed as (210), (220), (332)/(422), and (440) of continuous cubic *Ia*3*d* structure.

For subsequent fabrication of membranes on hollow fibers, I selected Torlon®, a poly(amide–imide), as the polymeric substrate material. Torlon® is chemically resistant and withstands high pressures up to 2,000 psi without plasticization [146]. These characteristics, as well the amenability of Torlon® for producing hollow fibers of controlled porosity, are expected to be important for separation applications.

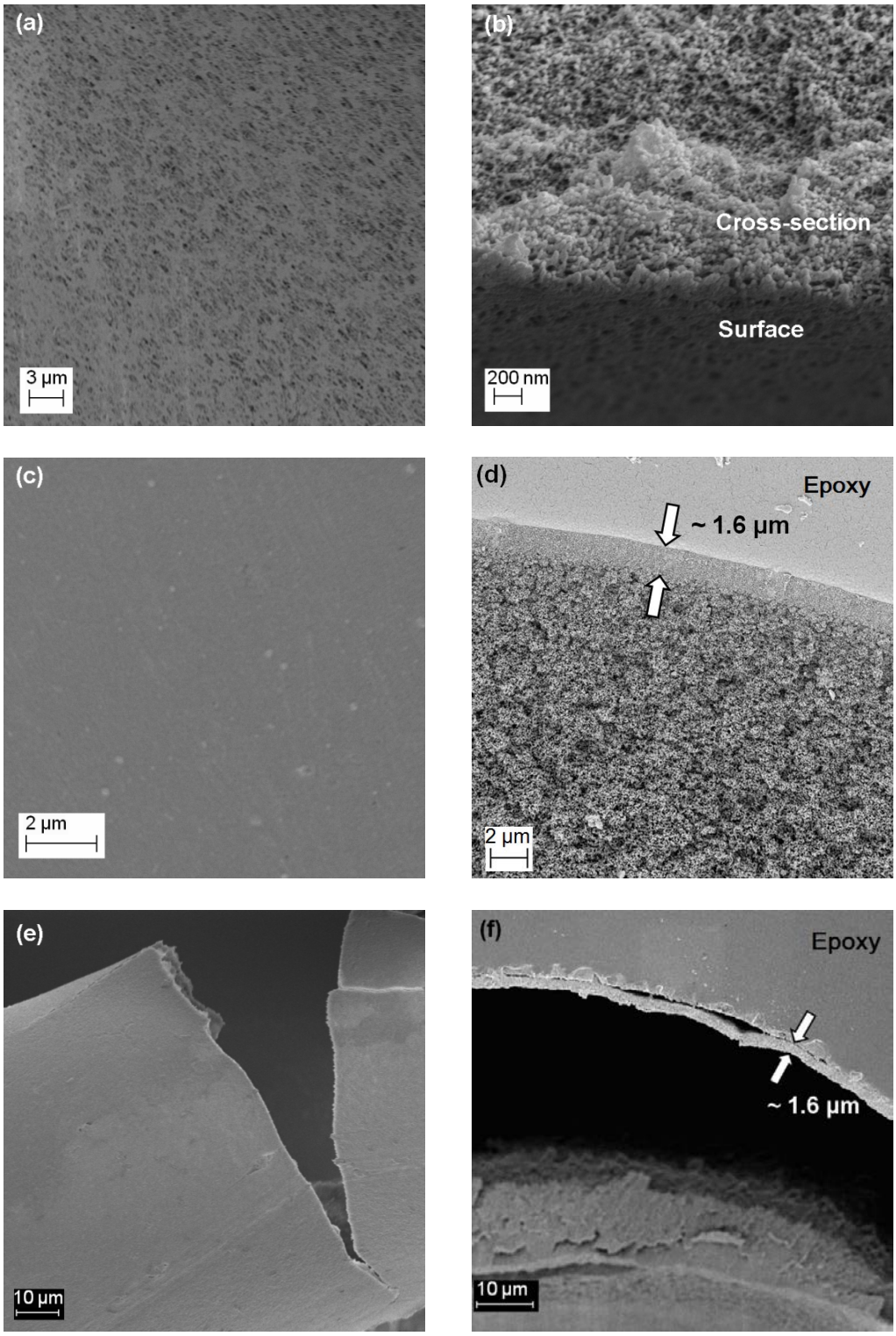

Figure 3-6. Surface and cross-section SEM images of **(a),(b)** bare Torlon® hollow fiber supports; **(c),(d)** mesoporous silica/Torlon® hollow fiber membranes; and **(e),(f)**

remaining silica layers after dissolving out the Torlon® supports, respectively. The mesoporous silica layer in **(e)** is free-standing, whereas the layer in **(f)** is adhered to an epoxy resin which was used to mount the fiber before polymer dissolution.

Figures 3-6(c), 3-6(d), and 3-7 show surface and cross-sectional SEM images of the mesoporous silica/Torlon® hollow fiber membranes after completion of the membrane formation, TEOS vapor treatment, and surfactant extraction steps. Continuous and uniform silica layers are formed in a facile and highly reproducible manner. The apparent thickness of the mesoporous silica layer is 1.6 μm. The morphology of the silica layer is further revealed by dissolving the Torlon® fiber with a strong solvent, *N*,*N*-dimethylformamide (Figures 3-6(e), 3-6(f), and 3-8). The SEM images suggest that in addition to the thin silica layer formed above the Torlon® fiber surface, the silica layer extends inside the pores of the fiber. The composition of the mesoporous silica/Torlon® layer was also confirmed by EDS (Figure 3-9). I speculate that the composite that the composite (polymer/silica) nature of the membrane layer may prevent the formation of continuous domains of highly ordered MCM-48.

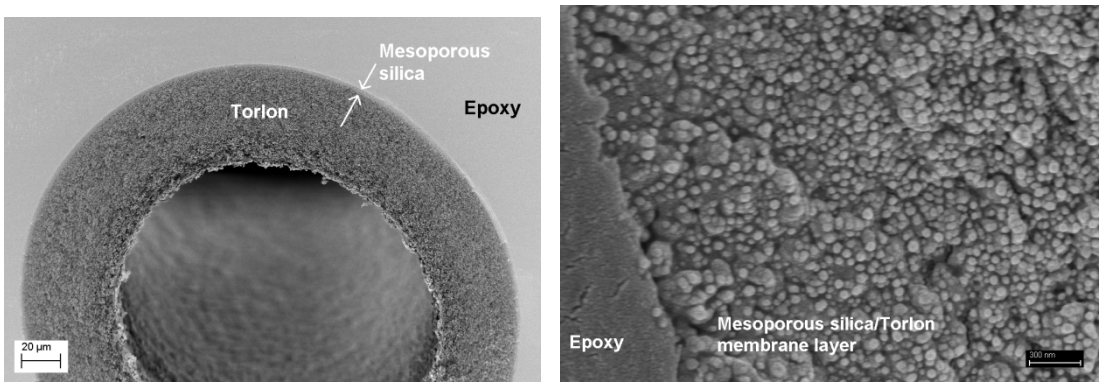

Figure 3-7. Cross-section SEM images of the mesoporous silica/Torlon® hollow fiber membrane after surfactant extraction.

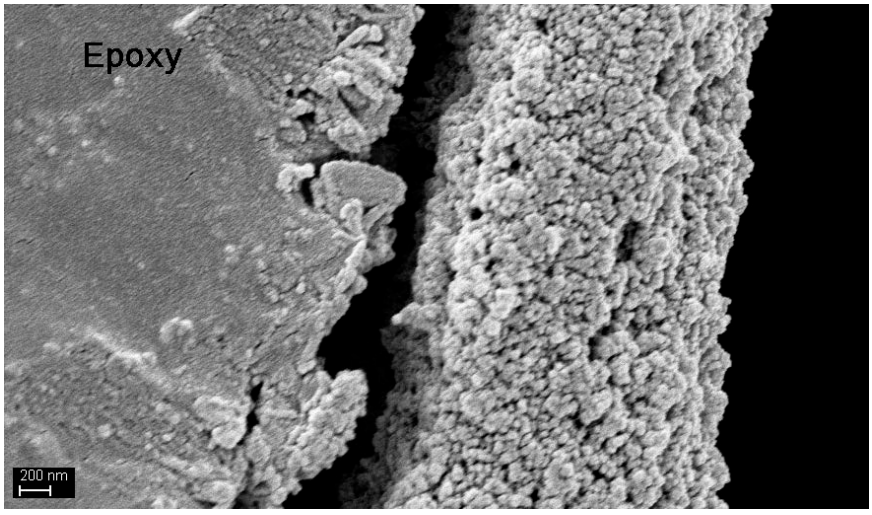

Figure 3-8. Cross-section SEM image of the remaining silica layer after dissolving out the Torlon® support. The membrane was mounted in an epoxy resin before dissolution of the Torlon® polymer.

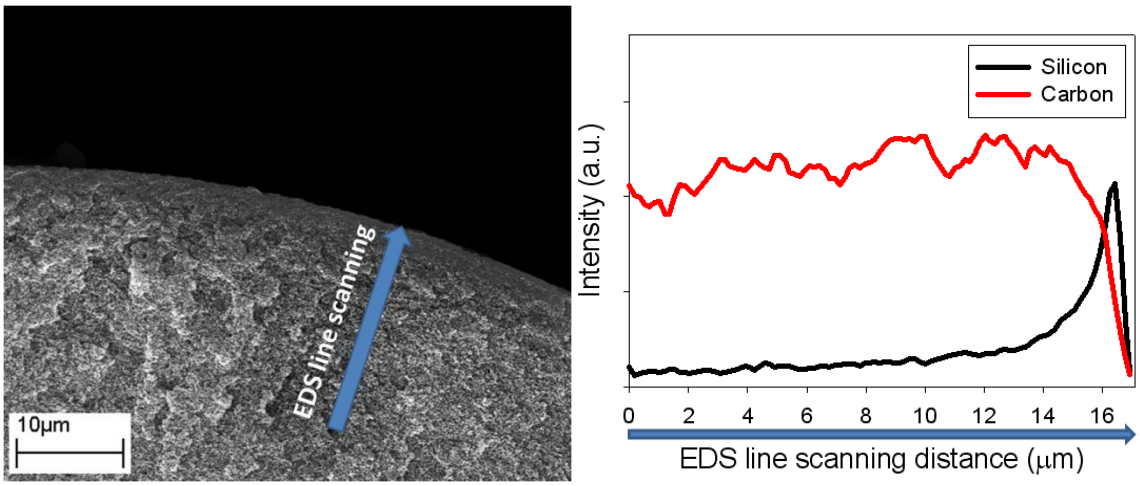

Figure 3-9. EDS line scanning analysis of the mesoporous silica/Torlon® hollow fiber membrane.

Table 3-1 summarizes pure-component CO_2 and N_2 gas permeation properties of the membranes at sequential stages of processing. The results support the formation of a continuous, defect-free mesoporous silica coating on the hollow fiber, and the activation of the mesopores after surfactant extraction leading to a high permeability. The membrane has non-zero permeability even before surfactant extraction, as gas molecules permeate through the low-density surfactant phase in the mesopores. CO_2 and N_2 permeances of the mesoporous silica/Torlon® hollow fiber after surfactant extraction were measured at 308 K and in a feed pressure range of 50 psig. The CO_2 permeability of the asymmetric mesoporous silica hollow fiber membrane is calculated to be 7,000 Barrer, a value significantly higher than that reported for MCM-48 membranes grown hydrothermally on ceramic disks (4,600 Barrer) [32]. Figure 3-10 shows pure-component gas permeabilities of the surfactant-free MCM-48 membranes versus the reciprocal square root of the gas molecular weight (M_w). The slight deviation of CO_2 from the

molecular weight trend may be due its stronger adsorption, both on the silica surface and on remaining surfactants.

Table 3-1. Pure-component gas permeation properties of mesoporous silica/Torlon® hollow fiber membranes at various stages of processing. All measurements were made at 308 K, and a feed pressure of 50 psig.[a]

Membrane	CO_2 permeance (GPU)	N_2 permeance (GPU)	CO_2/N_2 permeance ratio
Mesoporous silica/Torlon® after TEOS vapor treatment	11	5.9	1.9
Mesoporous silica/Torlon® after extraction with ethanol for 2 hours	730	390	1.9
Mesoporous silica/Torlon® after extraction with ethanol for 24 hours	1,700	1,900	0.9
Mesoporous silica/Torlon® after extraction with 0.05 N HCl/ethanol for 24 hours	4,400	3,300	1.3

[a] 1 psi = 6.89 kPa.

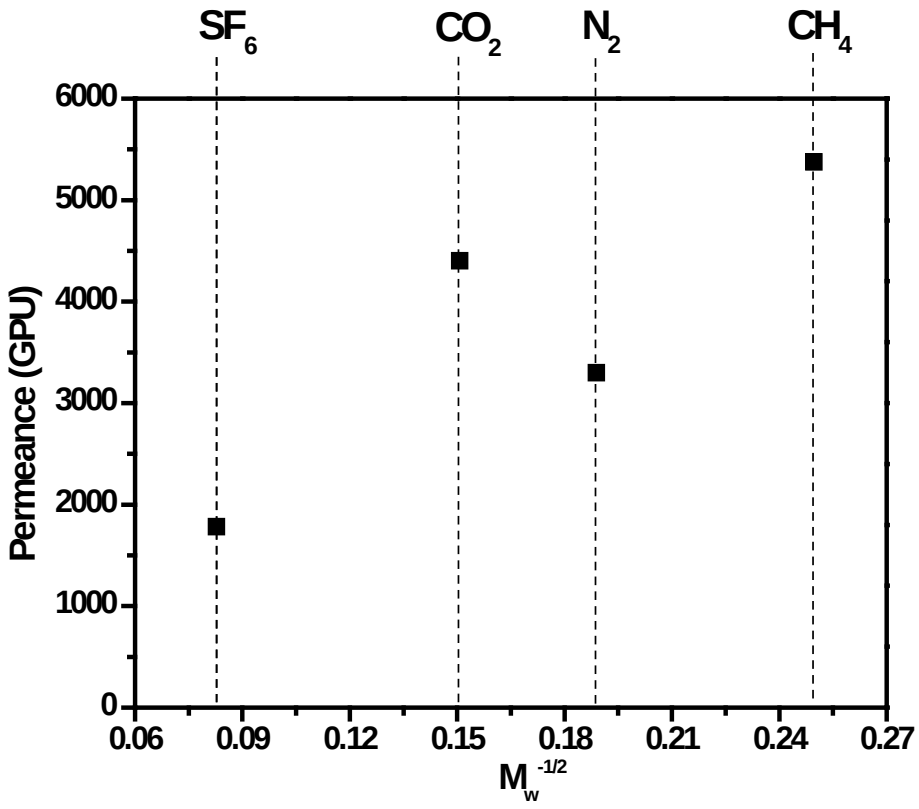

Figure 3-10. Pure-component gas permeation properties of mesoporous silica/Torlon® hollow fiber membranes at 308 K.

3.3.2 Evacuation and silylation of mesoporous membrane

Figures 3-11(a), 3-11(b) show SEM images of the mesoporous silica/Torlon® hollow fiber membranes after evacuation. Continuous and uniform silica layers are obtained in a highly reproducible manner. The membrane thickness is maintained at 1.6 μm after evacuation. Figures 3-11(c), 3-11(d) show SEM images of the subsequent HMDS-silylated mesoporous silica/Torlon® hollow fiber membranes. The continuous and uniform silica layers are not damaged by silylation. Also, there is no change in the membrane thickness or morphology after silylation.

Figure 3-12 shows single gas permeation data at 308 K for the extracted, evacuated, and subsequently silylated mesoporous silica/Torlon® hollow fiber membranes at varying feed pressures. Compared to the non-evacuated membrane, the permeances of the evacuated membranes increase from 3,300 to 20,000 GPU for N_2 and from 4,400 to 18,000 GPU for CO_2. This indicates successful removal of adsorbed water and other species at 423 K. Moreover, the relative permeance of N_2 and CO_2 (1.11) is closer to the Knudsen ratio. (Knudsen ratio: $N_2/CO_2 = 1.25$). Removal of residual species by evacuation activates the mesopores properly for subsequent pore modification.

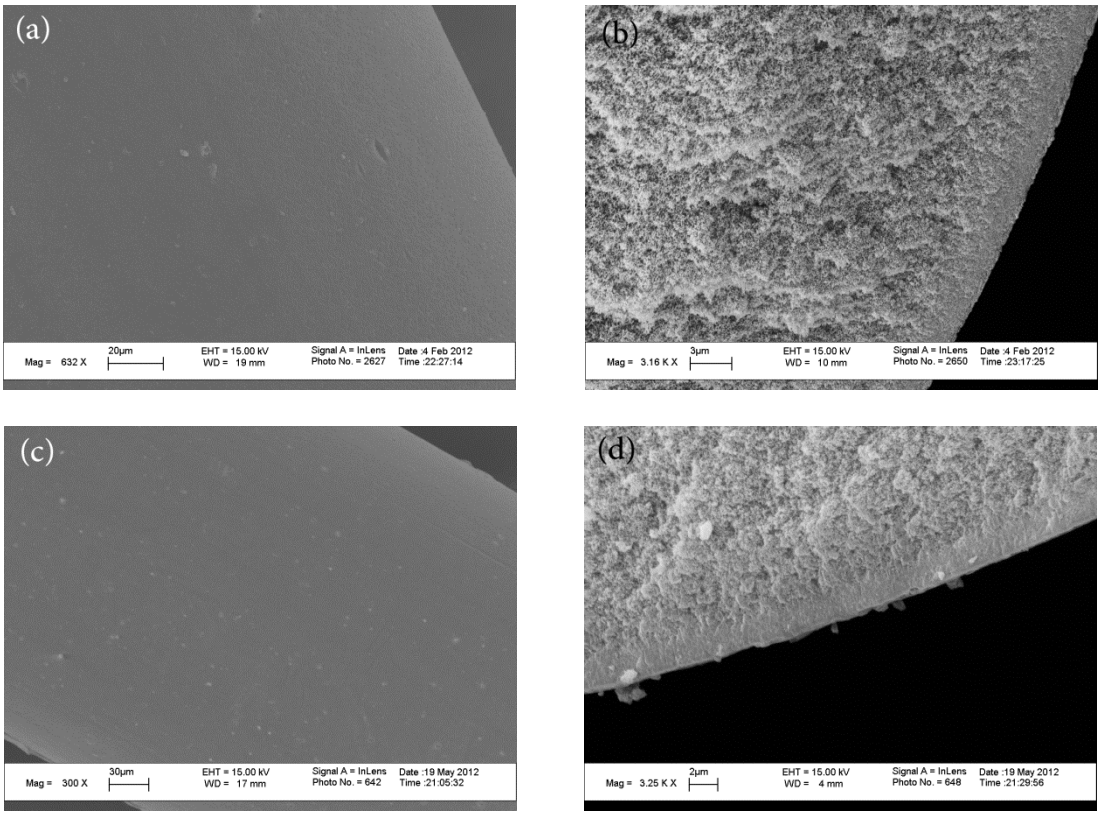

Figure 3-11. SEM images of **(a)** top view and **(b)** cross section of evacuated mesoporous silica/Torlon® hollow fiber membranes; and **(c)** top view **(d)** cross section of HMDS-silylated mesoporous silica/Torlon® hollow fiber membranes.

The gas permeances of the silylated mesoporous membranes were also measured. Permeances of N_2 and CO_2 decrease substantially after silylation, consistent with a reduction in porosity and decreased adsorption due to pore functionalization with trimethylsilyl groups. However, CO_2 shows less reduction, possibly due to its stronger adsorption on the silylated surface. As in the case of other mesoporous membranes (templated-extracted and evacuated membranes), the silylated mesoporous membranes have a constant permeance regardless of feed pressure, consistent with gas molecule transport being governed by a Knudsen-like mechanism. Surprisingly, a significant

reduction of gas permeance may also be attributed to silylation of the Torlon® support. As shown in Figure 3-13, the silica-free Torlon® support also has a reduced permeance (~ 10,000 GPU) after silylation.

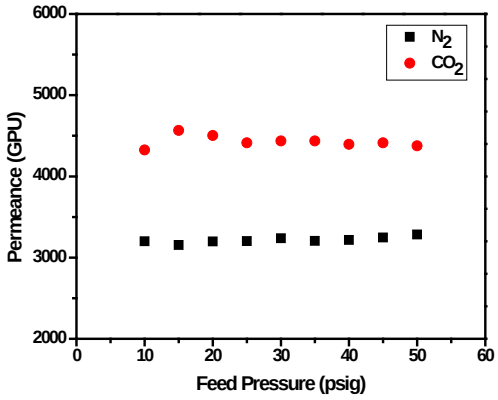

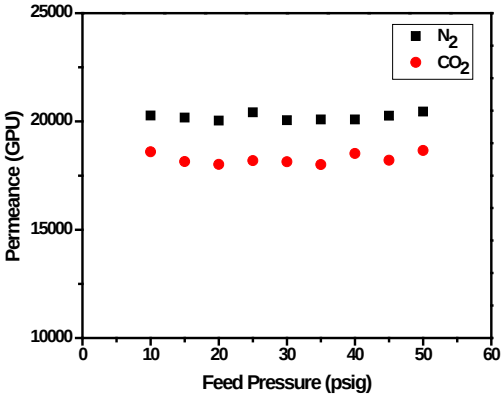

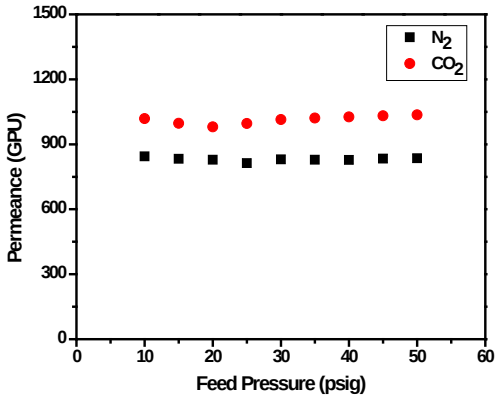

Figure 3-12. N_2 and CO_2 single gas permeation results for (top) template extracted, (middle) evacuated, and (bottom) silylated mesoporous silica/Torlon® hollow fiber membranes.

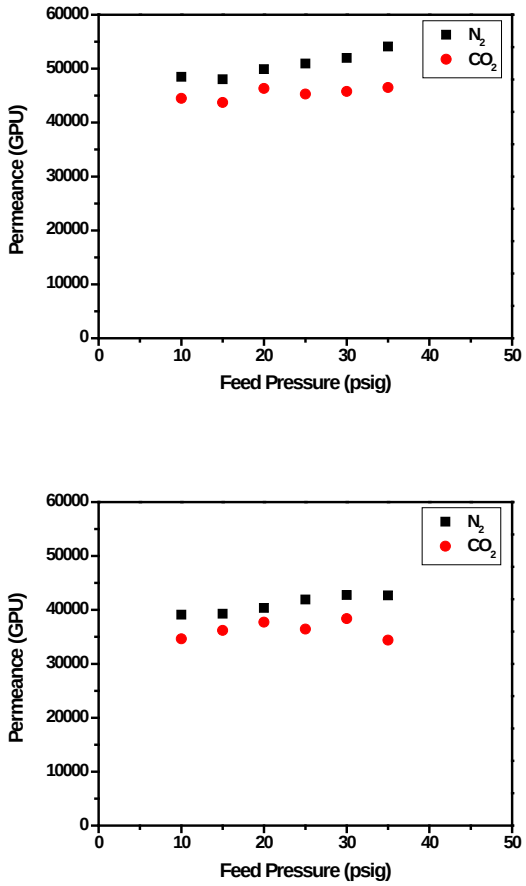

Figure 3-13. N_2 and CO_2 single gas permeation results for (top) silica-free Torlon® hollow fiber, and (bottom) the silylated Torlon® hollow fiber.

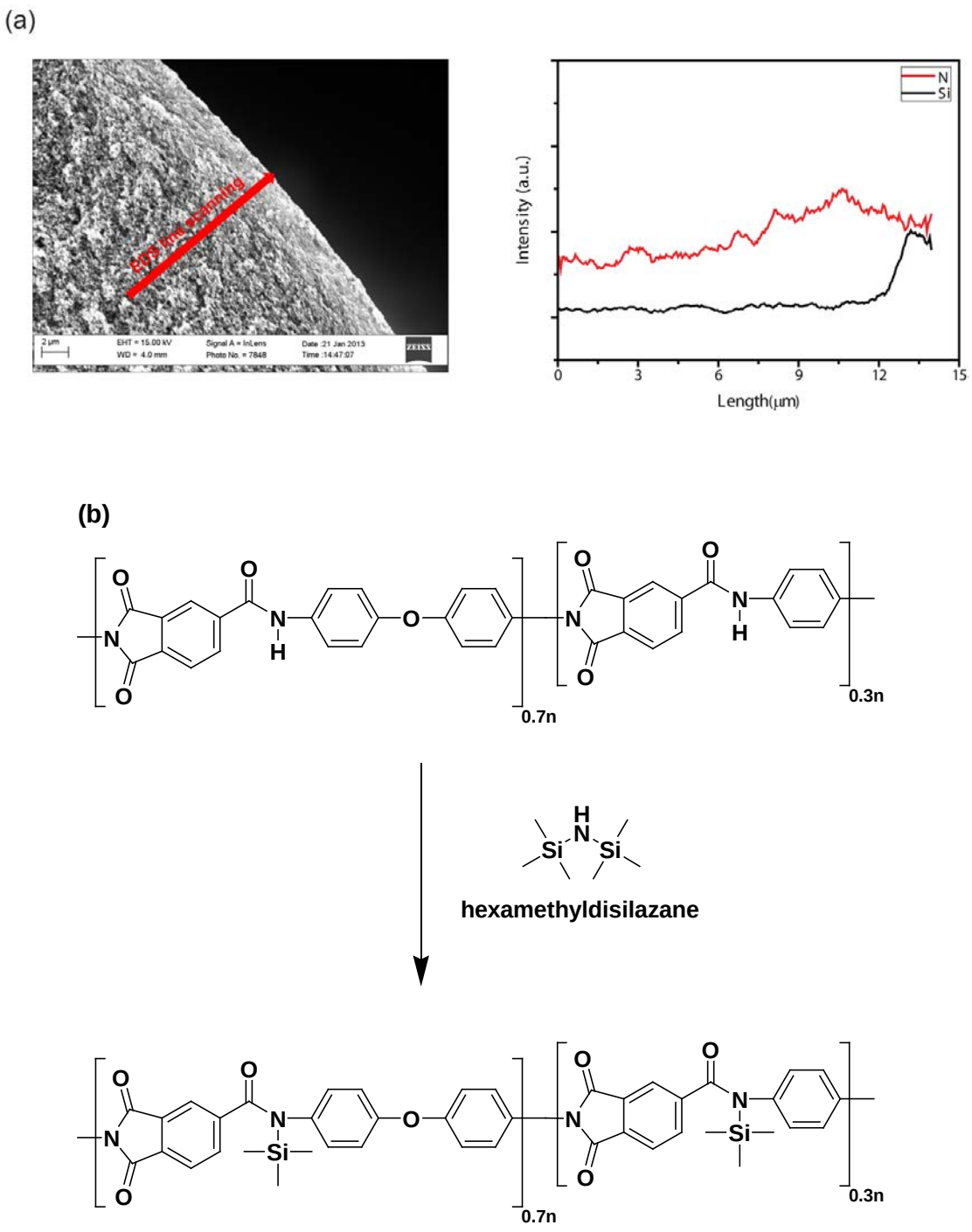

Figure 3-14. (a) Line scanning analysis of energy-dispersive X-ray spectroscopy (EDS) for the silylated Torlon® hollow fiber membrane, and **(b)** anticipated silylated Torlon® structure.

According to EDS analysis (Figure 3-14(a)), silicon species are detected on the outer surface of the Torlon® hollow fiber, which otherwise should not contain any silicon (Figure 3-15). Presumably, the amide group in the Torlon® structure is silylated by HMDS [147], as shown in the scheme of Figure 3-14(b). The theoretical permeances under conditions for Knudsen transport are also estimated (N_2=47,000 GPU, CO_2=38,000 GPU), using the structural tortuosity factor of 3 for the mesoporous silica membrane. Then, the theoretical estimate can be further corrected for the presence of significant gas-solid interactions (adsorption of gases on the mesopore walls) rather than an ideal Knudsen mechanism [42]. This correction is based on parameters obtained directly from Bhatia *et al* [97, 98] for silica mesopores approximately 3 nm in pore diameter. The corrected theoretical permeances of mesoporous membrane are 23,500 GPU for N_2 and 19,000 GPU for CO_2, which are slightly higher than those of our evacuated membrane. The slight deviation is probably due to pore constrictions or dense material at the mesoporous silica/Torlon® interface. Based on both gas permeation tests and comparison to theoretical values, it is clear that the mesoporous silica membranes on Torlon® hollow fiber supports are successfully fabricated in a controlled manner.

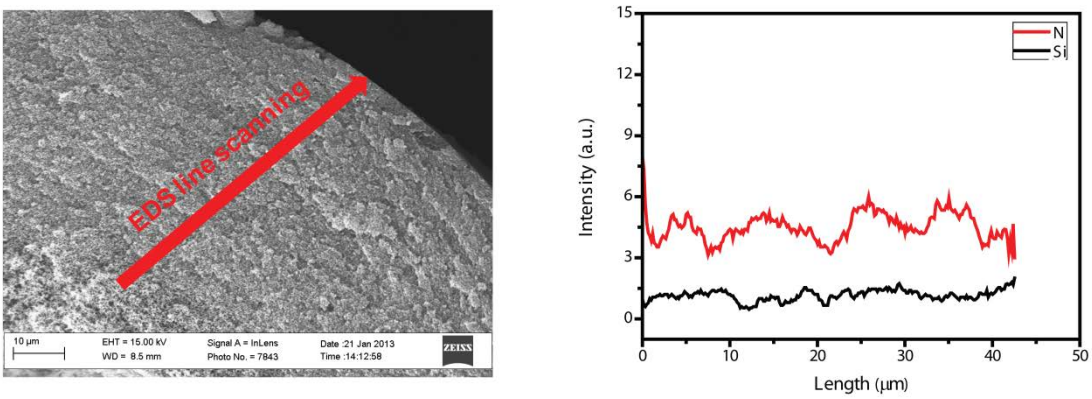

Figure 3-15. Line scanning analysis of energy-dispersive X-ray spectroscopy (EDS) for the Torlon® hollow fiber membrane.

The pore structure of the mesoporous silica membrane was investigated in further detail by XRD and TEM imaging. Figure 3-16 shows the low angle XRD patterns of the mesoporous silica membranes at several stages of processing (template-extracted, evacuated, and silylated). Although an intense diffraction signal is difficult to obtain due to the curved surface of the sample and the thin membrane layer, the existence of mesoporous silica is clearly indicated. The increase (Figure 3-16(b)) and decrease (Figure 3-16(c)) in peak intensity due to evacuation and silylation of the template-extracted membrane (Figure 3-16(a)) are due to the changes of electron density contrast between the mesopores and the silica walls, consistent with removal of residual species and modification of the pores with trimethylsilyl species, respectively.

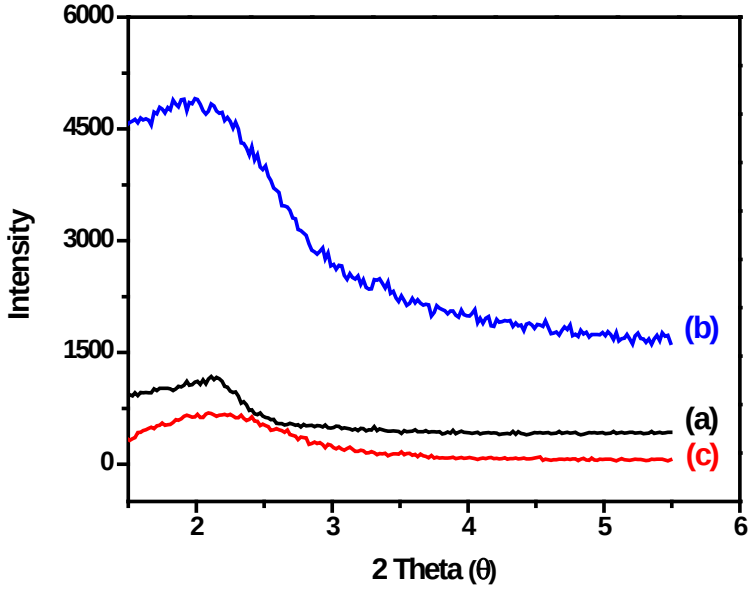

Figure 3-16. XRD patterns of **(a)** template-extracted, **(b)** evacuated, and **(c)** silylated mesoporous membranes.

The silica layers of the same set of membranes were examined by TEM (Figure 3-17) after dissolving away the Torlon® support fiber. The remaining silica structure containing worm-like channels is observed for the membranes in each stage. It has been reported that MCM-48 is formed by a transformation from either a worm-like or 2D hexagonal structure [148-150]. Worm-like mesoporous materials such as KIT-1 also have continuous channels, and possess a number of interesting properties different from ordered mesoporous silicas [151-154]. Moreover, image analysis results for the height and width of the pores show that the pore size is consistent with the presence of a mesoporous material with a diameter of about 2 nm (Figures 3-18, 3-19, and 3-20). For the pore size distribution analysis, I estimated the width and height of pores from the

TEM images using the ImageJ software. First, I selected areas of worm-like mesopores in TEM images, and cropped selected parts. Those selected images were analyzed by recognizing the pores as particles as shown in Figure 3-18, 3-19, and 3-20. Then, the software measured the width and height of each particle, and plotted the distributions, respectively. Interestingly, the pores of template-extracted (Figure 3-18) and silylated (Figure 3-20) membranes appear to be slightly smaller than those of the evacuated (Figure 3-19) mesoporous membrane, qualitatively indicating the reduction of the size of the pore channels due to the presence of surfactants and trimethylsilyl species. The analysis is consistent with the gas permeation measurements.

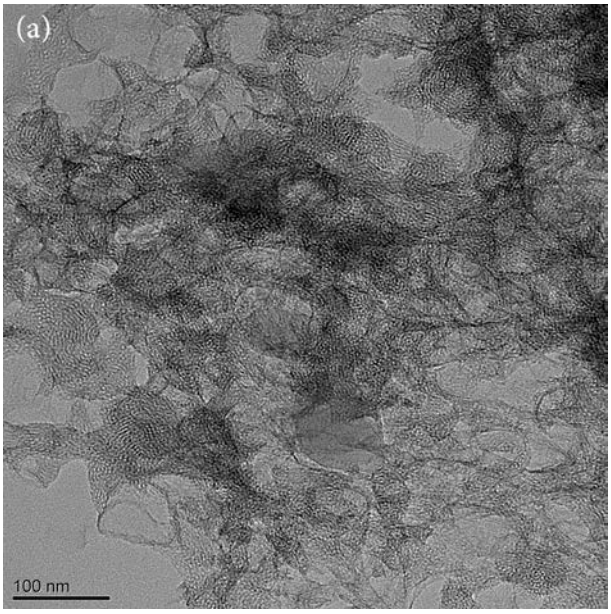

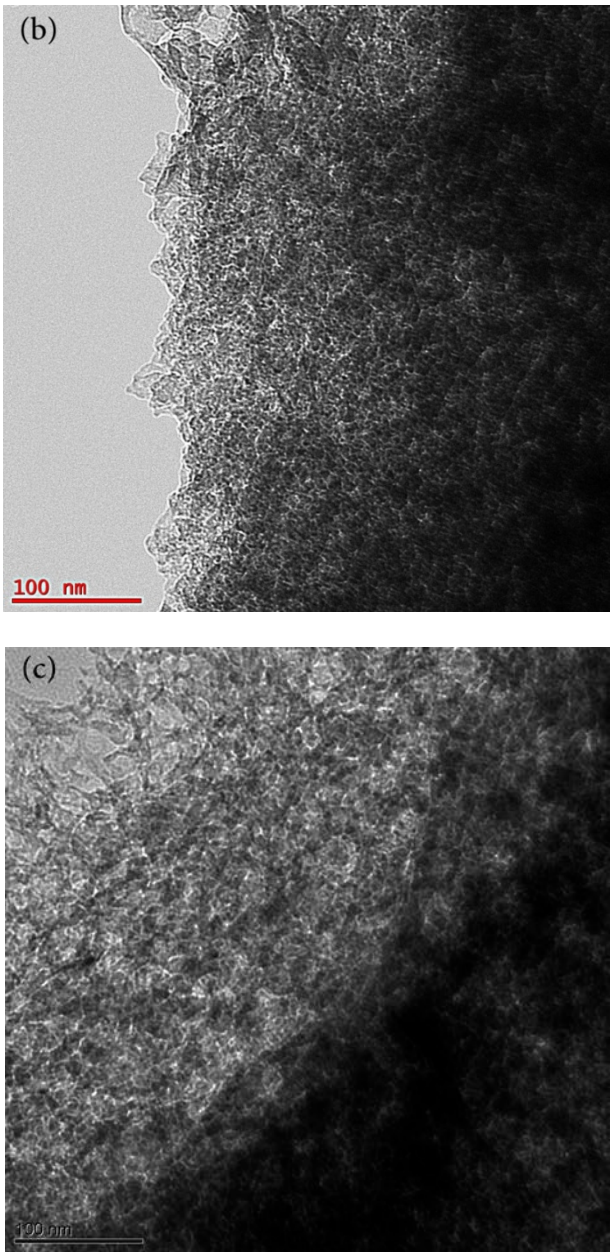

Figure 3-17. TEM images of the **(a)** template-extracted, **(b)** evacuated, and **(c)** silylated mesoporous membrane layers after dissolution of the Torlon® fiber.

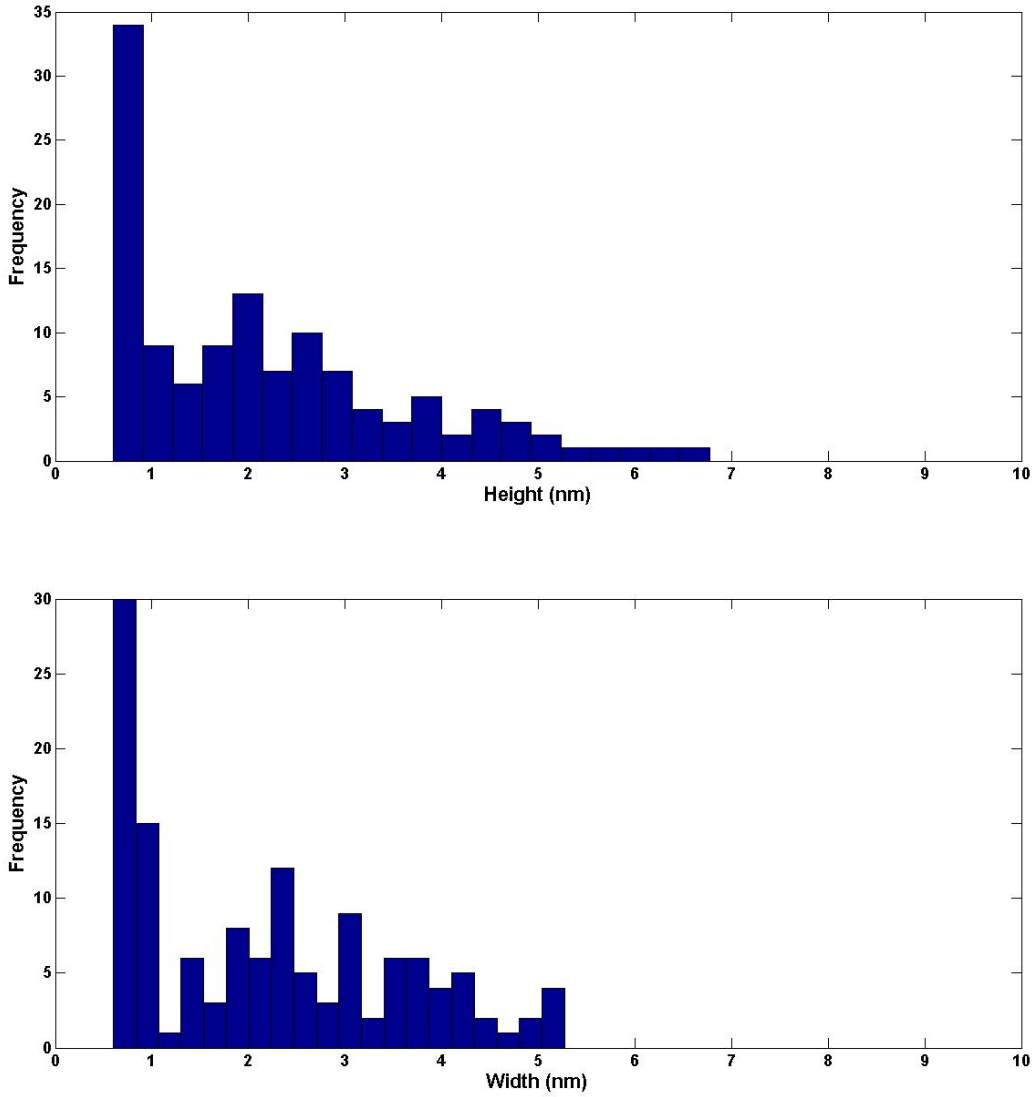

Figure 3-18. TEM analysis (height, width) for the extracted mesoporous silica/Torlon® hollow fiber membrane.

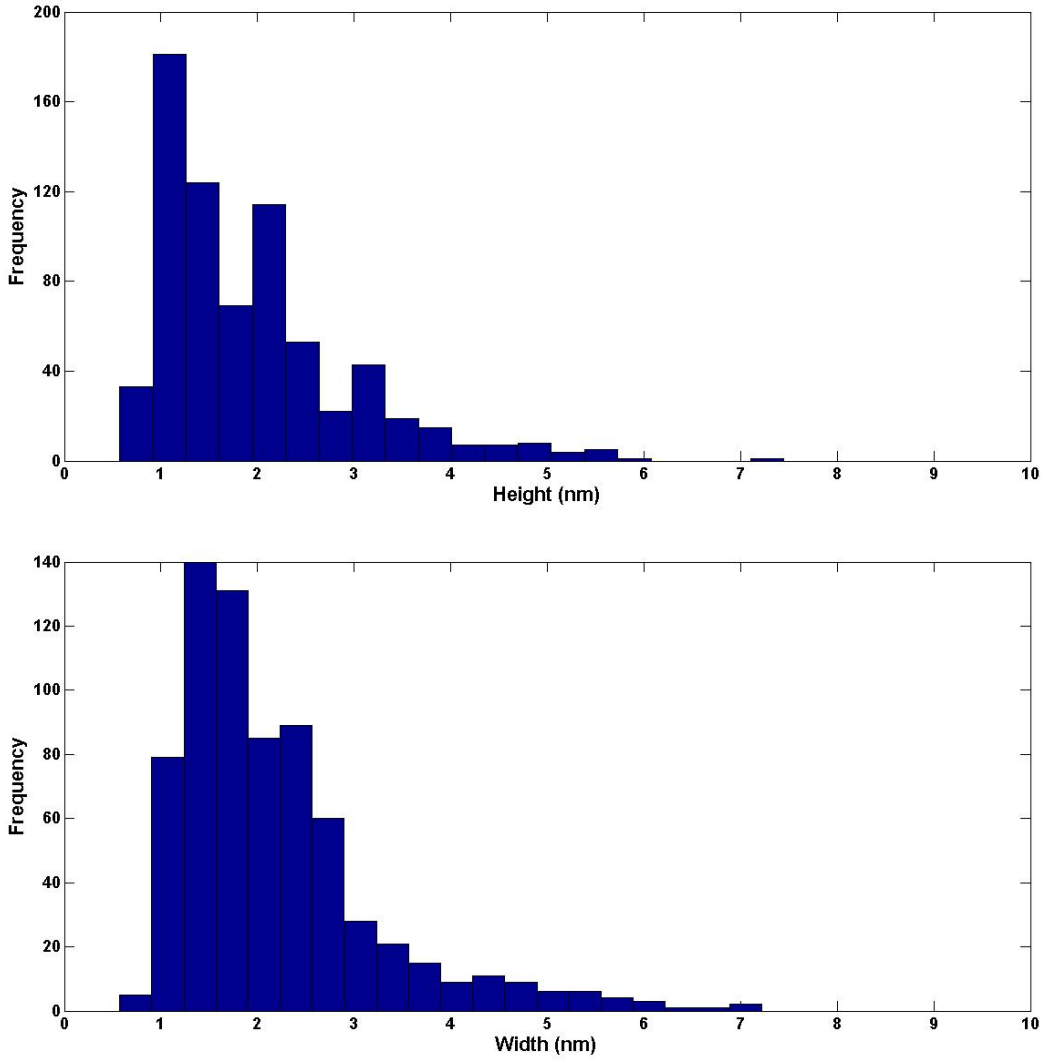

Figure 3-19. TEM analysis (height, width) for the evacuated mesoporous silica/Torlon® hollow fiber membrane.

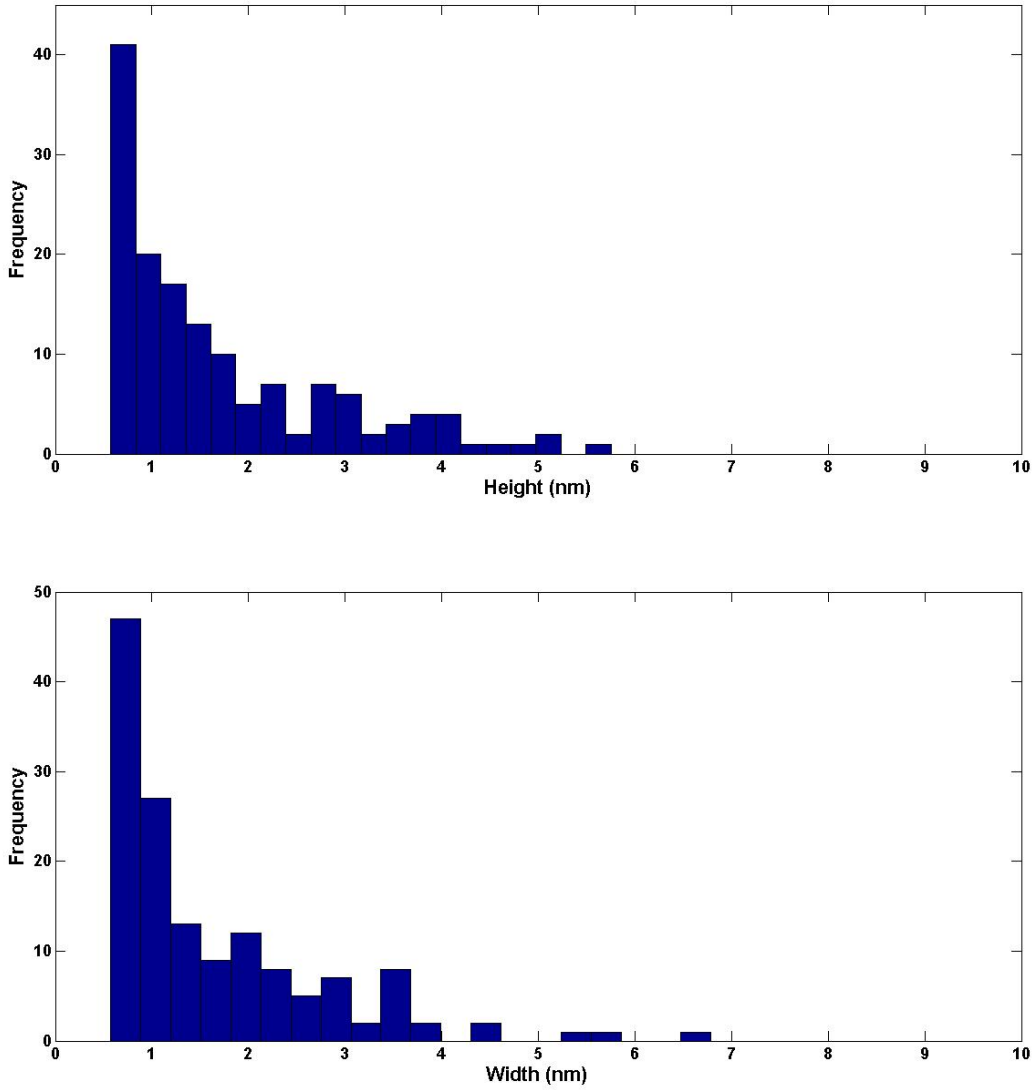

Figure 3-20. TEM analysis (height, width) for the silylated mesoporous silica/Torlon® hollow fiber membrane.

FT-ATR/IR was used to investigate the modification of the silica layer. Figure 3-22 shows the ATR/IR spectra of a mesoporous silica membrane at different stages of processing. The prepared samples were mounted on the poly(styrene) (PS) plates (Figure 3-21), and the PS plate itself was also measured to ensure that the ATR crystal was in

proper contact with the samples. The absorption peak around 1080 cm^{-1} is associated with the symmetric and asymmetric stretching vibrations of Si-O-Si linkages in mesoporous silica. After silylation of the mesoporous membrane, the intensity of this peak is significantly increased, which is likely due to the creation of additional Si-O-Si linkages by silylation. Also, the absorption peak around 800 cm^{-1} is more intense as compared to the template-extracted membrane. On the other hand, a relatively broad absorption peak located at 3200-3600 cm^{-1} is found in the template-extracted and evacuated membranes due to O-H stretching vibrations of the silanol groups and water molecules on the pore walls. These peaks completely disappear after silylation, suggesting that the surface silanols have been eliminated by condensation with the trimethylsilyl groups [155].

Figure 3-21. Illustration of mounted FT-ATR/IR sample.

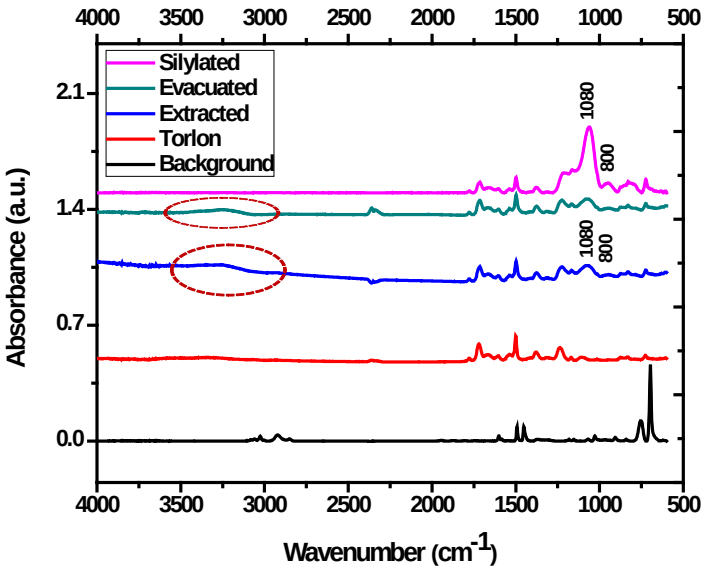

Figure 3-22. FT-ATR/IR absorption spectra of mesoporous silica/Torlon® hollow fiber membranes. The background spectrum is from the PS plate.

3.3.3 Pervaporation

Pervaporation data for five different organic/water mixtures are summarized in Figures 3-23, 3-24, and 3-25. To allow a comprehensive understanding of the permeation properties [100], the data are expressed in terms of flux, organic/water separation factor, permeance, permeability, and water/organic selectivity for template-extracted membranes, evacuated membranes, and silylated membranes, respectively. The feed mixtures used were (5/95 w/w) EtOH/water, MEK/water, EA/water, *i*-BuOH/water, and *n*-BuOH/water. The pervaporation experiments were performed at 303 K and 323 K.

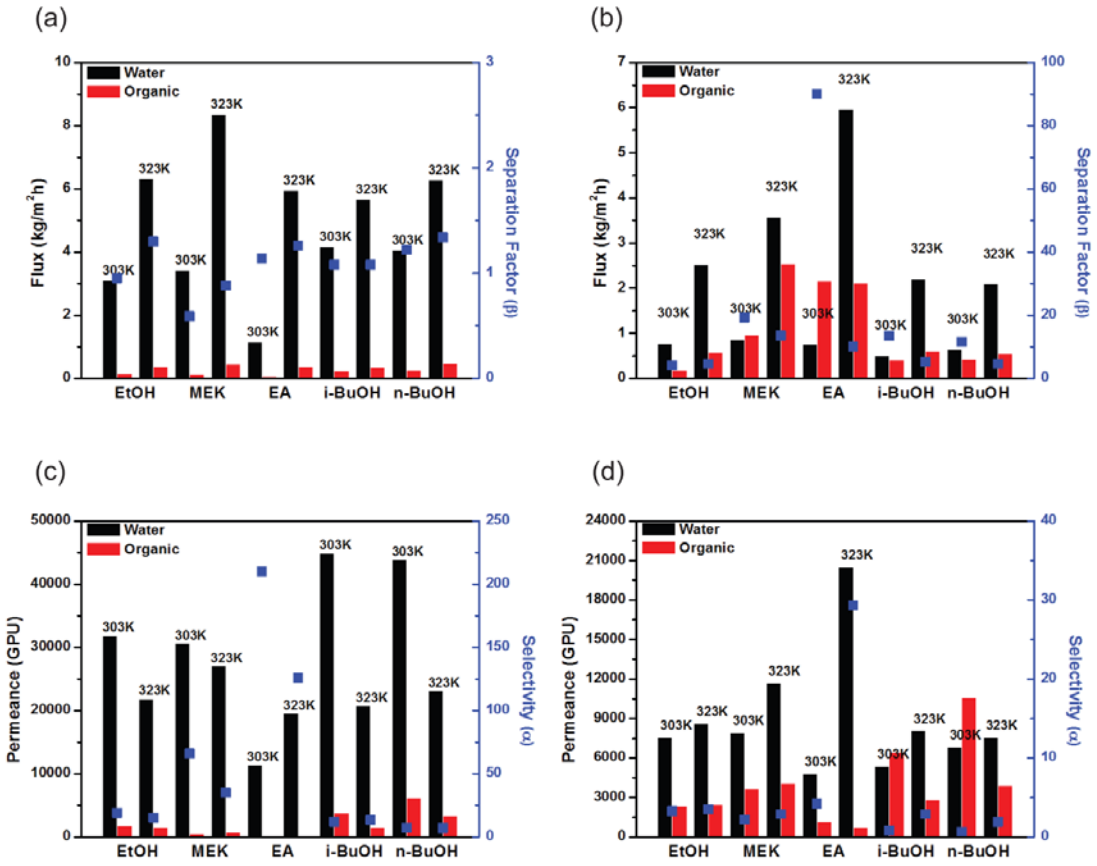

Figure 3-23. Pervaporation data (flux and organic/water separation factor) at 303 K and 323 K with 5 wt % organic/water feeds for **(a)** evacuated mesoporous membrane, and **(b)** silylated mesoporous membrane. Pervaporation data (permeance and water/organic selectivity) with 5 wt% organics/water feed mixtures for **(c)** evacuated mesoporous membrane, and **(d)** silylated mesoporous membrane.

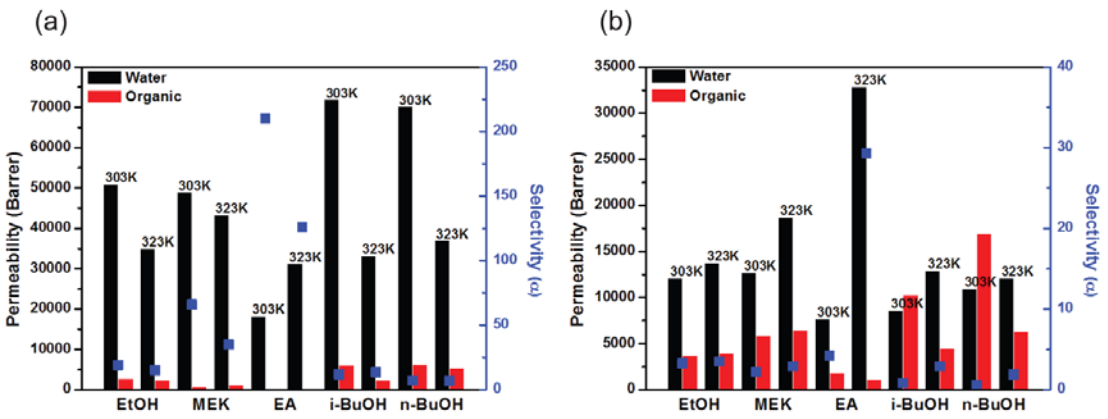

Figure 3-24. Pervaporation (permeability and selectivity) data with 5 wt % organics/water feed mixtures for **(a)** evacuated mesoporous membrane before silylation, and **(b)** silylated mesoporous membrane.

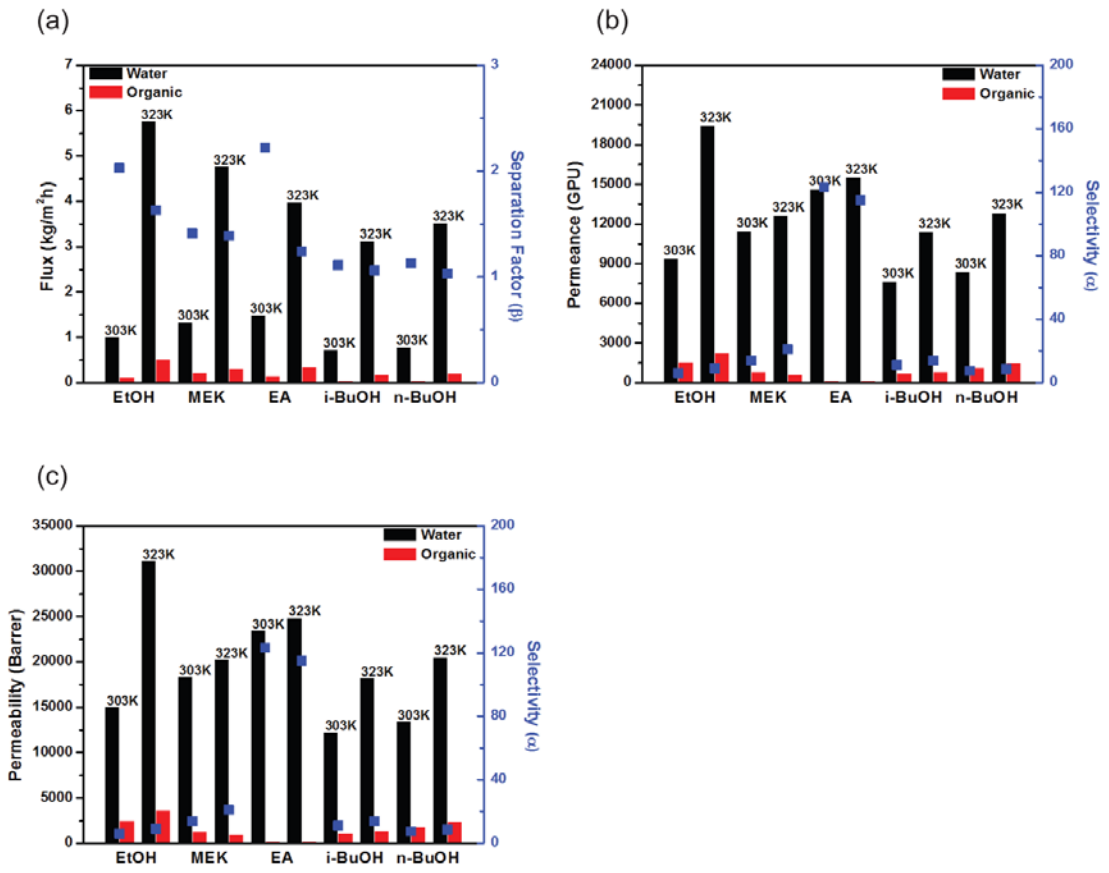

Figure 3-25. Pervaporation data with 5 wt % organics/water feed mixtures for extracted mesoporous membrane **(a)** flux and separation factor, **(b)** permeance and selectivity, and **(c)** permeability and selectivity.

Figures 3-23(a), and 3-23(b) show the fluxes and organic/water separation factors from the mixture pervaporation experiments. Beyond the model solutions composed of MEK and water or EA and water, the hydrophobic mesoporous membranes were also investigated for BuOH/water separations, due to the emerging importance of BuOH as a liquid fuel [156]. Both organic and water fluxes increase with temperature, but it is noteworthy that the water flux increases more than the organic flux. The separation factors of all the organic/water mixtures through the evacuated membranes range from

0.5 to 1.5, indicating that the membranes are not selective. They permeate almost the same amount of water and organic as is present in the feed mixture. However, the separation factor increases substantially after silylation, as this treatment renders the pore surface hydrophobic *via* modification by trimethylsilyl groups. The total fluxes somewhat increase or are maintained constant after silylation, and this is caused by a large increase in the fluxes of the organic species after silylation. The separation factors (*organics-over-water*) of the HMDS-treated mesoporous membrane at 303 K vary with the organic components in the order: EA (90) > MEK (19) > *i*-BuOH (13) > *n*-BuOH (11) > EtOH (4). On the other hand, higher water fluxes lead to decreased separation factors at the higher temperature of 323 K.

Figures 3-23(c), 3-23(d) show the permeances and *water-over-organic* selectivities (ratio of water and organic component permeances) for the two membranes, calculated from the membrane transport equation for any component *i*:

$$J_{\mathrm{i}} = \left(P_{\mathrm{m,i}}\right)\left(\gamma_{\mathrm{i}} x_{\mathrm{i}} p_{\mathrm{i}}^{\mathrm{sat}} - y_{\mathrm{i}} p_{\mathrm{p}}\right) \qquad (1)$$

where $\mathrm{J_i}$ is the molar flux of component *i*, $P_{\mathrm{m,i}}$ the permeance, γ_i the activity coefficient, x_{i} the feed mole fraction, $p_{\mathrm{i}}^{\mathrm{sat}}$ the saturated vapor pressure, y_{i} the permeate mole fraction, and p_{p} the permeate pressure.

Interestingly, the permeances of the organic species do not change much with increasing temperature, whereas the permeance of water increases significantly at 323 K. This result indicates that the permeance of the organic species is more highly dependent on adsorption of the components into the mesopores rather than diffusivity in the mesopores. Even though the silylated mesoporous membrane has high organic fluxes and

high organic separation factors (Figure 3-23(b)), it still has intrinsic water/organic selectivity in the range of 0.5-4 at 303 K. This is because the original non-silylated mesoporous membrane is highly hydrophilic and water selective. In other words, the trimethylsilyl groups are able to drastically decrease the flux of water through the membrane, but it still remains on the same order of magnitude as the organic fluxes. For completeness, Figure 3-24 shows the same information as Figures 3-23(c), (d) except that the permeability is displayed instead of permeance. It is seen that the silylated membranes display high permeabilities (on the order of 1,000 Barrer) for the organic species. Figure 3-25 represents the pervaporation data for the template-extracted mesoporous membrane. Similar to the evacuated membrane, the extracted membrane shows low organic separation factors (1-2.5) and high water selectivities (6-130). However, it has a significantly lower flux and permeance, because the residual surfactants and solvents partially block permeation.

As a result of the pervaporation properties discussed above, I find that the present silylated mesoporous silica/Torlon® hollow fiber membranes are able to upgrade 5 wt % organic/water feed mixtures are to 19 % EtOH, 53 % MEK, 83 % EA, 45 % *i*-BuOH, and 40 % *n*-BuOH permeate streams in a single pass at 303 K (Table 3-2). As shown in Table 3-2, this separation performance is considerably better than that of the template-evacuated membranes, and also (for completeness) the template-extracted mesoporous silica membranes (Table 3-3).

Table 3-2. Concentration upgrade from feed to permeate at 303 K.

	Evacuated membrane		Silylated membrane	
Feed solution	**Feed (wt %)**	**Permeate (wt %)**	**Feed (wt %)**	**Permeate (wt %)**
EtOH/water	4.7	4.7	5.4	19.1
MEK/water	6.0	3.6	5.4	52.6
EA/water	4.4	5.0	5.1	82.8
i-BuOH/water	5.2	5.6	5.7	44.7
n-BuOH/water	4.8	5.8	5.4	39.8

Table 3-3. Concentration upgrade from feed to permeate at 303 K for the template-extracted mesoporous silica/Torlon® hollow fiber membrane.

	Template-extracted membrane	
Feed solution	**Feed (wt %)**	**Permeate (wt %)**
EtOH/water	5.7	11.0
MEK/water	5.5	7.6
EA/water	4.0	8.5
i-BuOH/water	5.2	5.7
n-BuOH/water	4.8	5.4

In Table 3-4, the performance of the present membranes is compared to other hydrophobic membranes recently applied for organic/water pervaporation. The comparison focuses on two quantities of interest: the total flux through the membrane (F, in $kg.m^{-2}h^{-1}$) and the organic/water separation factor (β). Polymeric membranes show the

trade-off between flux and separation factor. The fluxes are extremely low for the membranes that have high separation factors, and *vice versa*. For example, a commercial PDMS membrane [157] has a comparable flux with the membranes presented in this work, but the separation factor is half of the silylated mesoporous silica membranes. Hydrophobic zeolite membranes show high performance in terms of both flux and separation factors [158]. However, there are very few reports describing separation of larger organic molecules such as MEK and EA from water with pure zeolite membranes [159, 160], because the water/organic diffusion selectivity counteracts the organic/water adsorption selectivity and leads to lower separation factors. Thus, zeolite membranes have been more successful in the dehydration of organic streams [158]. Two issues in the application of zeolite membranes are their high cost and uncertainties in the reliability of their fabrication in a defect-free manner. Small numbers of defects in zeolite membranes may have a large effect in lowering their hydrophobicity [158]. Zeolite membranes are about 10-50 times more expensive than polymeric membranes [161], and defect-free commercial-scale zeolite membranes are difficult to manufacture [162]. Composite membranes can combine the properties of polymers and zeolites, yielding improved performance [158]. However, the scale-up of such membranes to high-surface-area modules is an ongoing research topic. The present silylated mesoporous silica membranes are directly prepared on porous polymeric hollow fiber supports and can potentially be scaled up to very large surfaces areas. As seen from Table 3-4, silylation with HMDS already produces mesoporous silica hollow fiber membranes with high organic fluxes and good separation factors. The availability of a number of modifying agents and techniques for organic functionalization of mesoporous silica creates optimism that membranes with

higher performance can be attained starting from the platform studied in this chapter.

Table 3-4. Comparison of performance of hydrophobic membranes applied to organic/water pervaporation, including silylated mesoporous silica/Torlon® membranes in this work. PDMS: Polydimethylsiloxane, PVDF: polyvinylidene fluoride, POMS: polyoctylmethyl siloxane, TOA: trioctylamine, PTFE: polytetrafluoroethylene, PTMSP: poly(1-trimethylsilyl-1-propyne), PEBA: poly (ether) block amide, PVP: polyvinylpyrrolidone, HFP: hexafluoropropene, *: organic flux only reported.

Material Type	**Membrane**	**Molecule**	***F*** **($kg.m^{-2}h^{-1}$)**	β	**Ref #**
Polymers and Ionic Liquids	Commercial PDMS (Sulzer)	EtOH	0.8	2.1	[157]
	PDMS	MEK	0.06	100	[163]
	POMS	EtOH	1.2	8	[164]
	PDMS/PVDF	EtOH	0.45	15	[165]
	Polyphosphazene	EtOH	0.26	6.1	[166]
	Porous PTFE	EtOH	12	2	[167]
	PEBA	MEK	0.12	13.5	[163]
	Chitosan/PVP	EtOH	0.5	250	[168]
	Oleyl alcohol/POMS	*n*-BuOH	0.096	279	[169]
	Tetracyanoborate ionic liquid	*n*-BuOH	0.56	23	[170]
	P(VDF-HFP)[bmim]BF_4 ionic liquid	EA	0.66	144	[171]
	TOA liquid	EtOH	0.06	100	[172]
	Polyurethaneurea	EA	0.256	655	[173]
	PVDF-HFP	EA	1.9*	180	[174]
	Ethylene-vinyl acetate	EA	0.55*	118	[175]
	Poly(ethylene-co-vinyl acetate)	EA	0.72	120	[176]
	P(VDF-co-HFP)	EA	0.95	175	[177]
Zeolites	ZSM-5	EtOH	1.4	40	[178]
	ZSM-5	EtOH	9	5	[179]
		n-BuOH	4	10	
	Zr-Silicalite-1	EtOH	1	73	[180]
	MFI on YSZ hollow fiber	EtOH	7.4	47	[181]
	B-ZSM-11	MEK	0.6	220	[160]
	Silicalite	EtOH	0.04	35	[182]

		n-BuOH	0.01	90	
	Silicalite	*n*-BuOH	0.04	440	[183]
	Silicalite	MEK	0.25	32000	[184]
	Silicalite	EtOH	1.5	39	[185]
		n-BuOH	0.1	150	
Composites	PEBA/Silicalite (pure-silica MFI)	EtOH	0.8	3.6	[186]
	PTMSP/Cab-O-Sil TS 530 (commercial) hydrophobic silica	EtOH	9.5	18.3	[187]
		n-BuOH	9.5	104	
	PDMS/Silicalite	EtOH	0.06	10	[188]
		n-BuOH	0.040	70	
	PDMS/Silicalite	*i*-BuOH	5-11	25-42	[189]
	PDMS/ZrO_2-Al_2O_3	*n*-BuOH	0.46	26	[190]
	PDMS/Silicalite	*n*-BuOH	0.22	145	[191]
	PDMS/ZSM-5	EtOH	0.2	28	[192]
(Meso)Porous Silica	Phenyl-functionalized amorphous silica	EA	1.94	216	[193]
	Silylated MCM-48	EA	4.3	251	[155]
	Silylated MCM-48	EtOH	0.26	11	[139]
		MEK	1.4	201	
		EA	6.2	351	
	Silylated MCM-48	EtOH	0.15	3	[92]
		MEK	0.52	10	
		EA	0.55	17	
	Silylated mesoporous silica on Torlon® hollow fiber	EtOH	1	4	This work
		MEK	1.8	19	
		EA	2.9	90	
		n-BuOH	0.9	13	

3.4 Conclusion

In conclusion, the fabrication of continuous mesoporous silica membranes on polymeric hollow fibers *via* a facile, low-temperature process has been demonstrated, thereby suggesting a technologically scalable platform for separations with inorganic membranes. The membranes are defect-free and have a high gas flux (e.g., ~20,000 GPU for N_2). The open mesopores can be filled or modified with a variety of functional groups to tailor the selective properties of the membrane.

Hydrophobic trimethylsilyl groups are successfully incorporated on the surfaces of the mesopores, and the mesoporous silica layer remains intact and defect-free, based on XRD, electron microscopy, and gas permeation measurements. The silylated mesoporous membranes are selective for permeation of organic molecules in aqueous EtOH/water, MEK/water, EA/water, *i*-BuOH/water, and *n*-BuOH/water pervaporation experiments, whereas the bare membranes are selective for water. The good separation performance in organic/water mixtures can be attributed primarily to the hydrophobic nature of the silylated pores and the preferential adsorption of organics in the membrane. In relation to other types of organics/water separation membranes, the performance of the present membranes is quite promising for a range of potential organic/water separations. An important advantage of the present mesoporous silica/Torlon® hollow fiber membranes is their scalable, low-cost processing methodology. Due to the large possibilities in the selection of the functionalizing agents and the mesopore modification techniques, it is quite possible that the membrane performance can be greatly enhanced.

CHAPTER 4

SYNTHESIS AND GAS PERMEATION PROPERTIES OF AZIRIDINE-FUNCTIONALIZED MESOPOROUS-SILICA MEMBRANES ON POLYMERIC HOLLOW FIBERS

4.1 Introduction

Increased CO_2 concentration in the atmosphere due to combustion of fossil fuel has caused concerns about global climate change [194, 195]. Today the United States, the world's largest economy and consumer of energy, generates a quarter of global CO_2 emissions. Therefore, significant reduction of CO_2 emissions from the current level is necessary to stabilize atmospheric concentration of CO_2. A number of technologies, such as CO_2 capture and sequestration, and CO_2 utilization, are currently under investigation [196-199]. The current commercial technologies for CO_2 capture from flue gas are based on absorption using liquid amines [8, 200, 201]. The major drawback of using liquid amines is the large amount of energy required for their regeneration to release the captured CO_2 for compression and storage. Employing polymeric membranes is another approach for CO_2 separation from the flue gas [198, 202, 203]. For a polymeric membrane to be economically attractive, it should provide both high gas permeability and selectivity. Numerous studies have established a trade-off between the permeability and selectivity in polymer membranes [19]. The CO_2 permeability and CO_2/N_2 selectivity values for the polymer membranes used for CO_2 separation are significantly lower than desired cost-effective membrane based separation [18].

Koros *et al.* [20] suggested the use of mesoporous inorganic particles

incorporated to the polymer matrix as an attractive composite membrane for gas separations. They studied a variety of glassy polymers with inherently good diffusivity-based separation characteristics and found that the selectivity in O_2/N_2 separation significantly improved when the mesoporous silica particles were incorporated into the polymer matrix. They proposed that specific and nonspecific energetic interactions between the polymer and silica modify the packing of the polymer to create a better material for sieving.

Mesoporous silica membranes and thin films have a unique advantage that their pore size can be varied from 2-50 nm [21, 24, 25, 36], which can graft large polymeric molecules in the pores. Another unique feature of these membranes is that various amino groups (primary, secondary, and tertiary) can be attached to their surface silanol groups, which provide sites for CO_2 adsorption and facilitate its separation from N_2. I hypothesized that aziridine functionalized worm-like mesoporous silica membranes may show interesting properties for CO_2 separation from N_2 in the presence and absence of water vapor. I chose aziridine because it yields primary, secondary, and tertiary amino groups when polymerized, and these groups have high affinities for acidic CO_2 [204]. Thus, the final product is a hyper-branched amino silica (HAS) membrane. The presence of hyper-branched amine groups in the pores of mesoporous silica should provide a high CO_2/N_2 solubility selectivity [27, 205], because amine groups provide high CO_2 adsorption capacity and negligible N_2 adsorption capacity. The host mesoporous silica membrane possesses a worm-like pore structure, which decreases diffusion limitations. The worm-like mesoporous silica membranes contain a large concentration of surface silanol groups, which could be easily functionalized by amine-containing polymers. The

functionalization of mesoporous silica membranes with aziridine was hypothesized prevent the permeation of weakly interacting gases such as N_2, and lead to CO_2 selective properties.

On the other hand, some reports [206, 207] have suggested that the CO_2/N_2 selectivities significantly lower than 1 are obtained at very high polymer solubility parameters where the affinity between polymer segments and CO_2 reaches a maximum. Freeman *et al*. [207] showed that the CO_2/H_2 solubility selectivity afforded by polyethyleneimine (PEI) molecules was more than offset by the increase in H_2/CO_2 diffusivity selectivity due to PEI addition. Strong interactions between PEI molecules and CO_2 significantly hinder the diffusion of CO_2 and hence lead to H_2/CO_2 diffusivity selectivities significantly greater than 1. Therefore, the mesoporous silica membranes that are slightly N_2 selective on modification with aziridine may also become highly N_2 selective because of enhanced N_2/CO_2 diffusion selectivity owing to strong interaction of CO_2 (and hence slow diffusion) with polymeric amine molecules.

In this chapter, I describe the successful modification of worm-like mesoporous silica membranes on polymeric hollow fibers with aziridine to fabricate defect-free HAS membranes for CO_2 separation. Furthermore, I observed a counter-intuitive N_2 selectivity for HAS membranes in the dry gas permeation experiments. Considering kinetic diameter and affinity with amine groups of gas molecules, N_2 molecules are supposed to flow faster than CO_2 molecules when passing through amine modified pores. The HAS membranes showed CO_2 selective properties in the presence of water vapor. These phenomena are considered in more detail in the following sections. To the best of our knowledge, there have not been any studies of bi-functional (N_2 selective and CO_2

selective) permeation properties of any type of membrane.

4.2 Materials and Methods

4.2.1 Materials

The following reagents were obtained from the commercial suppliers and used as received without further purification: 2-chloroethylamine hydrochloride (Aldrich, 99%), sodium hydroxide (EMD, ACS grade, 97%), tetraethylorthosilicate (TEOS, 98% Sigma-Aldrich), cetyl trimethylammonium bromide (CTAB, Sigma-Aldrich), 1 N aqueous hydrochloric acid (HCl) solution (Sigma-Aldrich), ethanol (EtOH, BDH), Torlon® 4000T-LV (Solvay Advanced Polymers).

4.2.2 Synthesis of mesoporous silica membrane on Torlon® hollow fiber

Macroporous Torlon® (polyamide-imide) hollow fiber supports were fabricated by a dry-jet/wet-quench method, described in detail elsewhere [140]. The outer and inner diameters of the support fibers were ca. 380 μm and 230 μm, respectively. The fibers did not possess skin layers and had open pores of ~100 nm size at the outer surface. The mesoporous silica membrane was fabricated as described in our previous report [208]. Before the membrane coating, both ends of the fiber support were sealed with epoxy to prevent the membrane growth in the interior of the fiber support. The support Torlon hollow fibers were immersed in the coating solution for 5 hours at room temperature. The mixture had the molar composition of 1 TEOS : 0.425 CTAB : 0.00560 HCI : 62.2 H_2O. The hollow fiber membranes were aged with saturated TEOS vapor prior to use. A 22 cm-long fiber membrane was placed with 25 μL of TEOS in a closed vessel at 373 K for

24 hours. For surfactant extraction, the fiber membranes were washed with 0.05 N HCl/ethanol under stirring for 24 hours.

4.2.3 Synthesis of aziridine

Aziridine was synthesized from 2-chloroethylamine according to the previous report [204] with some modifications in the purification step. To a 250 mL round-bottom flask containing 2-chloroethylamine hydrochloride (30 g) was added a sodium hydroxide aqueous solution (25.8 g of sodium hydroxide in 170 g of deionized water). The resultant solution was heated to 323 K and stirred at this temperature for 2 hours. Aziridine was then recovered by a partial static vacuum distillation at 348 K. The collected distillate was dried over sodium hydroxide pellets and kept in a freezer overnight. Aziridine that phase-separated as an upper layer of liquid was recovered. The purified aziridine was obtained as colorless oil in 70-80 % yield and stored in a freezer. ^{1}H NMR (400.0 MHz, $(CD_3)_2SO$, TMS): δ (ppm) 1.17, 1.53; ^{13}C NMR (100.6 MHz, $(CD_3)_2SO$, TMS): δ (ppm) 17.4 [209]. Aziridine may be a carcinogen and reproductive hazard. Use extreme caution when handling these compounds. Only handle in a well-ventilated fume hood and always wear proper personal protection equipment.

4.2.4 Aziridine functionalization of mesoporous silica membrane

Polymerization of aziridine on the mesoporous membrane supports via vapor phase transport was carried out in a 290 mL glass pressure tube. Prior to aziridine functionalization, the surfactant-extracted mesoporous silica membranes were evacuated in a vacuum oven at 423 K under 0.07 atm, to remove physically adsorbed moisture and

residual surfactant. Also, the non-evacuated mesoporous silica membranes were functionalized with same way. A small glass test tube (12 × 75 mm, VWR) containing 3 g of aziridine was then placed inside the pressure tube. The pressure tube was closed tightly and maintained to a room temperature for 7 days of reaction time. After functionalization, the membranes were washed with ethanol for 30 min in a separate container under stirring to remove the physisorbed aziridine and polyamines from the sample surface. Then, the coated membranes were dried at room temperature before preparing the gas permeation module.

4.2.5 Characterization methods

Scanning electron microscopy (SEM) was performed with a LEO 1530 instrument to examine the membranes. The membrane samples were prepared on carbon tape and coated with gold to prevent image distortion due to surface charging.

4.2.6 Gas permeation measurements

Pure gas permeation was measured using a hollow fiber permeation testing system (Figure 4-1), constructed in-house as described earlier [143, 144]. Gases were fed into the bore (“tube side”) of the fiber interior at one end of the module. The temperature of the system was maintained at 308 K during the measurement. The flux through the walls of the fiber was measured on the “shell side” connected to a bubble flow meter. Atmospheric pressure was maintained on the downstream side. The permeance can also be expressed as the flux normalized by the transmembrane pressure (Δp_i), as shown by following equation.

$$P_i = \frac{F_i}{\Delta p_i} \quad (1)$$

A commonly used unit for gas permeance is the GPU (Gas Permeation Unit), where 1 GPU = 10^{-6} cm^3 (STP) cm^{-2} s^{-1} $cmHg^{-1}$. The ideal selectivity of the membrane is the ratio of the permeances of the individual gases. For single gas A and B, the ideal selectivity is described by:

$$\alpha_{A/B} = \frac{P_A}{P_B} \quad (2)$$

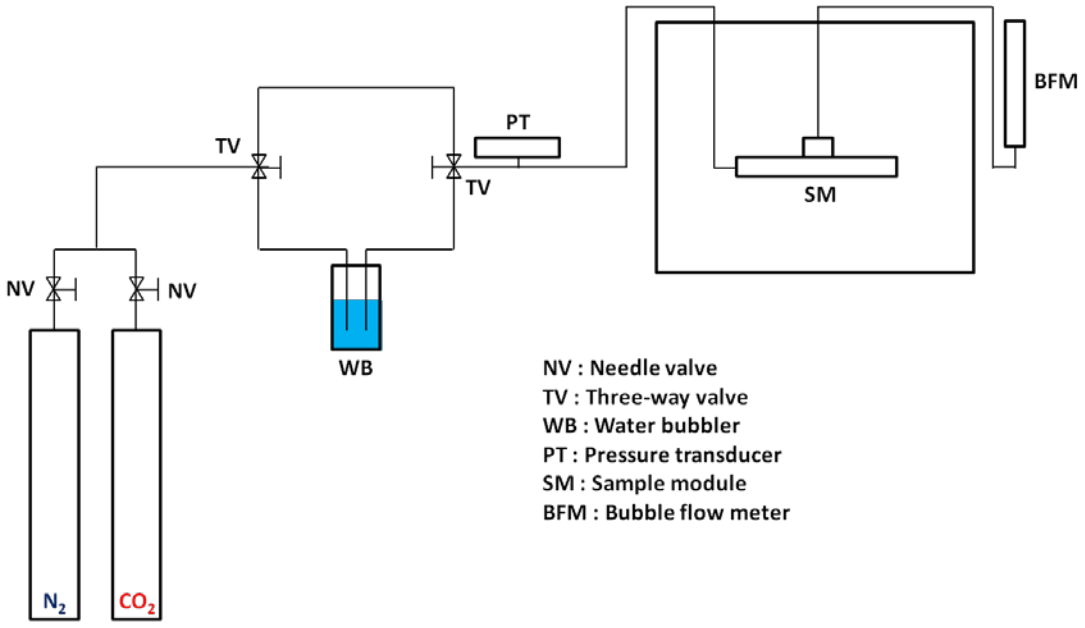

Figure 4-1. Schematic diagram of the experimental setup for permeation measurements.

Separate HAS membranes were measured with an in situ membrane degassing procedure. HAS membranes were degassed at 323 K under N_2 flow before measurement, and confirmed that initial and steady-state permeation values are corresponding to the data below.

4.3 Results and Discussion

4.3.1 Membrane characterization

Figures 4-2 shows cross-sectional SEM images of the aziridine functionalized mesoporous silica/Torlon® hollow fiber membranes without and with the evacuation process. Continuous and uniform silica layers are obtained on the outer surface of the hollow fiber in a highly reproducible manner. Figure 4-3 shows top-view SEM images of the aziridine functionalized mesoporous silica/Torlon® hollow fiber membranes without and with the evacuation process. The continuous and crack-free silica layers indicate that the membranes are not damaged by aziridine functionalization. Also, there is no change in the membrane morphology after amine-functionalization.

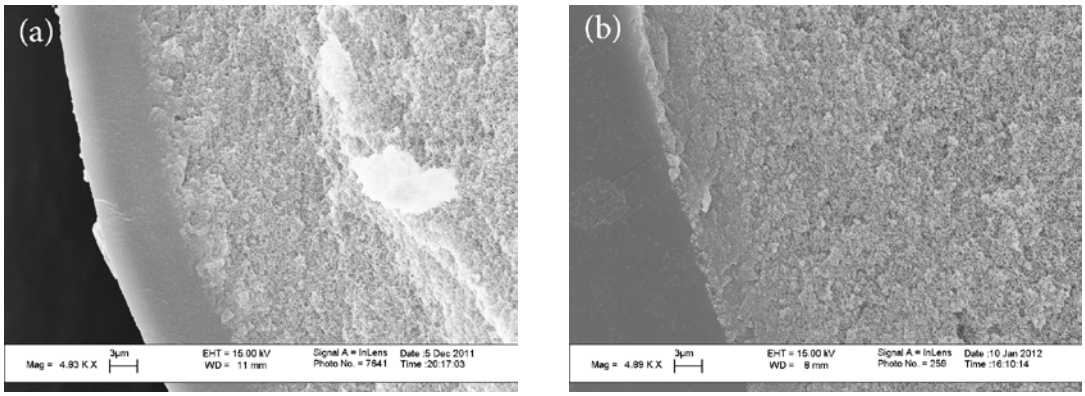

Figure 4-2. Cross-sectional SEM images of aziridine functionalized membranes **(a)** without evacuation, and **(b)** with evacuation.

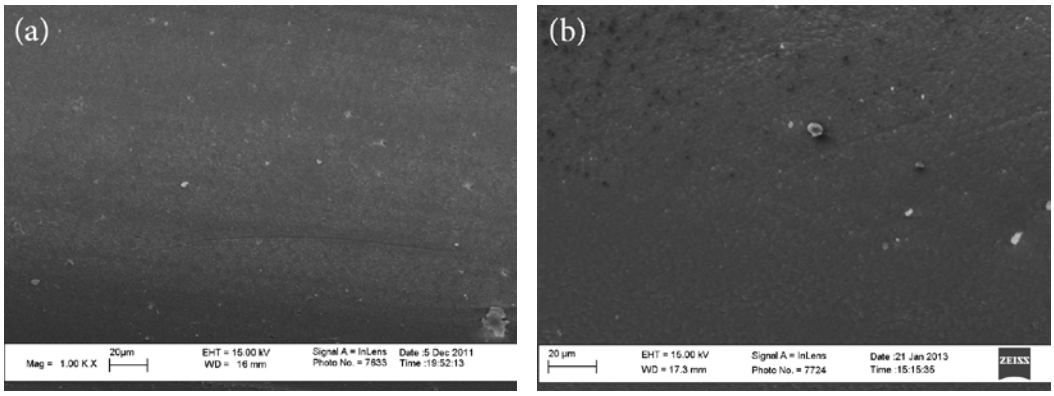

Figure 4-3. Top-view SEM images of aziridine functionalized membranes **(a)** without evacuation, and **(b)** with evacuation.

4.3.2 Gas permeation characteristics

Mesoporous silica membranes after pore modification with aziridine were characterized by pure N_2 and CO_2 gas permeation to study the effect of aziridine attachment on gas permeation and to confirm the synthesis of defect-free HAS membranes. Figure 4-4 shows cyclic dry gas permeation data for CO_2 and N_2 for an aziridine functionalized mesoporous silica membrane. Each gas is contacted with the membrane for 1500 min before switching to the other gas. Overall, permeances of both gases are significantly decreased after aziridine-functionalization of both the extracted and evacuated membranes, suggesting decreased pore sizes and pore volumes due to modification. Observing the huge reduction of permeances after amine functionalization, it is inferred that the incorporated aziridine forms HAS in the membrane pores. For example, the N_2 permeance decreased from 3,000 GPU to 10 GPU for the extracted membrane (Figure 4-4 (a)), from 20,000 GPU to 12 GPU for the evacuated membrane (Figure 4-4 (b)). These kinds of significant reduction are not based on the single aziridine

molecule, but due to hyper-branched amines. More interestingly, CO_2 permeance values for the HAS membrane were decreased as the permeation time was increased, indicating CO_2 molecules are strongly adsorbed to the amine groups. The adsorbed CO_2 molecules almost block the pores by reducing effective pore size, and causing stabilized permeance less than 2 GPU. When I switched the gas from CO_2 to N_2, the gas permeance was gradually recovered to the initial values (before CO_2 adsorption) in a short period of time, suggesting the adsorbed CO_2 molecules are desorbed out by N_2 flow and the effective pore size is recovered. Finally, this counter-intuitive phenomenon brings a conclusion of reverse selectivity (N_2/CO_2) of 5-7. Also, the cyclic test suggests that this reverse selectivity occurs reversibly. Figure 4-5 and Figure 4-6 show same information as Figure 4-4, but in a more stretched manner to identify the steady state point.

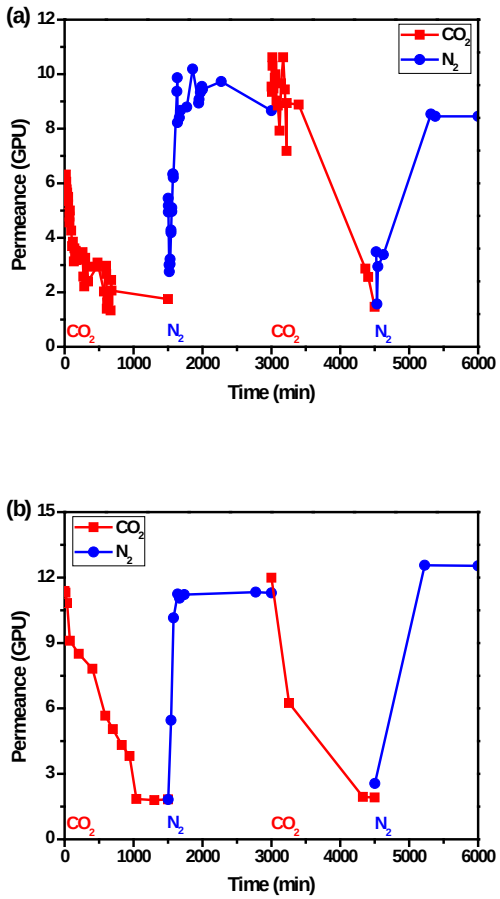

Figure 4-4. Cyclic dry gas permeation of CO_2 → N_2 → CO_2 → N_2 at 308 K for aziridine functionalized mesoporous silica/Torlon® hollow fiber membranes synthesized **(a)** without evacuation, and **(b)** after evacuation.

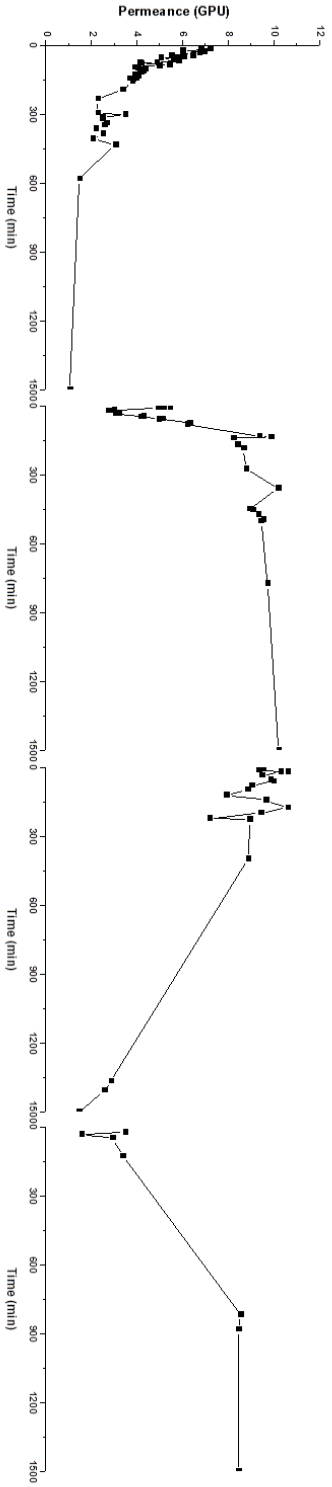

Figure 4-5. Cyclic dry gas permeation CO_2 → N_2 → CO_2 → N_2 for aziridine functionalized mesoporous silica/Torlon® hollow fiber membranes without evacuation at 308 K.

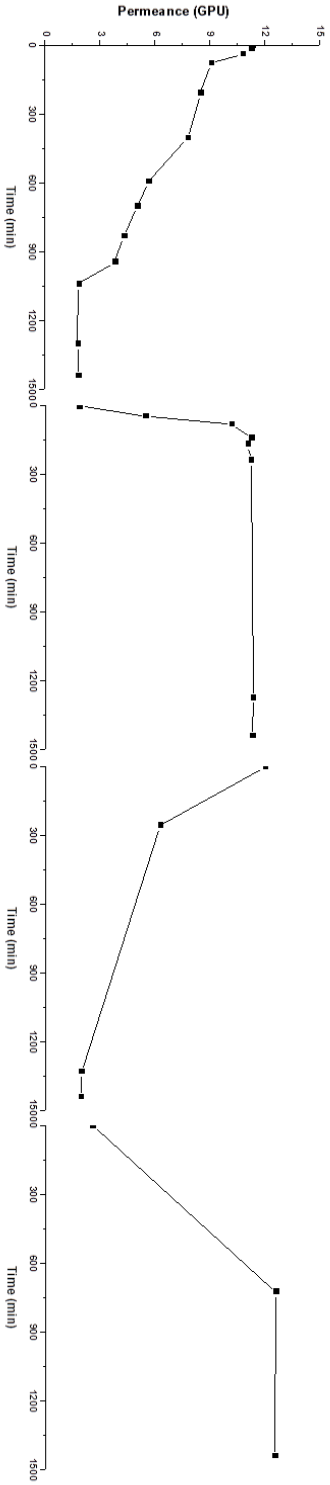

Figure 4-6. Cyclic dry gas permeation CO_2 → N_2 → CO_2 → N_2 for aziridine functionalized mesoporous silica/Torlon® hollow fiber membranes after evacuation at 308 K.

CO_2 adsorption to the HAS during dry gas permeation occurs on the amine pairs of primary-primary, primary-secondary, and secondary-secondary amines, as shown in Figure 4-7, and barely occurs on the pairs of primary-tertiary and secondary-tertiary due to the steric hindrance. By this acid-base reaction, CO_2 molecule is covalently bonded to the one of the amines, and the other amine is converted to an alkylammonium ion. Different from primary and secondary amines, tertiary amine pairs are not involved in the CO_2 adsorption [210]. Figure 4-8 describes the schematic of a pore channel of the HAS membrane, and the CO_2 molecule adsorbed HAS membrane. Amine groups are positioned closely due to the crosslinking when reacted with CO_2 gas molecules. As a result, the effective pore size is significantly decreased.

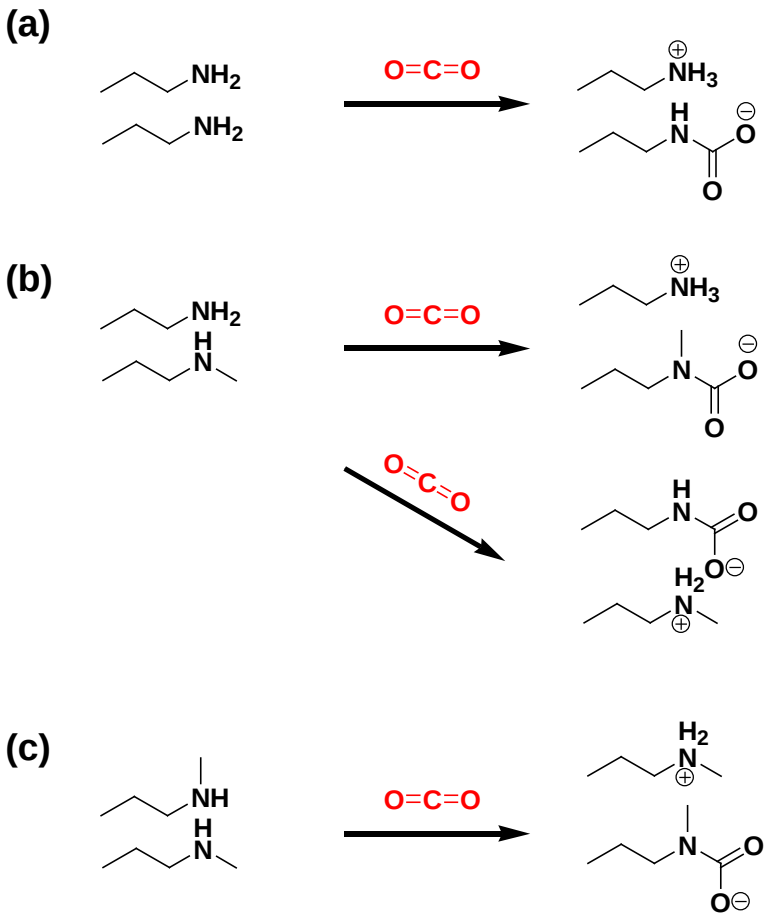

Figure 4-7. Mechanisms of CO_2 adsorption to the pairs of **(a)** primary-primary, **(b)** primary-secondary, and **(c)** secondary-secondary amines.

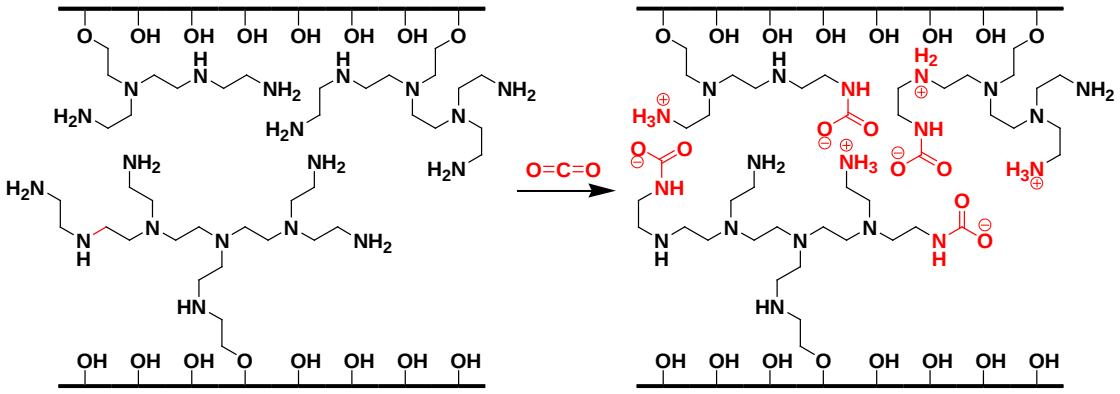

Figure 4-8. Mechanism of CO_2 gas adsorption through crosslinking (leading to reverse selectivity) by aziridine functionalized membrane.

In the presence of water vapor, the N_2 permeances were much lower than those of dry gas permeation (Figure 4-9), but CO_2 permeances were slightly increased. Thus, the ratios of N_2 and CO_2 permeances in single gas permeation experiments were much lower than those of dry gas permeation. In the presence of water vapor, the CO_2 adsorption capacity of the HAS membrane increases considerably, leading to higher CO_2 solubility [211]. Additionally, there is probably a slight contribution of adsorption by tertiary-tertiary amine pairs in the presence of water vapor [210]. In particular, the aziridine-functionalized membrane after evacuation shows a CO_2/N_2 selectivity of 2.7. The decrease in gas permeance of N_2 is a result of water vapor adsorption in HAS membranes, expected to lower the free volume available for permeation. From this result, I speculate that the evacuated membrane is modified with aziridine in a more controlled manner.

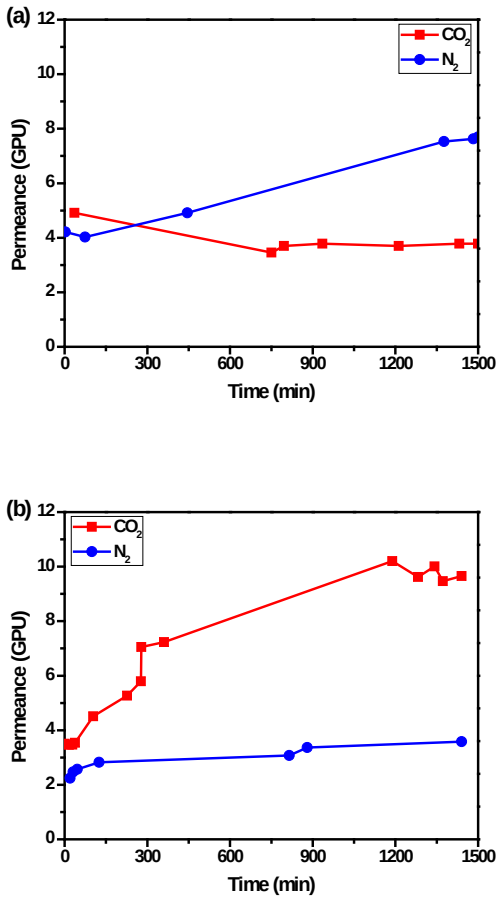

Figure 4-9. Wet gas permeation of N_2 and CO_2 at 308 K for aziridine functionalized mesoporous silica/Torlon® hollow fiber membranes synthesized **(a)** without evacuation, and **(b)** after evacuation.

The nature of the chemical interactions between the HAS membrane and CO_2 changes in the presence of moisture. Figure 4-10 shows the CO_2 hypothesized adsorption mechanism to the primary amine groups in the presence and absence of moisture. The interaction between the basic surface and acidic CO_2 molecules is thought to result in the formation of surface ammonium carbamates under anhydrous conditions and in the formation of ammonium bicarbonate and carbonate species in the presence of water. Thus,

in dry CO_2 permeation, adsorption capacities are limited to one mole of CO_2 for every two moles of surface-bound amine groups; in the presence of water, adsorption capacities may increase up to two moles of CO_2 per two moles of surface-bound amine groups. Additionally, amine groups are less close to each other, because each amine reacts with the CO_2 molecule separately. Additionally, CO_2 molecules are hopping through amine groups due to the high adsorption capacity in the presence of water, because there are available adsorption sites locally.

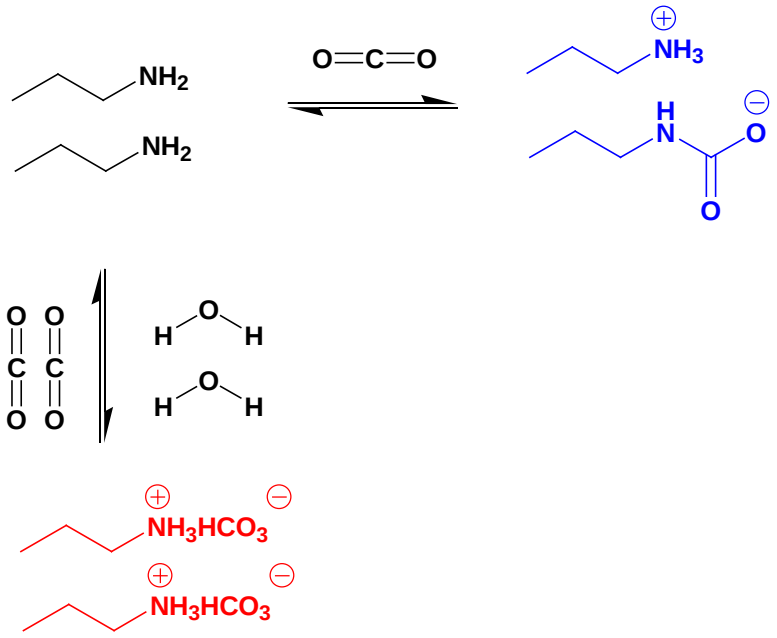

Figure 4-10. Surface reaction of tethered amine groups with CO_2.

Table 4-1 summarizes the steady state single gas (N_2 and CO_2) permeation results for two different HAS membranes at 308 K. Both membranes show N_2 selectivity in dry gas permeation, and this transforms into CO_2 selective behavior in wet gas permeation. As a result, I suggest that the evacutated membrane to remove moisture and residual

surfactant is modified in a more controlled manner by aziridine. As a result, the HAS membrane shows CO_2 selective properties due to facilitated transport of CO_2 by hopping from one amine site to the other in presence of water.

Table 4-1. Steady-state single gas permeation results at 308 K.

Membranes	Gas	N_2	CO_2	Selectivity (N_2/CO_2)
Aziridine functionalization w/o evacuation	Dry	8.6	1.6	5.4
	Wet	7.7	3.8	2.0
Aziridine functionalization after evacuation	Dry	12	1.8	6.7
	Wet	3.6	9.7	0.37

On the basis of combined permeation data, it is concluded that the HAS membrane can be N_2 selective in dry-gas permeation. I speculate that the hyper-branched amines are highly modifying the pores, and additional CO_2 adsorption blocking most of the remained spaces. On the other hand, it is also concluded that the HAS membrane can be CO_2 selective in wet gas permeation, because water facilitates the CO_2 hopping by reducing the activation energy for hopping between amine sites.

4.4 Conclusions

Aziridine was successfully introduced into the worm-like mesopore channels of mesoporous membranes on polymeric hollow fiber supports, where it reacts to form HAS

structures on the internal pore surfaces. The HAS-containing membranes were selective for N_2 over CO_2 at 308 K in anhydrous pure gas permeation. However, the same membranes were selective to CO_2 over N_2 in the presence of water vapor. This change in behavior is less clear in the non-evacuated membranes, which have residual surfactant in the pores,thereby causing the low concentration of modifiable surface silanol groups. Overall, this study describes unequivocally gas permeation characteristic of aziridine-functionalized mesoporous silica membranes in the absence and presence of water vapor.

CHAPTER 5

SUMMARY AND FUTURE WORK

5.1 Summary

The work described in this thesis develops the science and engineering of mesoporous silica membranes for molecular transport and separations. A number of significant challenges along this path were addressed by a strategy that combined new approaches for supported membrane fabrication, silylation, amine-functionalization, application to liquid & gas separations, surface property investigations, and characterization techniques. These investigations have addressed several challenges of mesoporous silica membrane technology and created opportunities for applying mesoporous silica materials in a scalable membrane separation platform.

5.1.1 Silylated MCM-48 membrane on α-alumina disk for organic/water separation

In chapter 2, the fabrication of continuous MCM-48 membranes on α-alumina disks via seed layer deposition and hydrothermal growth was presented. The seeded MCM-48 membranes have low defect density and high gas fluxes. By means of the seed layer deposition, MCM-48 membranes can be formed on the top of α-alumina supports with little silica infiltration into the macroporous supports. Also, the porosity of intact MCM-48 membranes was assessed by nitrogen physisorption for the first time. Compared to the unseeded MCM-48 membrane, the seeded membrane has a larger pore volume and surface area.

The obtained membranes were silylated with hexamethyldisilazane (HMDS) to

tailor selective properties of the membrane. The HMDS-treated MCM-48 membranes were selective for permeation of organic molecules in aqueous ethanol (EtOH)/water, methyl ethyl ketone (MEK)/water, and ethyl acetate (EA)/water permeation experiments, whereas the unmodified membranes were significantly selective for water. The good separation performance in organic/water mixtures can be attributed primarily to the hydrophobic nature of the silylated pores and the preferential adsorption of organics on the membrane.

5.1.2 Mesoporous silica membrane on polymeric hollow fiber for organic/water separation

To apply mesoporous silica membrane as technologically scalable platform for separations, the fabrication of continuous mesoporous silica membranes on polymeric hollow fibers *via* a facile, low-temperature process was demonstrated. The membranes synthesized by this approach are defect-free and have a high gas flux. The open mesopores were modified with trimethylsilyl groups to tailor the hydrophobic properties of the membrane, and the mesoporous silica layer remained intact and defect-free, as exhibited by X-ray diffraction, electron microscopy, and gas permeation measurements.

The silylated mesoporous membranes are selective for permeation of organic molecules in aqueous EtOH/water, MEK/water, EA/water, *iso*-butanol/water, and *n*-butanol/water pervaporation experiments, whereas the bare membranes are selective for water. The good separation performance in organic/water mixtures can be attributed primarily to the hydrophobic nature of the silylated pores and the preferential adsorption of organics in the membrane. In relation to other types of organics/water separation

membranes, the performance of the present membranes is quite promising for a range of potential organic/water separations. An important advantage of the present mesoporous silica/Torlon® hollow fiber membranes is their scalability, and as well as their low-cost processing methodology.

5.1.3 Mesoporous silica membrane on polymeric hollow fiber for gas separation

Synthesis and gas transport properties of aziridine-functionalized mesoporous silica membranes on polymeric hollow fibers have also been investigated. The synthesized worm-like mesoporous silica membranes on polymeric hollow fiber were amine-functionalized with aziridine and their transport properties were studied to understand the effects of surface functionalization on gas separations. This new hybrid aminosilica membrane had very interesting and counter-intuitive N_2 selective permeation properties in dry gas permeation. Detailed characterization of the membrane structure and its permeation behavior showed this was due to strong adsorption of CO_2 leading to reduced gas flux due to CO_2-induced amine crosslinking. This hyper branched amino silica membrane is a very promising new material for acid gas capture from flue gas streams. More interestingly, this membrane showed CO_2 selective property when applied to humid gas permeation. Water in humid gas affect the adsorption of CO_2 molecules by reducing crosslinking, and finally the CO_2 flows through facilitated transport by hopping of CO_2 molecules. While the selectivity values in this particular example (CO_2/N_2 separation) were not high, this work demonstrates that such properties can be controlled and used in other separations as well.

5.2 Future Works

The present work leads to several interesting avenues for further research, some of which are outlined below.

5.2.1 Extension of silylation techniques to other mesoporous M41S membranes

MCM-48 and worm-like mesoporous silica have an extensive literature and were used as model materials in this thesis. However, they are not necessarily the best materials for a particular separation application. There are several mesoporous silicas that can be used in the fabrication of modified silica membranes, such as MCM-41 and MCM-50 (Figure 5-1). The pore modification developed in this study can be applied to the pore of these mesoporous silicas to control the loading of functionalizing agents and selective properties. This is one of the potential advantages of the methods developed in this thesis over compatibilization using silane and amine chemistry. It is expected that membranes have not only high flux but also have more desirable structure for homogeneous pore modification when the MCM-41 membranes are synthesized perpendicular to support materials [212, 213]. With further optimization of the silylation conditions (loading and the type of silyl group) on 2D membranes, this technique has potential for significant performance enhancements. More interestingly, the study of pore size dependency is also possible by applying the pore-expanded mesoporous silicas [214, 215] to the membrane configuration and further silylation.

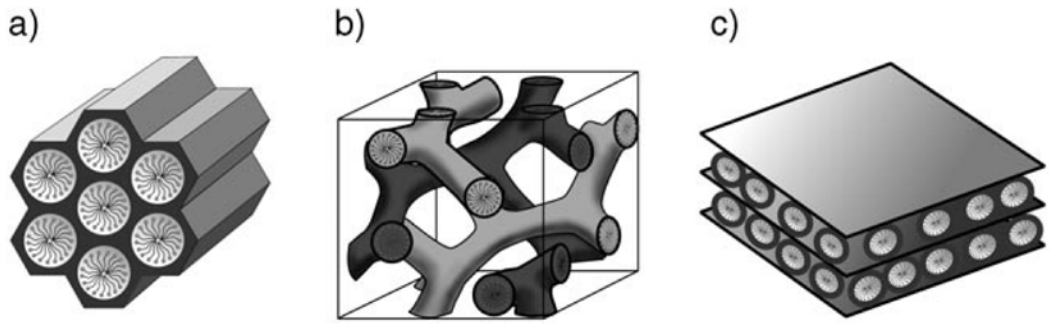

Figure 5-1. Structures of mesoporous M41S materials: **(a)** MCM-41 (2D hexagonal, space group *p6mm*), **(b)** MCM-48 (cubic, space group *Ia3d*), and **(c)** MCM-50 (lamellar, space group *p2*) [45].

5.2.2 Direct characterization of organic loading and pore structure for modified mesoporous silica membranes

The structural characterization of thin organic-modified silica membranes is general quite challenging, and most previous works are focused on silica powder characterizations as a surrogate for the membrane characterizations [31, 32, 138]. However, in this thesis it has been shown that the organic-modification characteristics of membranes can be different from those of powders. Properties such as the organic loading in the mesopores as well as details of the pore morphology in the for modified mesoporous silica membranes are still unknown due to the limitations of conventional characterization methods. Two factors causing this situation are the small amount of membrane sample on top of the much thicker polymeric support, and the curvature of hollow fiber support. This impedes the effectiveness of techniques such as X-ray diffraction and FT-ATR/IR. The use of thicker membranes on a flat support could be useful in gaining more precise information on the organic-modified silica membrane layer.

After dissolving out the polymer support, sufficient amount of sample may be obtained for direct characterizations such as thermogravimetric analysis and N_2 physisorption. In addition, thicker modified mesoporous silica membranes on flat supports can allow more detailed X-ray/synchrotron and FT-ATR/IR studies.

5.2.3 Application to dehydration of organic using hydrophilic mesoporous silica membranes

In this thesis, silylated hydrophobic mesoporous silica membranes have been studied for the organic/water separations. On the other hand, hydrophilic membranes are also of interest, for example in the dehydration of organic-rich streams as shown in Figure 5-2. As discussed in previous chapters, the as-synthesized mesoporous silica membranes are hydrophilic due to the large number of surface silanol groups. Incorporation of amino groups enables further hydrophilization of these organic-inorganic hybrid materials. It has been recently shown that the polar nature of amine groups resulted in increased adsorption of water molecules in the functionalized mesopores, and this observation was applied to the dehydration of organics [216]. Since the present mesoporous silica membranes are already synthesized in a hollow fiber configuration as described in this thesis, they may also comprise a technologically scalable platform for water separations with hydrophilic membranes.

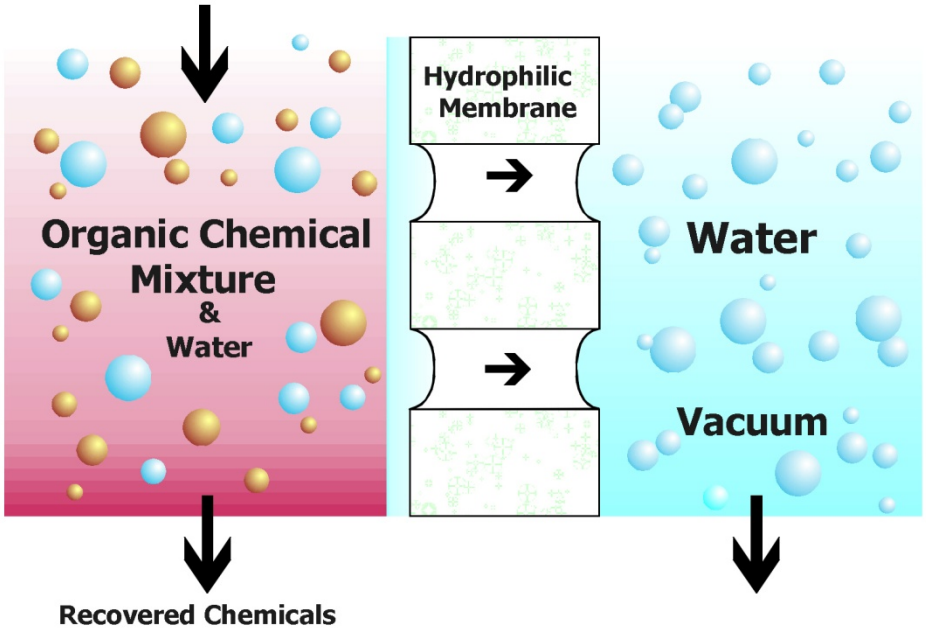

Figure 5-2. Hydrophilic membranes used to remove water from a chemical or mixture of chemicals.

REFERENCES

[1] R. Anwander, I. Nagl, M. Widenmeyer, G. Engelhardt, O. Groeger, C. Palm and T. Roser, Surface characterization and functionalization of MCM-41 silicas via silazane silylation, Journal of Physical Chemistry B, 104 (2000) 3532-3544.

[2] C. T. Kresge, M. E. Leonowicz, W. J. Roth, J. C. Vartuli and J. S. Beck, Ordered mesoporous molecular-sieves synthesized by a liquid-crystal template mechanism, Nature, 359 (1992) 710-712.

[3] L. Wang, X. L. Han, J. D. Li, L. Qin and D. J. Zheng, Preparation of modified mesoporous MCM-41 silica spheres and its application in pervaporation, Powder Technology, 231 (2012) 63-69.

[4] D. Y. Zhao, Q. S. Huo, J. L. Feng, B. F. Chmelka and G. D. Stucky, Nonionic triblock and star diblock copolymer and oligomeric surfactant syntheses of highly ordered, hydrothermally stable, mesoporous silica structures, J. Am. Chem. Soc., 120 (1998) 6024-6036.

[5] J. S. Beck, J. C. Vartuli, W. J. Roth, M. E. Leonowicz, C. T. Kresge, K. D. Schmitt, C. T. W. Chu, D. H. Olson, E. W. Sheppard, S. B. Mccullen, J. B. Higgins and J. L. Schlenker, A new family of mesoporous molecular-sieves prepared with liquid-crystal templates, J. Am. Chem. Soc., 114 (1992) 10834-10843.

[6] D. Y. Zhao, J. L. Feng, Q. S. Huo, N. Melosh, G. H. Fredrickson, B. F. Chmelka and G. D. Stucky, Triblock copolymer syntheses of mesoporous silica with periodic 50 to 300 angstrom pores, Science, 279 (1998) 548-552.

[7] Y. S. Lin, I. Kumakiri, B. N. Nair and H. Alsyouri, Microporous inorganic membranes, Separation and Purification Methods, 31 (2002) 229-379.

[8] E. B. Rinker, S. S. Ashour and O. C. Sandall, Absorption of carbon dioxide into aqueous blends of diethanolamine and methyldiethanolamine, Industrial & Engineering Chemistry Research, 39 (2000) 4346-4356.

[9] N. Hiyoshi, K. Yogo and T. Yashima, Adsorption of carbon dioxide on amine modified SBA-15 in the presence of water vapor, Chemistry Letters, 33 (2004) 510-511.

[10] T. W. Kim, R. Ryoo, M. Kruk, K. P. Gierszal, M. Jaroniec, S. Kamiya and O. Terasaki, Tailoring the pore structure of SBA-16 silica molecular sieve through the use of copolymer blends and control of synthesis temperature and time, Journal of Physical Chemistry B, 108 (2004) 11480-11489.

[11] T. Yu, H. Zhang, X. W. Yan, Z. X. Chen, X. D. Zou, P. Oleynikov and D. Y. Zhao, Pore structures of ordered large cage-type mesoporous silica FDU-12s, Journal of Physical Chemistry B, 110 (2006) 21467-21472.

[12] S. Ruthstein, J. Schmidt, E. Kesselman, R. Popovitz-Biro, L. Omer, V. Frydman, Y. Talmon and D. Goldfarb, Molecular level processes and nanostructure evolution during the formation of the cubic mesoporous material KIT-6, Chemistry of Materials, 20 (2008) 2779-2792.

[13] T. Yokoi, H. Yoshitake and T. Tatsumi, Synthesis of anionic-surfactant-templated mesoporous silica using organoalkoxysilane-containing amino groups, Chemistry of Materials, 15 (2003) 4536-4538.

[14] T. W. Kim, R. Ryoo, K. P. Gierszal, M. Jaroniec, L. A. Solovyov, Y. Sakamoto and O. Terasaki, Characterization of mesoporous carbons synthesized with SBA-16 silica template, Journal of Materials Chemistry, 15 (2005) 1560-1571.

[15] W. J. Roth and J. C. Vartuli, Synthesis of mesoporous molecular sieves, Zeolites and

Ordered Mesoporous Materials: Progress and Prospects, 157 (2005) 91-110.

[16] W. Z. Zhou, Mesoporous crystals of transition metal oxides, Perspectives of Nanoscience and Nanotechnology, 140 (2008) 37-45.

[17] T. L. Chew, A. L. Ahmad and S. Bhatia, Ordered mesoporous silica (OMS) as an adsorbent and membrane for separation of carbon dioxide (CO_2), Adv. Colloid Interface Sci., 153 (2010) 43-57.

[18] M. T. Ho, G. Allinson and D. E. Wiley, Comparison of CO_2 separation options for geo-sequestration: are membranes competitive?, Desalination, 192 (2006) 288-295.

[19] L. M. Robeson, Correlation of Separation Factor Versus Permeability for Polymeric Membranes, Journal of Membrane Science, 62 (1991) 165-185.

[20] M. Moaddeb and W. J. Koros, Gas transport properties of thin polymeric membranes in the presence of silicon dioxide particles, Journal of Membrane Science, 125 (1997) 143-163.

[21] M. Ogawa and N. Masukawa, Preparation of transparent thin films of lamellar, hexagonal and cubic silica-surfactant mesostructured materials by rapid solvent evaporation methods, Microporous and Mesoporous Materials, 38 (2000) 35-41.

[22] G. G. Qi, Y. B. Wang, L. Estevez, X. N. Duan, N. Anako, A. H. A. Park, W. Li, C. W. Jones and E. P. Giannelis, High efficiency nanocomposite sorbents for CO_2 capture based on amine-functionalized mesoporous capsules, Energy & Environmental Science, 4 (2011) 444-452.

[23] V. Zelenak, M. Badanicova, D. Halamova, J. Cejka, A. Zukal, N. Murafa and G. Goerigk, Amine-modified ordered mesoporous silica: Effect of pore size on carbon dioxide capture, Chemical Engineering Journal, 144 (2008) 336-342.

[24] N. Yao, A. Y. Ku, N. Nakagawa, T. Lee, D. A. Saville and I. A. Aksay, Disorder-order transition in mesoscopic silica thin films, Chemistry of Materials, 12 (2000) 1536-1548.

[25] M. Klotz, A. Ayral, C. Guizard and L. Cot, Synthesis and characterization of silica membranes exhibiting an ordered mesoporosity. Control of the porous texture and effect on the membrane permeability, Separation and Purification Technology, 25 (2001) 71-78.

[26] Y. F. Lu, R. Ganguli, C. A. Drewien, M. T. Anderson, C. J. Brinker, W. L. Gong, Y. X. Guo, H. Soyez, B. Dunn, M. H. Huang and J. I. Zink, Continuous formation of supported cubic and hexagonal mesoporous films by sol gel dip-coating, Nature, 389 (1997) 364-368.

[27] X. C. Xu, C. S. Song, B. G. Miller and A. W. Scaroni, Adsorption separation of carbon dioxide from flue gas of natural gas-fired boiler by a novel nanoporous "molecular basket" adsorbent, Fuel Processing Technology, 86 (2005) 1457-1472.

[28] V. V. Guliants, M. A. Carreon and Y. S. Lin, Ordered mesoporous and macroporous inorganic films and membranes, Journal of Membrane Science, 235 (2004) 53-72.

[29] P. Kumar and V. V. Guliants, Periodic mesoporous organic-inorganic hybrid materials: Applications in membrane separations and adsorption, Microporous and Mesoporous Materials, 132 (2010) 1-14.

[30] A. Yamaguchi and N. Teramae, Fabrication and analytical applications of hybrid mesoporous membranes, Analytical Sciences, 24 (2008) 25-30.

[31] P. Kumar, J. Ida, S. Kim, V. V. Guliants and J. Y. S. Lin, Ordered mesoporous membranes: Effects of support and surfactant removal conditions on membrane quality, J. Membr. Sci., 279 (2006) 539-547.

[32] P. Kumar, J. C. Ida and V. V. Guliants, High flux mesoporous MCM-48 membranes: effects of support and synthesis conditions on membrane permeance and quality, Micropor. Mesopor. Mater., 110 (2008) 595-599.

[33] N. W. Ockwig and T. M. Nenoff, Membranes for hydrogen separation, Chemical Reviews, 107 (2007) 4078-4110.

[34] B. A. McCool, N. Hill, J. DiCarlo and W. J. DeSisto, Synthesis and characterization of mesoporous silica membranes via dip-coating and hydrothermal deposition techniques, Journal of Membrane Science, 218 (2003) 55-67.

[35] S. J. Yoo, D. M. Ford and D. F. Shantz, Synthesis and characterization of uniform alumina-mesoporous silica hybrid membranes, Langmuir, 22 (2006) 1839-1845.

[36] K. J. Edler and S. J. Roser, Growth and characterization of mesoporous silica films, International Reviews in Physical Chemistry, 20 (2001) 387-466.

[37] K. Domansky, J. Liu, L. Q. Wang, M. H. Engelhard and S. Baskaran, Chemical sensors based on dielectric response of functionalized mesoporous silica films, Journal of Materials Research, 16 (2001) 2810-2816.

[38] J. L. Gu, J. L. Shi, Z. Hua, L. M. Xiong, L. X. Zhang and L. Li, Highly dispersed gold nanowires within the pore channels of mesoporous silica thin films prepared from organic-inorganic hybrid films functionalized with basic moieties, Chemistry Letters, 34 (2005) 114-115.

[39] N. Petkov, S. Mintova, B. Jean, T. Metzger and T. Bein, Functionalized cubic mesostructured silica films, Materials Science & Engineering C-Biomimetic and Supramolecular Systems, 23 (2003) 827-831.

[40] S. Tanaka, J. Kaihara, N. Nishiyama, Y. Oku, Y. Egashira and K. Ueyama,

Incorporation of organic groups within the channel wall of spin-on mesostructured silica films by a vapor infiltration technique, Langmuir, 20 (2004) 3780-3784.

[41] W. Yantasee, Y. H. Lin, X. H. Li, G. E. Fryxell, T. S. Zemanian and V. V. Viswanathan, Nanoengineered electrochemical sensor based on mesoporous silica thin-film functionalized with thiol-terminated monolayer, Analyst, 128 (2003) 899-904.

[42] L. Nicole, C. Boissiere, D. Grosso, A. Quach and C. Sanchez, Mesostructured hybrid organic-inorganic thin films, Journal of Materials Chemistry, 15 (2005) 3598-3627.

[43] J. C. Hicks, J. H. Drese, D. J. Fauth, M. L. Gray, G. G. Qi and C. W. Jones, Designing adsorbents for CO_2 capture from flue gas-hyperbranched aminosilicas capable,of capturing CO_2 reversibly, Journal of the American Chemical Society, 130 (2008) 2902-2903.

[44] X. S. Zhao and G. Q. Lu, Modification of MCM-41 by surface silylation with trimethylchlorosilane and adsorption study, Journal of Physical Chemistry B, 102 (1998) 1556-1561.

[45] F. Hoffmann, M. Cornelius, J. Morell and M. Froba, Silica-based mesoporous organic-inorganic hybrid materials, Angewandte Chemie-International Edition, 45 (2006) 3216-3251.

[46] Y. Sakamoto, K. Nagata, K. Yogo and K. Yamada, Preparation and CO_2 separation properties of amine-modified mesoporous silica membranes, Micropor. Mesopor. Mater., 101 (2007) 303-311.

[47] S. Kim, J. Ida, V. V. Guliants and J. Y. S. Lin, Tailoring pore properties of MCM-48 silica for selective adsorption of CO_2, Journal of Physical Chemistry B, 109 (2005) 6287-6293.

[48] D.-H. Park, N. Nishiyama, Y. Egashira and K. Ueyama, Separation of organic/water mixtures with silylated MCM-48 silica membranes, Micropor. Mesopor. Mater., 66 (2003) 69-76.

[49] B. A. McCool and W. J. DeSisto, Amino-functionalized silica membranes for enhanced carbon dioxide permeation, Advanced Functional Materials, 15 (2005) 1635-1640.

[50] D. H. Park, N. Nishiyama, Y. Egashira and K. Ueyama, Enhancement of hydrothermal stability and hydrophobicity of a silica MCM-48 membrane by silylation, Ind. Eng. Chem. Res., 40 (2001) 6105-6110.

[51] S. Higgins, B. A. McCool, C. P. Tripp, D. M. Ruthven and W. J. DeSisto, Covalent Attachment of Monochlorosilanes to Mesoporous Silica Membranes using Supercritical Fluid Deposition, Separation Science and Technology, 43 (2008) 4113-4128.

[52] H. Lin and B. D. Freeman, Gas solubility, diffusivity and permeability in poly(ethylene oxide), Journal of Membrane Science, 239 (2004) 105-117.

[53] P. Bernardo, E. Drioli and G. Golemme, Membrane gas separation: a review/state of the art, Ind. Eng. Chem. Res., 48 (2009) 4638-4663.

[54] C. C. Striemer, T. R. Gaborski, J. L. McGrath and P. M. Fauchet, Charge and size-based separation of macromolecules using ultrathin silicon membranes, Nature, 445 (2007) 749-753.

[55] L. M. Robeson, Correlation of separation factor versus permeability for polymeric membranes, J. Membr. Sci., 62 (1991) 165-185.

[56] L. M. Robeson, The upper bound revisited, J. Membr. Sci., 320 (2008) 390-400.

[57] M. Mulder, Basic principles of membrane technology, Kluwer Academic Publishers,

Dordrecht, The Netherlands, (1991).

[58] J. Choi, H. K. Jeong, M. A. Snyder, J. A. Stoeger, R. I. Masel and M. Tsapatsis, Grain boundary defect elimination in a zeolite membrane by rapid thermal processing, Science, 325 (2009) 590-593.

[59] M. Kanezashi, J. O'Brien-Abraham, Y. S. Lin and K. Suzuki, Gas permeation through DDR-type zeolite membranes at high temperatures, AIChE J., 54 (2008) 1478-1486.

[60] W. C. Yoo, J. A. Stoeger, P. Lee, M. Tsapatsis and A. Stein, High-performance randomly oriented zeolite membranes using brittle seeds and rapid thermal processing, Angew. Chem. Int. Ed., 122 (2010) 8699-8703.

[61] N. Nishiyama, D. H. Park, A. Koide, Y. Egashira and K. Ueyama, A mesoporous silica (MCM-48) membrane: preparation and characterization, J. Membr. Sci., 182 (2001) 235-244.

[62] W. Chaikittisilp, H. J. Kim and C. W. Jones, Mesoporous alumina-supported amines as potential steam-stable adsorbents for capturing CO_2 from simulated flue gas and ambient air, Energy Fuel, 25 (2011) 5528-5537.

[63] A. J. Crisci, M. H. Tucker, M. Y. Lee, S. G. Jang, J. A. Dumesic and S. L. Scott, Add-functionalized SBA-15-type silica catalysts for carbohydrate dehydration, ACS Catal., 1 (2011) 719-728.

[64] C. Duncan, A. V. Biradar and T. Asefa, Aminotroponate/aminotroponiminate zinc complexes functionalized mesoporous silica catalysts for intramolecular hydroamination of non-activated alkenes with varied steric and electronic properties, ACS Catal., 1 (2011) 736-750.

[65] J. C. Hicks and C. W. Jones, Controlling the density of amine sites on silica surfaces using benzyl spacers, Langmuir, 22 (2006) 2676-2681.

[66] R. P. Hodgkins, A. Ahniyaz, K. Parekh, L. M. Belova and L. Bergström, Maghemite nanocrystal impregnation by hydrophobic surface modification of mesoporous silica, Langmuir, 23 (2007) 8838-8844.

[67] J. A. Melero, R. Grieken, van and G. Morales, Advances in the synthesis and catalytic applications of organosulfonic-functionalized mesostructured materials, Chem. Rev., 106 (2006) 3790-3812.

[68] A. P. Wight and M. E. Davis, Design and preparation of organic-inorganic hybrid catalysts, Chem. Rev., 102 (2002) 3589-3613.

[69] D. Bek, H. Balcar, N. Zilkova, A. Zukal, M. Horacek and J. Cejka, Grubbs catalysts immobilized on mesoporous molecular sieves via phosphine and pyridine linkers, ACS Catal., 1 (2011) 709-718.

[70] Y. J. Pagan-Torres, J. M. R. Gallo, D. Wang, H. N. Pham, J. A. Libera, C. L. Marshall, J. W. Elam, A. K. Datye and J. A. Dumesic, Synthesis of highly ordered hydrothermally stable mesoporous niobia catalysts by atomic layer deposition, ACS Catal., 1 (2011) 1234-1245.

[71] S. B. Hartono, S. Z. Qiao, K. Jack, B. P. Ladewig, Z. Hao and G. Q. Lu, Improving adsorbent properties of cage-like ordered amine functionalized mesoporous silica with very large pores for bioadsorption, Langmuir, 25 (2009) 6413-6424.

[72] K.-S. Jang, H.-J. Kim, J. R. Johnson, W.-g. Kim, W. J. Koros, C. W. Jones and S. Nair, Modified mesoporous silica gas separation membranes on polymeric hollow fibers, Chem. Mater., 23 (2011) 3025-3028.

[73] S. Lu, D. Wang, S. P. Jiang, Y. Xiang, J. Lu and J. Zeng, HPW/MCM-41 phosphotungstic acid/mesoporous silica composites as novel proton-exchange membranes for elevated-temperature fuel cells, Adv. Mater., 22 (2010) 971-976.

[74] T. Sen, A. Sebastianelli and I. J. Bruce, Mesoporous silica-magnetite nanocomposite: fabrication and applications in magnetic bioseparations J. Am. Chem. Soc., 128 (2006) 7130-7131.

[75] S. K. Sheshadri, H. M. Alsyouri and Y. S. Lin, Counter diffusion self assembly synthesis of ordered mesoporous silica membranes in straight pore supports, Micropor. Mesopor. Mater., 129 (2010) 228-237.

[76] L. Zhang, S. Qiao, Y. Jin, H. Yang, S. Budihartono, F. Stahr, Z. Yan, X. Wang, Z. Hao and G. Q. Lu, Fabrication and size-selective bioseparation of magnetic silica nanospheres with highly ordered periodic mesostructure, Adv. Funct. Mater., 18 (2008) 3203-3212.

[77] M. Pedernera, O. d. l. Iglesia, R. Mallada, Z. Lin, J. Rocha, J. Coronas and J. Santamaría, Preparation of stable MCM-48 tubular membranes, J. Membr. Sci., 326 (2009) 137-144.

[78] S. F. Wu, J. Q. Wang, G. L. Liu, Y. Yang and J. M. Lu, Separation of ethyl acetate (EA)/water by tubular silylated MCM-48 membranes grafted with different alkyl chains, J. Membr. Sci., 390 (2012) 175-181.

[79] H. Ji, Y. Q. Fan, W. Q. Jin, C. L. Chen and N. P. Xu, Synthesis of Si-MCM-48 membrane by solvent extraction of the surfactant template, J. Non-Cryst. Solids, 354 (2008) 2010-2016.

[80] C. Y. Liu, L. Q. Wang, W. Z. Ren, Z. H. Rong, X. Q. Wang and J. Q. Wang,

Synthesis and characterization of a mesoporous silica (MCM-48) membrane on a large-pore alpha-Al_2O_3 ceramic tube, Micropor. Mesopor. Mater., 106 (2007) 35-39.

[81] A. Gouzinis and M. Tsapatsis, On the preferred orientation and microstructural manipulation of molecular sieve films prepared by secondary growth, Chem. Mater., 10 (1998) 2497-2504.

[82] S. Nair, Z. P. Lai, V. Nikolakis, G. Xomeritakis, G. Bonilla and M. Tsapatsis, Separation of close-boiling hydrocarbon mixtures by MFI and FAU membranes made by secondary growth, Micropor. Mesopor. Mater., 48 (2001) 219-228.

[83] G. Xomeritakis, Z. P. Lai and M. Tsapatsis, Separation of xylene isomer vapors with oriented MFI membranes made by seeded growth, Ind. Eng. Chem. Res., 40 (2001) 544-552.

[84] K. Schumacher, M. Grün and K. K. Unger, Novel synthesis of spherical MCM-48, Micropor. Mesopor. Mater., 27 (1999) 201-206.

[85] Y. Liu, Y. S. Li and W. S. Yang, Fabrication of highly b-oriented MFI film with molecular sieving properties by controlled in-plane secondary growth, J. Am. Chem. Soc., 132 (2010) 1768-1769.

[86] C. Y. Liu, J. Q. Wang and Z. H. Rong, Mesoporous MCM-48 silica membrane synthesized on a large-pore alpha-Al_2O_3 ceramic tube, J. Membr. Sci., 287 (2007) 6-8.

[87] S. F. Wu, J. H. Yang, J. M. Lu, Z. H. Zhou, C. L. Kong and J. Q. Wang, Synthesis of thin and compact mesoporous MCM-48 membrane on vacuum-coated alpha-Al_2O_3 tube, J. Membr. Sci., 319 (2008) 231-237.

[88] N. Nishiyama, S. Tanaka, Y. Egashira, Y. Oku and K. Ueyama, Enhancement of structural stability of mesoporous silica thin films prepared by spin-coating, Chem.

Mater., 14 (2002) 4229-4234.

[89] S. Tanaka, N. Nishiyama, Y. Oku, Y. Egashira and K. Ueyama, Improved thermal stability of mesoporous molecular sieves by vapor infiltration treatment, Micropor. Mesopor. Mater., 63 (2003) 105-112.

[90] K. Hammond, G. Tompsett, S. Auerbach and W. Conner, Apparatus for measuring physical adsorption on intact supported porous membranes, J. Porous Mater., 14 (2007) 409-416.

[91] K. D. Hammond, M. Hong, G. A. Tompsett, S. M. Auerbach, J. L. Falconer and W. C. Conner, High-resolution physical adsorption on supported borosilicate MFI zeolite membranes: comparison with powdered samples, J. Membr. Sci., 325 (2008) 413-419.

[92] H. J. Kim, K. S. Jang, P. Galebach, C. Gilbert, G. Tompsett, W. C. Conner, C. W. Jones and S. Nair, Seeded growth, silylation, and organic/water separation properties of MCM-48 membranes, Journal of Membrane Science, 427 (2013) 293-302.

[93] W. W. Lukens, P. Schmidt-Winkel, D. Y. Zhao, J. L. Feng and G. D. Stucky, Evaluating pore sizes in mesoporous materials: a simplified standard adsorption method and a simplified Broekhoff-de Boer method, Langmuir, 15 (1999) 5403-5409.

[94] N. J. Harrick, Internal reflection spectroscopy, John Wiley and Sons, New York, 1967.

[95] F. M. Mirabella, Internal reflection spectroscopy—Theory and application, Marcel Dekker, New York, 1993.

[96] S. Brunauer, L. S. Deming, W. E. Deming and E. Teller, On a theory of the van der Waals adsorption of gases, J. Am. Chem. Soc., 62 (1940) 1723-1732.

[97] S. K. Bhatia, Modeling Pure Gas Permeation in Nanoporous Materials and

Membranes, Langmuir, 26 (2010) 8373-8385.

[98] S. K. Bhatia and D. Nicholson, Some pitfalls in the use of the Knudsen equation in modelling diffusion in nanoporous materials, Chemical Engineering Science, 66 (2011) 284-293.

[99] R. Anwander, I. Nagl, M. Widenmeyer, G. Engelhardt, O. Groeger, C. Palm and T. Roser, Surface characterization and functionalization of MCM-41 silicas via silazane silylation, J. Phys. Chem. B, 104 (2000) 3532-3544.

[100] R. W. Baker, J. G. Wijmans and Y. Huang, Permeability, permeance and selectivity: a preferred way of reporting pervaporation performance data, J. Membr. Sci., 348 (2010) 346-352.

[101] P. Bernardo, E. Drioli and G. Golemme, Membrane Gas Separation: A Review/State of the Art, Industrial & Engineering Chemistry Research, 48 (2009) 4638-4663.

[102] C. C. Striemer, T. R. Gaborski, J. L. McGrath and P. M. Fauchet, Charge- and size-based separation of macromolecules using ultrathin silicon membranes, Nature, 445 (2007) 749-753.

[103] I. F. J. Vankelecom, Polymeric membranes in catalytic reactors, Chemical Reviews, 102 (2002) 3779-3810.

[104] H. Strathmann, Membrane separation processes: Current relevance and future opportunities, Aiche Journal, 47 (2001) 1077-1087.

[105] L. M. Robeson, The upper bound revisited, Journal of Membrane Science, 320 (2008) 390-400.

[106] J. A. Gonzalez-Marcos, C. Lopez-Dehesa and J. R. Gonzalez-Velasco, Effect of

operation conditions in the pervaporation of ethanol-water mixtures with poly(1-trimethylsilyl-1-propyne) membranes, Journal of Applied Polymer Science, 94 (2004) 1395-1403.

[107] K. Jian, P. N. Pintauro and R. Ponangi, Separation of dilute organic/water mixtures with asymmetric poly(vinylidene fluoride) membranes, Journal of Membrane Science, 117 (1996) 117-133.

[108] H. O. E. Karlsson and G. Tragardh, Pervaporation of Dilute Organic-Waters Mixtures - a Literature-Review on Modeling Studies and Applications to Aroma Compound Recovery, Journal of Membrane Science, 76 (1993) 121-146.

[109] M. E. Williams, J. A. Hestekin, C. N. Smothers and D. Bhattacharyya, Separation of organic pollutants by reverse osmosis and nanofiltration membranes: Mathematical models and experimental verification, Industrial & Engineering Chemistry Research, 38 (1999) 3683-3695.

[110] S. B. Hartono, S. Z. Qiao, K. Jack, B. P. Ladewig, Z. P. Hao and G. Q. Lu, Improving Adsorbent Properties of Cage-like Ordered Amine Functionalized Mesoporous Silica with Very Large Pores for Bioadsorption, Langmuir, 25 (2009) 6413-6424.

[111] T. Sen, A. Sebastianelli and I. J. Bruce, Mesoporous silica-magnetite nanocomposite: Fabrication and applications in magnetic bioseparations, Journal of the American Chemical Society, 128 (2006) 7130-7131.

[112] L. Zhang, S. Z. Qiao, Y. G. Jin, H. G. Yang, S. Budihartono, F. Stahr, Z. F. Yan, X. L. Wang, Z. P. Hao and G. Q. Lu, Fabrication and Size-Selective Bioseparation of Magnetic Silica Nanospheres with Highly Ordered Periodic Mesostructure, Advanced Functional Materials, 18 (2008) 3203-3212.

[113] A. A. Kittur, S. S. Kulkarni, M. I. Aralaguppi and M. Y. Kariduraganavar, Preparation and characterization of novel pervaporation membranes for the separation of water-isopropanol mixtures using chitosan and NaY zeolite, Journal of Membrane Science, 247 (2005) 75-86.

[114] Q. Xu, Y. Yang, X. Z. Wang, Z. H. Wang, W. Q. Jin, J. Huang and Y. Wang, Atomic layer deposition of alumina on porous polytetrafluoroethylene membranes for enhanced hydrophilicity and separation performances, Journal of Membrane Science, 415 (2012) 435-443.

[115] J. Choi, H. K. Jeong, M. A. Snyder, J. A. Stoeger, R. I. Masel and M. Tsapatsis, Grain Boundary Defect Elimination in a Zeolite Membrane by Rapid Thermal Processing, Science, 325 (2009) 590-593.

[116] Q. Q. Ge, Z. B. Wang and Y. S. Yan, High-Performance Zeolite NaA Membranes on Polymer-Zeolite Composite Hollow Fiber Supports, Journal of the American Chemical Society, 131 (2009) 17056-+.

[117] M. Kanezashi, J. O'Brien-Abraham, Y. S. Lin and K. Suzuki, Gas permeation through DDR-type zeolite membranes at high temperatures, Aiche Journal, 54 (2008) 1478-1486.

[118] L. Xu and H. K. Lee, Zirconia hollow fiber: Preparation, characterization, and microextraction application, Analytical Chemistry, 79 (2007) 5241-5248.

[119] W. C. Yoo, J. A. Stoeger, P. S. Lee, M. Tsapatsis and A. Stein, High-Performance Randomly Oriented Zeolite Membranes Using Brittle Seeds and Rapid Thermal Processing, Angewandte Chemie-International Edition, 49 (2010) 8699-8703.

[120] Y. Huang, R. W. Baker and L. M. Vane, Low-Energy Distillation-Membrane

Separation Process, Industrial & Engineering Chemistry Research, 49 (2010) 3760-3768.

[121] L. M. Vane, F. R. Alvarez, Y. Huang and R. W. Baker, Experimental validation of hybrid distillation-vapor permeation process for energy efficient ethanol-water separation, Journal of Chemical Technology and Biotechnology, 85 (2010) 502-511.

[122] L. M. Vane, V. V. Namboodiri and R. G. Meier, Factors affecting alcohol-water pervaporation performance of hydrophobic zeolite-silicone rubber mixed matrix membranes, Journal of Membrane Science, 364 (2010) 102-110.

[123] A. R. Dacosta and A. G. Fane, Net-Type Spacers - Effect of Configuration on Fluid-Flow Path and Ultrafiltration Flux, Industrial & Engineering Chemistry Research, 33 (1994) 1845-1851.

[124] J. C. Hicks and C. W. Jones, Controlling the density of amine sites on silica surfaces using benzyl spacers, Langmuir, 22 (2006) 2676-2681.

[125] R. P. Hodgkins, A. Ahniyaz, K. Parekh, L. M. Belova and L. Bergstrom, Maghemite nanocrystal impregnation by hydrophobic surface modification of mesoporous silica, Langmuir, 23 (2007) 8838-8844.

[126] J. A. Melero, R. van Grieken and G. Morales, Advances in the synthesis and catalytic applications of organosulfonic-functionalized mesostructured materials, Chemical Reviews, 106 (2006) 3790-3812.

[127] A. P. Wight and M. E. Davis, Design and preparation of organic-inorganic hybrid catalysts, Chemical Reviews, 102 (2002) 3589-3613.

[128] W. Chaikittisilp, H. J. Kim and C. W. Jones, Mesoporous Alumina-Supported Amines as Potential Steam-Stable Adsorbents for Capturing CO_2 from Simulated Flue Gas and Ambient Air, Energy & Fuels, 25 (2011) 5528-5537.

[129] T. L. Chew, A. L. Ahmad and S. Bhatia, Ordered mesoporous silica (OMS) as an adsorbent and membrane for separation of carbon dioxide (CO_2), Advances in Colloid and Interface Science, 153 (2010) 43-57.

[130] P. Kumar, J. C. Ida and V. V. Guliants, High flux mesoporous MCM-48 membranes: Effects of support and synthesis conditions on membrane permeance and quality, Microporous and Mesoporous Materials, 110 (2008) 595-599.

[131] N. Nishiyama, D. H. Park, A. Koide, Y. Egashira and K. Ueyama, A mesoporous silica (MCM-48) membrane: preparation and characterization, Journal of Membrane Science, 182 (2001) 235-244.

[132] M. Pedernera, O. de la Iglesia, R. Mallada, Z. Lin, J. Rocha, J. Coronas and J. Santamaria, Preparation of stable MCM-48 tubular membranes, Journal of Membrane Science, 326 (2009) 137-144.

[133] Y. Sakamoto, K. Nagata, K. Yogo and K. Yamada, Preparation and CO_2 separation properties of amine-modified mesoporous silica membranes, Microporous and Mesoporous Materials, 101 (2007) 303-311.

[134] S. F. Lu, D. L. Wang, S. P. Jiang, Y. Xiang, J. L. Lu and J. Zeng, HPW/MCM-41 Phosphotungstic Acid/Mesoporous Silica Composites as Novel Proton-Exchange Membranes for Elevated-Temperature Fuel Cells, Advanced Materials, 22 (2010) 971-976.

[135] J. C. McKeen, Y. S. Yan and M. E. Davis, Proton Conductivity of Acid-Functionalized Zeolite Beta, MCM-41, and MCM-48: Effect of Acid Strength, Chemistry of Materials, 20 (2008) 5122-5124.

[136] S. J. Park, D. H. Lee and Y. S. Kang, High temperature proton exchange

membranes based on triazoles attached onto SBA-15 type mesoporous silica, Journal of Membrane Science, 357 (2010) 1-5.

[137] S. K. Seshadri, H. M. Alsyouri and Y. S. Lin, Counter diffusion self assembly synthesis of ordered mesoporous silica membranes in straight pore supports, Microporous and Mesoporous Materials, 129 (2010) 228-237.

[138] P. Kumar, S. Kim, J. Ida and V. V. Guliants, Polyethyleneimine-modified MCM-48 membranes: Effect of water vapor and feed concentration on N_2/CO_2 selectivity, Industrial & Engineering Chemistry Research, 47 (2008) 201-208.

[139] D. H. Park, N. Nishiyama, Y. Egashira and K. Ueyama, Separation of organic/water mixtures with silylated MCM-48 silica membranes, Microporous and Mesoporous Materials, 66 (2003) 69-76.

[140] A. J. Brown, J. R. Johnson, M. E. Lydon, W. J. Koros, C. W. Jones and S. Nair, Continuous Polycrystalline Zeolitic Imidazolate Framework-90 Membranes on Polymeric Hollow Fibers, Angewandte Chemie-International Edition, 51 (2012) 10615-10618.

[141] A. Belwalkar, E. Grasing, W. Van Geertruyden, Z. Huang and W. Z. Misiolek, Effect of processing parameters on pore structure and thickness of anodic aluminum oxide (AAO) tubular membranes, Journal of Membrane Science, 319 (2008) 192-198.

[142] T. J. Collins, ImageJ for microscopy, Biotechniques, 43 (2007) 25-30.

[143] M. Al-Juaied and W. J. Koros, Performance of natural gas membranes in the presence of heavy hydrocarbons, Journal of Membrane Science, 274 (2006) 227-243.

[144] D. Q. Vu, W. J. Koros and S. J. Miller, High pressure CO_2/CH_4 separation using carbon molecular sieve hollow fiber membranes, Industrial & Engineering Chemistry Research, 41 (2002) 367-380.

[145] R. W. Baker, J. G. Wijmans and Y. Huang, Permeability, permeance and selectivity: A preferred way of reporting pervaporation performance data, Journal of Membrane Science, 348 (2010) 346-352.

[146] M. R. Kosuri and W. J. Koros, Defect-free asymmetric hollow fiber membranes from Torlon (R), a polyamide-imide polymer, for high-pressure CO_2 separations, Journal of Membrane Science, 320 (2008) 65-72.

[147] G. P. Beaurecard, Y. H. Hu, D. W. Grainger and S. P. James, Silylation of poly-L-lysine hydrobromide to improve dissolution in apolar organic solvents, Journal of Applied Polymer Science, 79 (2001) 2264-2271.

[148] C. C. Landry, S. H. Tolbert, K. W. Gallis, A. Monnier, G. D. Stucky, F. Norby and J. C. Hanson, Phase transformations in mesostructured silica/surfactant composites. Mechanisms for change and applications to materials synthesist, Chemistry of Materials, 13 (2001) 1600-1608.

[149] L. A. Solovyov, O. V. Belousov, R. E. Dinnebier, A. N. Shmakov and S. D. Kirik, X-ray diffraction structure analysis of MCM-48 mesoporous silica, Journal of Physical Chemistry B, 109 (2005) 3233-3237.

[150] S. H. Tolbert, C. C. Landry, G. D. Stucky, B. F. Chmelka, P. Norby, J. C. Hanson and A. Monnier, Phase transitions in mesostructured silica/surfactant composites: Surfactant packing and the role of charge density matching, Chemistry of Materials, 13 (2001) 2247-2256.

[151] D. M. Dabbs and I. A. Aksay, Self-assembled ceramics produced by complex-fluid templation, Annual Review of Physical Chemistry, 51 (2000) 601-+.

[152] R. Ryoo, J. M. Kim, C. H. Ko and C. H. Shin, Disordered molecular sieve with

branched mesoporous channel network, Journal of Physical Chemistry, 100 (1996) 17718-17721.

[153] R. Ryoo, C. H. Ko, S. J. Cho and J. M. Kim, Optically transparent, single-crystal-like oriented mesoporous silica films and plates, Journal of Physical Chemistry B, 101 (1997) 10610-10613.

[154] S. Y. Tao, G. T. Li and H. S. Zhu, Metalloporphyrins as sensing elements for the rapid detection of trace TNT vapor, Journal of Materials Chemistry, 16 (2006) 4521-4528.

[155] S. F. Wu, J. Q. Wang, G. L. Liu, Y. Yang and J. M. Lu, Separation of ethyl acetate (EA)/water by tubular silylated MCM-48 membranes grafted with different alkyl chains, Journal of Membrane Science, 390 (2012) 175-181.

[156] G. H. Schoutens and W. J. Groot, Economic-Feasibility of the Production of Iso-Propanol-Butanol-Ethanol Fuels from Whey Permeate, Process Biochemistry, 20 (1985) 117-121.

[157] L. Li, Z. Y. Xiao, S. J. Tan, P. Liang and Z. B. Zhang, Composite PDMS membrane with high flux for the separation of organics from water by pervaporation, Journal of Membrane Science, 243 (2004) 177-187.

[158] T. C. Bowen, R. D. Noble and J. L. Falconer, Fundamentals and applications of pervaporation through zeolite membranes, Journal of Membrane Science, 245 (2004) 1-33.

[159] S. Das, A. K. Banthia and B. Adhikari, Improved conversion to ethyl acetate through removal of water of esterification by membrane pervaporation, Indian Journal of Chemical Technology, 14 (2007) 552-559.

[160] V. A. Tuan, S. G. Li, R. D. Noble and J. L. Falconer, Preparation and pervaporation

properties of a MEL-type zeolite membrane, Chemical Communications, (2001) 583-584.

[161] J. Caro, M. Noack and P. Kolsch, Zeolite membranes: From the laboratory scale to technical applications, Adsorption-Journal of the International Adsorption Society, 11 (2005) 215-227.

[162] S. L. Wee, C. T. Tye and S. Bhatia, Membrane separation process-Pervaporation through zeolite membrane, Separation and Purification Technology, 63 (2008) 500-516.

[163] R. Thiyagarajan, S. Ravi and P. K. Bhattacharya, Pervaporation of methyl-ethyl ketone and water mixture: Determination of concentration profile, Desalination, 277 (2011) 178-186.

[164] M. Garcia, M. T. Sanz and S. Beltran, Separation by pervaporation of ethanol from aqueous solutions and effect of other components present in fermentation broths, Journal of Chemical Technology and Biotechnology, 84 (2009) 1873-1882.

[165] X. Zhan, J. D. Li, J. Q. Huang and C. X. Chen, Enhanced Pervaporation Performance of Multi-layer PDMS/PVDF Composite Membrane for Ethanol Recovery from Aqueous Solution, Applied Biochemistry and Biotechnology, 160 (2010) 632-642.

[166] Y. W. Huang, J. W. Fu, Y. Pan, X. B. Huang and X. Z. Tang, Pervaporation of ethanol aqueous solution by polyphosphazene membranes: Effect of pendant groups, Separation and Purification Technology, 66 (2009) 504-509.

[167] A. Aroujalian and A. Raisi, Pervaporation as a means of recovering ethanol from lignocellulosic bioconversions, Desalination, 247 (2009) 509-517.

[168] Q. G. Zhang, W. W. Hu, A. M. Zhu and Q. L. Liu, UV-crosslinked chitosan/polyvinylpyrrolidone blended membranes for pervaporation, Rsc Advances, 3 (2013) 1855-1861.

[169] A. B. Beltran, G. M. Nisola, E. L. Vivas, W. Cho and W. J. Chung, Poly(octylmethylsiloxane)/oleyl alcohol supported liquid membrane for the pervaporative recovery of 1-butanol from aqueous and ABE model solutions, Journal of Industrial and Engineering Chemistry, 19 (2013) 182-189.

[170] S. Heitmann, J. Krings, P. Kreis, A. Lennert, W. R. Pitner, A. Gorak and M. M. Schulte, Recovery of n-butanol using ionic liquid-based pervaporation membranes, Separation and Purification Technology, 97 (2012) 108-114.

[171] Y. Q. Dong, M. Wang, L. Chen and M. J. Li, Preparation, characterization of P(VDF-HFP)/[bmim]BF4 ionic liquids hybrid membranes and their pervaporation performance for ethyl acetate recovery from water, Desalination, 295 (2012) 53-60.

[172] A. Thongsukmak and K. K. Sirkar, Extractive pervaporation to separate ethanol from its dilute aqueous solutions characteristic of ethanol-producing fermentation processes, Journal of Membrane Science, 329 (2009) 119-129.

[173] Y. X. Bai, J. W. Qian, C. F. Zhang, L. Zhang, Q. F. An and H. L. Chen, Cross-linked HTPB-based polyurethaneurea membranes for recovery of ethyl acetate from aqueous solution by pervaporation, Journal of Membrane Science, 325 (2008) 932-939.

[174] X. Z. Tian and X. Jiang, Poly(vinylidene fluoride-co-hexafluoropropene) (PVDF-HFP) membranes for ethyl acetate removal from water, Journal of Hazardous Materials, 153 (2008) 128-135.

[175] Y. X. Bai, J. W. Qian, Q. F. An, Z. H. Zhu and P. Zhang, Pervaporation characteristics of ethylene-vinyl acetate copolymer membranes with different composition for recovery of ethyl acetate from aqueous solution, Journal of Membrane Science, 305 (2007) 152-159.

[176] Y. X. Bai, J. W. Qian, Q. Zhao, Z. H. Zhu and P. Zhang, Effect of formation conditions of poly(ethylene-co-vinyl acetate) membrane on the membrane physical structure and pervaporation properties in the recovery of ethyl acetate from aqueous solution, Journal of Membrane Science, 299 (2007) 45-53.

[177] B. K. Zhu, X. Z. Tian and Y. Y. Xu, Recovering ethyl acetate from aqueous solution using P(VDF-co-HFP) membrane based pervaporation\, Desalination, 184 (2005) 71-78.

[178] J. Kuhn, S. Sutanto, J. Gascon, J. Gross and F. Kapteijn, Performance and stability of multi-channel MFI zeolite membranes detemplated by calcination and ozonication in ethanol/water pervaporation, Journal of Membrane Science, 339 (2009) 261-274.

[179] D. Korelskiy, T. Leppajarvi, H. Zhou, M. Grahn, J. Tanskanen and J. Hedlund, High flux MFI membranes for pervaporation, Journal of Membrane Science, 427 (2013) 381-389.

[180] P. Chen, X. B. Chen, X. S. Chen, Z. W. An and H. Kita, Pervaporation Separation and Catalysis Activity of Novel Zirconium Silicalite-1 Zeolite Membrane, Chinese Journal of Chemistry, 27 (2009) 1692-1696.

[181] X. J. Shu, X. R. Wang, Q. Q. Kong, X. H. Gu and N. P. Xu, High-Flux MFI Zeolite Membrane Supported on YSZ Hollow Fiber for Separation of Ethanol/Water, Industrial & Engineering Chemistry Research, 51 (2012) 12073-12080.

[182] K. Sakaki, H. Habe, H. Negishi and T. Ikegami, Pervaporation of aqueous dilute 1-butanol, 2-propanol, ethanol and acetone using a tubular silicalite membrane, Desalination and Water Treatment, 34 (2011) 290-294.

[183] H. Negishi, K. Sakaki and T. Ikegami, Silicalite Pervaporation Membrane Exhibiting a Separation Factor of over 400 for Butanol, Chemistry Letters, 39 (2010)

1312-1314.

[184] X. S. Chen, X. Lin, P. Chen and H. Kita, Pervaporation of ketone/water mixtures through silicalite membrane, Desalination, 234 (2008) 286-292.

[185] D. Shen, W. Xiao, J. H. Yang, N. B. Chu, J. M. Lu, D. H. Yin and J. Q. Wang, Synthesis of silicalite-1 membrane with two silicon source by secondary growth method and its pervaporation performance, Separation and Purification Technology, 76 (2011) 308-315.

[186] J. Gu, X. Shi, Y. X. Bai, H. M. Zhang, L. Zhang and H. Huang, Silicalite-Filled Polyether-block-amides Membranes for Recovering Ethanol from Aqueous Solution by Pervaporation, Chemical Engineering & Technology, 32 (2009) 155-160.

[187] S. Claes, P. Vandezande, S. Mullens, K. De Sitter, R. Peeters and M. K. Van Bael, Preparation and benchmarking of thin film supported PTMSP-silica pervaporation membranes, Journal of Membrane Science, 389 (2012) 265-271.

[188] H. L. Zhou, Y. Su, X. R. Chen and Y. H. Wan, Separation of acetone, butanol and ethanol (ABE) from dilute aqueous solutions by silicalite-1/PDMS hybrid pervaporation membranes, Separation and Purification Technology, 79 (2011) 375-384.

[189] X. L. Liu, Y. S. Li, Y. Liu, G. Q. Zhu, J. Liu and W. S. Yang, Capillary supported ultrathin homogeneous silicalite-poly(dimethylsiloxane) nanocomposite membrane for bio-butanol recovery, Journal of Membrane Science, 369 (2011) 228-232.

[190] G. P. Liu, D. Hou, W. Wei, F. J. Xiangli and W. Q. Jin, Pervaporation Separation of Butanol-Water Mixtures Using Polydimethylsiloxane/Ceramic Composite Membrane, Chinese Journal of Chemical Engineering, 19 (2011) 40-44.

[191] H. L. Zhou, Y. Su, X. R. Chen, S. L. Yi and Y. H. Wan, Modification of silicalite-1

by vinyltrimethoxysilane (VTMS) and preparation of silicalite-1 filled polydimethylsiloxane (PDMS) hybrid pervaporation membranes, Separation and Purification Technology, 75 (2010) 286-294.

[192] L. M. Vane, V. V. Namboodiri and T. C. Bowen, Hydrophobic zeolite-silicone rubber mixed matrix membranes for ethanol-water separation: Effect of zeolite and silicone component selection on pervaporation performance, Journal of Membrane Science, 308 (2008) 230-241.

[193] S. Araki, S. Imasaka, S. Tanaka and Y. Miyake, Pervaporation of organic/water mixtures with hydrophobic silica membranes functionalized by phenyl groups, Journal of Membrane Science, 380 (2011) 41-47.

[194] C. Azar and H. Rodhe, Targets for stabilization of atmospheric CO_2, Science, 276 (1997) 1818-1819.

[195] R. V. Siriwardane, M. S. Shen, E. P. Fisher and J. A. Poston, Adsorption of CO_2 on molecular sieves and activated carbon, Energy & Fuels, 15 (2001) 279-284.

[196] S. Elliott, K. S. Lackner, H. J. Ziock, M. K. Dubey, H. P. Hanson, S. Barr, N. A. Ciszkowski and D. R. Blake, Compensation of atmospheric CO_2 buildup through engineered chemical sinkage, Geophysical Research Letters, 28 (2001) 1235-1238.

[197] H. Herzog, What future for carbon capture and sequestration?, Environmental Science & Technology, 35 (2001) 148a-153a.

[198] S. I. Plasynski and Z. Y. Chen, Review of CO_2 capture technologies and some improvement opportunities., Abstracts of Papers of the American Chemical Society, 220 (2000) U391-U391.

[199] T. M. Yegulalp, K. S. Lackner and H. J. Ziock, A review of emerging technologies

for sustainable use of coal for power generation, Environmental Issues and Management of Waste in Energy and Mineral Production, (2000) 375-382.

[200] R. Bounaceur, N. Lape, D. Roizard, C. Vallieres and E. Favre, Membrane processes for post-combustion carbon dioxide capture: A parametric study, Energy, 31 (2006) 2556-2570.

[201] X. Zhang, C. F. Zhang, S. J. Qin and Z. S. Zheng, A kinetics study on the absorption of carbon dioxide into a mixed aqueous solution of methyldiethanolamine and piperazine, Industrial & Engineering Chemistry Research, 40 (2001) 3785-3791.

[202] R. W. Baker, Future directions of membrane gas separation technology, Industrial & Engineering Chemistry Research, 41 (2002) 1393-1411.

[203] P. H. M. Feron and A. E. Jansen, The production of carbon dioxide from flue gas by membrane gas absorption, Energy Conversion and Management, 38 (1997) S93-S98.

[204] J. C. Hicks, J. H. Drese, D. J. Fauth, M. L. Gray, G. G. Qi and C. W. Jones, Designing adsorbents for CO(2) capture from flue gas-hyperbranched aminosilicas capable,of capturing CO(2) reversibly, Journal of the American Chemical Society, 130 (2008) 2902-2903.

[205] X. C. Xu, C. S. Song, J. M. Andresen, B. G. Miller and A. W. Scaroni, Novel polyethylenimine-modified mesoporous molecular sieve of MCM-41 type as high-capacity adsorbent for CO_2 capture, Energy & Fuels, 16 (2002) 1463-1469.

[206] J. A. Davies and P. C. Griffiths, A phenomenological approach to separating the effects of obstruction and binding for the diffusion of small molecules in polymer solutions, Macromolecules, 36 (2003) 950-952.

[207] K. Ghosal, R. T. Chern, B. D. Freeman, W. H. Daly and I. I. Negulescu, Effect of

basic substituents on gas sorption and permeation in polysulfone, Macromolecules, 29 (1996) 4360-4369.

[208] K. S. Jang, H. J. Kim, J. R. Johnson, W. G. Kim, W. J. Koros, C. W. Jones and S. Nair, Modified Mesoporous Silica Gas Separation Membranes on Polymeric Hollow Fibers, Chemistry of Materials, 23 (2011) 3025-3028.

[209] W. Chaikittisilp, S. A. Didas, H. J. Kim and C. W. Jones, Vapor-Phase Transport as A Novel Route to Hyperbranched Polyamine-Oxide Hybrid Materials, Chemistry of Materials, 25 (2013) 613-622.

[210] P. Bollini, S. A. Didas and C. W. Jones, Amine-oxide hybrid materials for acid gas separations, Journal of Materials Chemistry, 21 (2011) 15100-15120.

[211] X. C. Xu, C. S. Song, B. G. Miller and A. W. Scaroni, Influence of moisture on CO_2 separation from gas mixture by a nanoporous adsorbent based on polyethylenimine-modified molecular sieve MCM-41, Industrial & Engineering Chemistry Research, 44 (2005) 8113-8119.

[212] K. F. Lam, H. Kassab, M. Pera-Titus, K. L. Yeung, B. Albela and L. Bonneviot, MCM-41 "LUS": Alumina Tubular Membranes for Metal Separation in Aqueous Solution, Journal of Physical Chemistry C, 115 (2011) 176-187.

[213] H. Saputra, R. Othman, M. H. Ani, A. G. E. Sutjipto and R. Muhida, High energy density zinc-air microbattery utilising inorganic MCM-41 membrane, Materials Research Innovations, 15 (2011) 114-117.

[214] J. H. Drese, S. Choi, S. A. Didas, P. Bollini, M. L. Gray and C. W. Jones, Effect of support structure on CO_2 adsorption properties of pore-expanded hyperbranched aminosilicas, Microporous and Mesoporous Materials, 151 (2012) 231-240.

[215] M. M. Wan, J. Y. Yang, Y. Qiu, Y. Zhou, C. X. Guan, Q. Hou, W. G. Lin and J. H. Zhu, Sustained Release of Heparin on Enlarged-Pore and Functionalized MCM-41, Acs Applied Materials & Interfaces, 4 (2012) 4113-4122.

[216] G. G. Paradis, R. Kreiter, M. M. A. van Tuel, A. Nijmeijer and J. F. Vente, Amino-functionalized microporous hybrid silica membranes, Journal of Materials Chemistry, 22 (2012) 7258-7264.